

Dissertation zur Erlangung des akademischen Grades

doctor rerum naturalium

(Dr. rer. nat.)

der Fakultät für Chemie und Pharmazie
der Ludwig-Maximilians-Universität München



The Effect of Lethal Toxin on the Respiratory Epithelium

Mandy Lehmann

aus

Frankfurt/Oder

2008

Erklärung

Diese Dissertation wurde im Sinne von § 13 Abs. 4 der Promotionsordnung vom 29. Januar 1998 von Frau Dr. U. G. Knaus betreut und von Frau Prof. Dr. A. M. Vollmar vor der Fakultät für Chemie und Pharmazie vertreten.

Ehrenwörtliche Versicherung

Diese Dissertation wurde selbständig, ohne unerlaubte Hilfe erarbeitet.

San Diego, am 02.03.2008

A handwritten signature in black ink that reads "Mandy Lehmann". The signature is written in a cursive style with a large initial 'M' and a long, sweeping underline.

Mandy Lehmann

Dissertation eingereicht am: 08.03.2008
1. Gutachter: Frau Prof. Dr. U. G. Knaus
2. Gutachter: Frau Prof. Dr. A. M. Vollmar
Mündliche Prüfung am: 17.04.2008

Dedicated to my mom

1 CONTENTS

<u>1</u>	<u>CONTENTS</u>	<u>1</u>
<u>2</u>	<u>INTRODUCTION</u>	<u>4</u>
2.1	BACILLUS ANTHRACIS INFECTION LEADS TO ANTHRAX	4
2.1.1	THE GENETICS BEHIND <i>BACILLUS ANTHRACIS</i>	5
2.1.2	ANTHRAX RECEPTORS TEM8 AND CMG2	10
2.1.3	ANTHRAX TOXIN CYCLE	11
2.2	BACTERIA AND TOXIN INTERACTION WITH THE EPITHELIUM	12
2.2.1	LETHAL TOXIN INFLUENCE ON JUNCTIONS AND ADHESION	13
2.2.2	GENERAL KNOWLEDGE ABOUT JUNCTIONS AND ADHESIONS	13
2.2.3	LETHAL TOXIN INFLUENCE ON THE CYTOSKELETON	14
2.2.4	GENERAL OVERVIEW OF THE CYTOSKELETON	15
2.3	LETHAL TOXIN INDUCED CELL DEATH IN MURINE CELLS	24
2.3.1	CYTOTOXICITY COMPARISON BETWEEN MOUSE AND HUMAN	26
2.3.2	CLINICAL SYMPTOMS AND TREATMENT OF INHALATIONAL ANTHRAX	27
<u>3</u>	<u>AIM OF THE WORK</u>	<u>28</u>
<u>4</u>	<u>MATERIAL AND METHODS</u>	<u>29</u>
4.1	CHEMICALS AND REAGENTS	29
4.1.1	KITS	30
4.1.2	INHIBITORS	30
4.1.3	MOLECULAR WEIGHT MARKERS	30
4.1.4	RADIOISOTOPES	31
4.1.5	BUFFERS	31
4.1.6	ANTIBODIES	32
4.1.7	PRIMERS	34
4.2	TECHNICAL EQUIPMENT	34
4.2.1	COMPUTER AND INTERNET PROGRAMS	35
4.3	CELL CULTURE	36
4.3.1	POLARIZED AIRWAY SYSTEM	36
4.3.2	CULTURING OF MURINE MACROPHAGES	38
4.4	GENE EXPRESSION	38
4.4.1	POLYMERASE CHAIN REACTION (PCR)	38

4.5	IMMUNOBLOT	39
4.6	IMMUNOCYTOCHEMISTRY AND MICROSCOPY	41
4.7	FLOW CYTOMETRY	42
4.7.1	DETERMINE CELL CYCLE CONTENT BY PROPIDIUM IODIDE (PI) STAIN	42
4.7.2	MEASUREMENT OF MITOCHONDRIAL POTENTIAL	42
4.8	LETHAL FACTOR ACTIVITY ASSAY	43
4.8.1	MAPK KIDE CLEAVAGE ASSAY	43
4.9	LENTIVIRUS PRODUCTION	43
4.10	CELL VIABILITY AND CELL DEATH	44
4.10.1	MTT ASSAY FOR CELL VIABILITY	44
4.10.2	TUNEL ASSAY TO DETERMINE DNA STRAND BREAKS	44
4.10.3	PHOSPHATIDYLSERINE EXPOSURE	44
4.10.4	CASPASE ACTIVATION	45
4.10.5	LDH RELEASE ASSAY	45
4.10.6	PROTEASOME ACTIVITY	45
4.11	EVALUATION OF THE POLARIZED AIRWAY SYSTEM	46
4.11.1	EPITHELIUM TRANSEPITHELIAL ELECTRICAL RESISTANCE	46
4.11.2	PERMEABILITY MEASUREMENTS	46
4.12	CELL ADHESION AND MIGRATION	47
4.12.1	ADHESION ASSAY	47
4.12.2	MIGRATION ASSAY IN BOYDEN CHAMBER	47
4.12.3	WOUND HEALING ASSAY	47
4.13	FRACTIONATION	47
4.13.1	FRACTIONATION OF MEMBRANE, CYTOSOL AND CYTOSKELETON	47
4.13.2	FRACTIONATION OF MEMBRANE AND CYTOSOL	48
5	RESULTS	49
5.1	CHARACTERIZATION OF AIRWAY EPITHELIAL CELLS	49
5.1.1	A MODEL TO STUDY ANTHRAX INFECTION	52
5.2	JUNCTION CHANGES AFTER LT TREATMENT	53
5.3	ALTERATION OF THE CYTOSKELETON AFTER LT TREATMENT	57
5.3.1	ACTIN AND TUBULIN CHANGES	57
5.3.2	MOTILITY DEFECTS	57
5.3.3	ADHESION ALTERATION AFTER LT TREATMENT	57
5.3.4	EFFECTER MOLECULES FOR CYTOSKELETON AND MOTILITY CHANGES	57
5.4	INVOLVEMENT OF THE MAPK PATHWAY	57
5.5	RESCUE EFFECT OF THE PERMEABILITY AND RESISTANCE	57
5.6	CELL VIABILITY AFTER LT TREATMENT	57

5.6.1	PROLIFERATION DECREASE DUE TO CELL CYCLE ARREST	57
5.6.2	MITOCHONDRIAL POTENTIAL CHANGES	57
5.6.3	PROTEASOME IMPAIRMENT	57
5.7	CONTINUES MAPKK CLEAVAGE DUE TO LETHAL TOXIN RESIDUES	57
5.8	MODIFICATION OF LETHAL FACTOR INFLUENCES ITS CYTOTOXIC EFFECT	57
6	<u>DISCUSSION</u>	57
6.1	POLARIZED LUNG EPITHELIAL - AN EXCELLENT MODEL TO STUDY LT INTOXICATION	57
6.2	LETHAL TOXIN DISRUPTS BARRIER FUNCTION IN LUNGS	57
6.3	LETHAL TOXIN ALTERS THE CYTOSKELETON	57
6.4	DEFECTIVE MOTILITY AND WOUND HEALING IN THE LUNGS CAUSED BY LETHAL FACTOR EXPOSURE	57
6.5	LETHAL FACTOR STORED IN MEMBRANE COMPARTMENTS CAUSING CONTINUE MAPKK CLEAVAGE	57
6.6	MINIMAL CYTOTOXICITY EFFECT OF LF IN HUMAN LUNG CELLS	57
6.7	THE MODIFICATION OF LF ON LYSINES ABOLISHED INDUCED CELL DEATH IN MURINE MACROPHAGES	57
7	<u>SUMMARY</u>	57
8	<u>REFERENCES</u>	57
9	<u>INDEX OF FIGURES</u>	57
10	<u>INDEX OF TABLES</u>	57
11	<u>INDEX OF MOVIES</u>	57
12	<u>APPENDIX</u>	57
12.1	SUMMARY OF CHARACTERISTICALLY MARKER OF LUNG CELLS	57
12.2	ABBREVIATIONS	57
12.3	ALPHABETICAL LIST OF COMPANIES	57
12.4	PUBLICATIONS	57
12.5	ACKNOWLEDGEMENTS	57
12.6	CURRICULUM VITAE	57

2 INTRODUCTION

2.1 *Bacillus Anthracis* Infection Leads to Anthrax

Bacillus anthracis is a Gram-positive, capsulated, aerobic and non-motile bacillus. It is related to the “*Bacillus cereus* group” of bacteria. To date, 89 strains have been identified. With a size of 3-5 μ m in length and 1-1.5 μ m in width, it is one of the largest bacteria. Under certain conditions *B. anthracis* forms spores that are extremely resistant to environmental insults. Therefore, they can survive for decades in air, water, soil and vegetation (saprophyte). Engulfment of the spores by the host leads to germination and conversion to the vegetative, actively dividing bacterium. (Figure 2-1) One of the striking features of the bacterium is its capsule, which protects it from the uptake by phagocytic cells. [1] The mechanism behind the conversion from the spore to the bacterium is not well understood. However, the change of the carbondioxide concentration and temperature between the environment and after uptake in the organism is believed to play a role. [2]

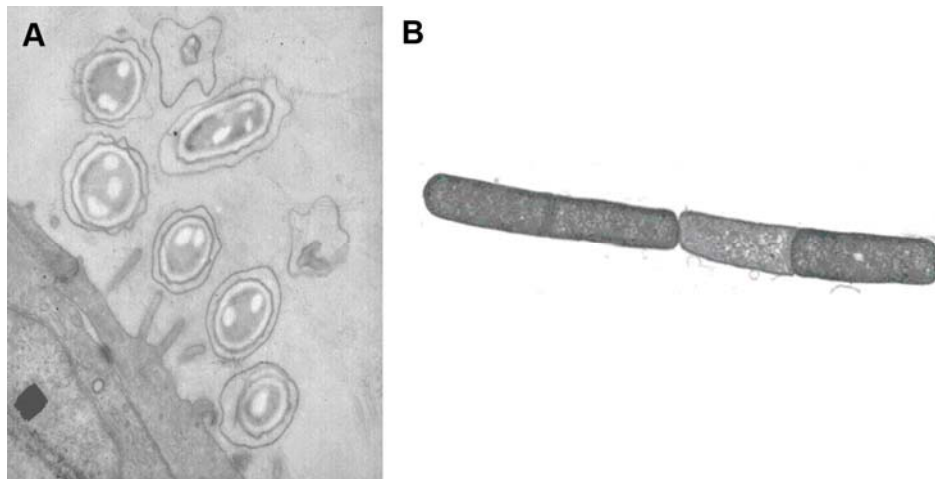


Figure 2-1: Electron microscopy of spores and vegetative form of anthrax.

A) Spores (Sterne strain) in close proximity to the apical side of in vitro differentiated airway epithelial cells. B) Vegetative form of *B. anthracis* (copied from [3])

The vegetative form of *B. anthracis* is known to cause anthrax, an acute infectious disease that is capable of inducing death to a variety of organisms, including humans. Three different forms of anthrax disease are known, depending on the entry route of the infectious bacteria. They are known as cutaneous, gastrointestinal and inhalational anthrax. The cutaneous form occurs after contact of spores with small skin lesions. Skin colonization with *B. anthracis* leads to the formation of black eschars that have given the disease its name (anthrax is the Greek word for coal). [4] It is treatable with antibiotics such as penicillin and therefore the least fatal but most common form. [5] Both gastrointestinal anthrax, which is caused by ingestion of contaminated meat [6], and inhalational anthrax have a much higher mortality rate (90-95%) among human cases.

In the past, certain outbreaks of the inhalational anthrax were reported, mostly caused by the exposure to contaminated animal material. [7-9] Improved hygiene and handling of those products decreased the number of cases. [10] Recently, attention was drawn to spore contaminated letters sent to federal departments in the

USA. This caused the infection and deaths of approximately 15 people. [11, 12] Interestingly, those spores were found to be genetically modified in their size and charge, making them highly aerosolized and even more infectious. Normal spores are much bigger. [13]

2.1.1 The Genetics Behind *Bacillus Anthracis*

The virulence factors of *Bacillus anthracis* are encoded by genes located on two plasmids called pXO1 and pXO2.

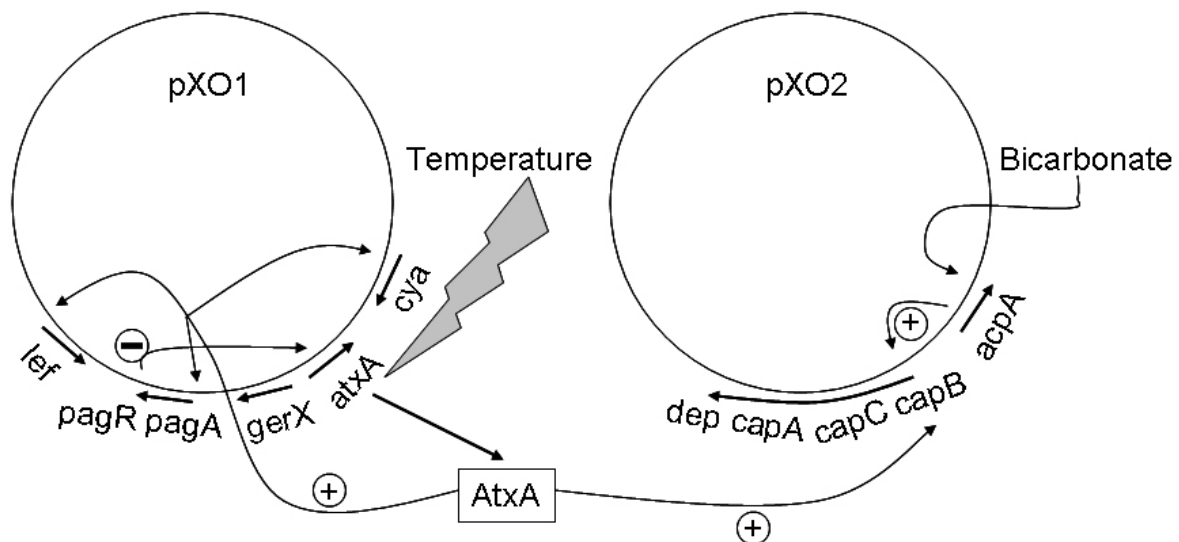


Figure 2-2: Plasmids pXO1 and pXO2 of *B. anthracis* contain genes, which encode virulence factors.

pXO1 contains the genes *pag*, *lef* and *cya* that encode protective antigen (PA, *pag*), lethal factor (LF, *lef*) and edema factor (EF, *cya*) and genes controlling capsule (*atxA*) production. pXO2 encodes proteins important for the biosynthesis and regulation of the polyglutamic acid capsule (*cap A*, *cap B*, *cap C*). [14-16] Furthermore, the *dep* gene is associated with depolymerization of the capsular polymer. [17] Bicarbonate is required for the capsule, and therefore genes for bicarbonate sensing are encoded on both plasmids. Atax (anthrax toxin activator) mediates CO₂-dependent regulation of transcription and expression. [18-21]

2.1.1.1 Protective Antigen – Structure and Function

Protective antigen is secreted by the vegetative form of *B. anthracis*. It needs to bind to the two known anthrax receptors (TEM8 and/or CMG2) to facilitate the translocation of LF and EF across the membrane to the cytosol. Therefore, PA needs to be proteolytically cleaved by a cell surface associated furin protease at the sequence RKKR¹⁶⁴⁻¹⁶⁷, resulting in the removal of a 20kDa fragment. [22] This process is required to form a barrel structure of seven PAs, allowing the attachment of lethal or edema factor. (Figure 2-9)

The crystal structure for PA revealed a 100Å tall, 50Å wide and 30Å deep molecule with a size of 83kDa. [23] (Figure 2-3) It contains four domains: Domain 1 (aa 1-258) which binds two calcium ions, can be viewed as two subdomains, termed PA20 and PA63. [24] PA20 corresponds to the residues 1-167. After its cleavage several hydrophobic residues become exposed, which are involved in LF and EF binding.

The remaining part (168-258) forms the N-terminus of the PA63. [25] Domain 2 (aa 259-487) is the longest domain, composed of charged or polar residues and is important for pore formation. Deletion mutations lacking F313 and F314 are defective in channel formation. [26] Domain 3 (aa 488-595) is the smallest domain and seems to be important for the self association of PA63, since mutagenesis of residue 510-518 inhibits oligomerization. [27, 28] Domain 4 (aa 596-735) is implicated in receptor binding, which was shown by deletion mutations of the C-terminus (679-693, 704-723, N682S). [29-32]

The heptameric prepore forms a ring shaped barrel structure. (Figure 2-3, B) The outside consists of domain 3 and 4 and inside of domain 1 and 2. [33] The lumen has an average diameter of 20Å and contains mainly polar and negatively charged residues. A maximum of three lethal and/or edema factor proteins can bind to the hydrophobic surface of domain 1. LF and EF unfold upon decrease of the pH and translocate through the narrow lumen into the pH-neutral cytosol, where they refold. To this end, a study by Melnyk et al. proposed a model in which the interaction of positive charged Lys397 loop (outside) and negative charged Asp426 (inside) contract the pore and bring the Phe427 of domain 2 closer together, which play a major role in the translocation of the protein through the pores. [34] This Phe clamp could function as a seal and trap LF at the N-terminus. After decreasing pH levels LF and EF unfold, translocate through the narrow lumen and refold in the neutral cytosol.

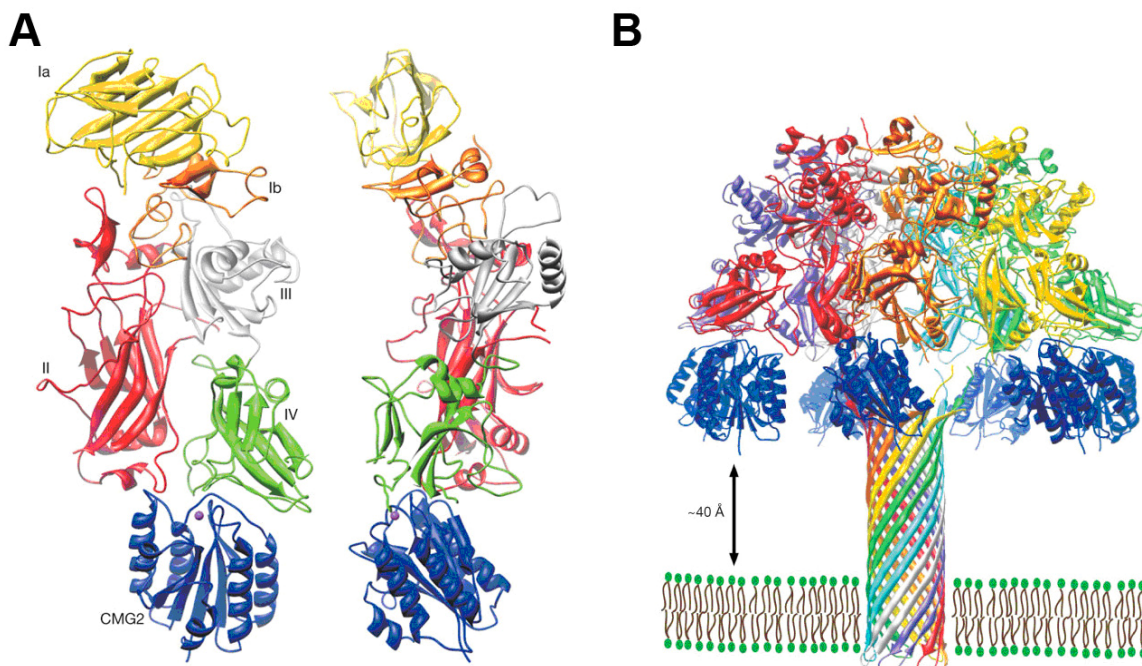


Figure 2-3: Protective antigen crystal structure and pore formation from [35].

A) Crystal structure of protective antigen bound to CMG2. The four domains are shown in different colors. B) Shape of the heptameric prepore displayed anchored in a lipid membrane. Abbreviation: Å, angstrom; CMG2, capillary morphogenesis gene 2.

2.1.1.2 Edema Factor / Edema Toxin – Structure and Function

EF is a calcium and calmodulin dependent adenylate cyclase, which shares homology of the catalytic adenylate cyclases domain with *Bordatella pertussis* and *Bordatella bronchiseptica*. [36]

It has been shown that treatment of macrophages with edema toxin leads to a wide variety of gene alterations. These genes are known to regulate processes such as inflammatory responses, apoptosis, adhesion, immune cell activation and transcription. [37] In addition to the altered gene expression profile, elevated intracellular cAMP levels are important for the establishment of infection. [38, 39] This is due to the dampening effect on the innate immune system by suppressing cytokine secretion. Treatment of murine bone-marrow derived macrophages with edema toxin inhibits IL-12p70 and TNF- α production. [40] Furthermore, decreased NADPH oxidase activation in human neutrophils through [cAMP] elevation leads to less production of superoxide, impeding effective killing of bacteria. [41] Independently of macrophages, neutrophil function is also affected. ET lowers the chemotactic response, phagocytosis and oxidative burst.

Effects of ET are also seen in the endothelium. Primary human microvascular endothelial cells (HMVECs) change their cytoskeleton and chemotaxis upon ET treatment by inducing transcription of Epac-related activators of Rap1, Epac2 (RapGEF4), and MR-GEF/RapGEF5. [42] Furthermore, the increased release of inflammatory proteins such as prostanoids and histamine causes enhanced endothelial permeability. [43] In addition, ET suppresses platelet aggregation by activation of protein kinase A. [44] The endothelial cell and platelet alterations could be the reason for inefficient wound closure causing bleeding in the interstitium.

Besides the inflammatory response, ET has been shown to increase hypertension caused by significant reduction of the left ventricular volumes and cardiac output. [45, 46]

2.1.1.3 Lethal Factor / Lethal Toxin – Structure and Function

The gene for lethal factor, called *lef*, was found on the pXO1 plasmid and generates a secreted protein of 90.2kDa. [47, 48] Lethal factor consists of four domains. (Figure 2-4)

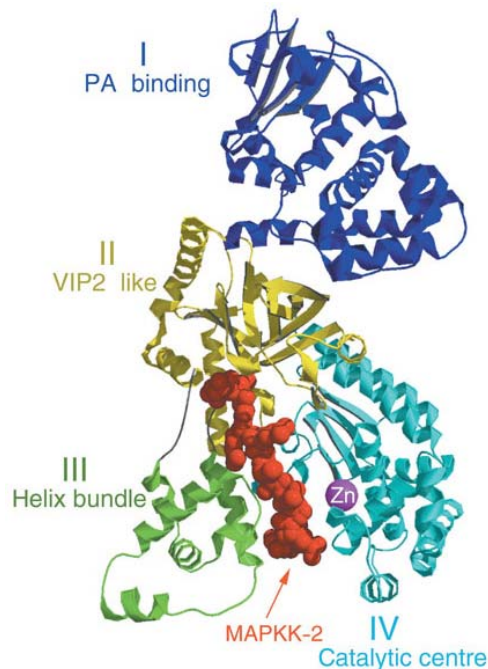


Figure 2-4: Crystal structure of lethal factor from [49].

Displayed are the four domains of lethal factor: protective antigen (I), MAPKK binding function (II) and the catalytic centre (IV). Abbreviation: MAPKK-2, mitogen-activated protein kinase kinase; PA, protective antigen; VIP2, vegetative insecticidal protein 2; Zn, zinc.

Domain 1 (aa 28-263) is homolog to the edema factor and is important for PA binding. Mutations in this region (D182, D187, D188, Y223, H229, L235 and Y236) inhibit PA recognition or binding. [50, 51] Domains 2-4 are inserted into each other. Domain 2 contains an ADP-ribosyltransferase unit, which is similar to the VIP2 protein, a toxin of *Bacillus cereus*. It contains mutations in the active site enhancing the substrate recognition. Point mutation studies (L293A, K294A, L514A, N516A, R491A: 10 to 50-fold reduction; N516A, L514A with either L293A, K294, or R491: complete reduction) showed that domain 2 plays an important role in the MAPKK cleavage. This indicates its involvement in the association with the MAPKK complex. [52] Domain 3 includes tandem repeats of the domain 2 and seems to be connected with it. Domain 4 forms the catalytic site, containing a HEFGHAV site (HEXXH, X can be any residue, aa 686-692), which is specific for metalloproteases. [49] Lethal factor is a zinc dependent metalloprotease. The protease activity was identified by protease inhibitors such as bestatin, which prevents the cytolysis of J774A.1 cells. Binding studies with zinc (^{65}Zn) proved that LF interacts with one or more zinc atoms. Also, mutagenesis of the histidines 686 and 690 to alanines (HEFGH, motif of metalloproteases) reduces cytotoxicity and zinc binding. [53, 54] However, a point mutation from cysteine to glutamine (E687C), which is still able to bind zinc, inhibits the activity of lethal factor to cleave MAPKK. Duesbery et al. and Vitale et al. discovered in 1998 the enzymatic substrates of lethal toxin, called mitogen-activated protein kinase kinase or MEK family (MKK1/2, MAPKK 1 and 2) with two different approaches, mutagenesis and yeast two-hybrid. [55, 56] LF acts preferably upon proline-containing peptides. [57] (Figure 2-5) Until recently, it was believed, that LT cuts the N-terminus of all MAPKK besides MKK5 [56-58], which is required for phosphorylation of their downstream effectors, ERK, p38 and JNK. (Figure 2-1)

MEK1	P	K	K	K	P	T	P	-	I	Q	L	N	P	A	P	8-9
MEK2	R	R	K	P	V	L	P	-	A	L	T	I	N	P	T	10-11
MKK3	K	R	K	K	D	L	R	-	I	S	C	M	S	K	P	26-27
MKK4	G	K	R	K	A	L	K	-	L	N	F	A	N	P	P	45-46
MKK4	P	F	K	S	T	A	R	-	F	T	L	N	P	N	P	58-59
MKK6	K	R	N	P	G	L	K	-	I	P	K	E	A	F	E	14-15
MKK7	R	P	R	P	T	L	Q	-	L	P	L	A	N	D	G	44-45
MKK7	R	P	R	H	M	L	G	-	L	P	S	T	L	F	T	76-77
consensus	+	+	+	+	X	φ	X	-	φ							

Figure 2-5: Alignment for MAPKK cleavage site.

N-terminus cleavage sites of all affected MAPKK are shown with their amino acid sequence and their consensus sequence. Adapted from [59]. Abbreviation: MEK, mitogen activating ERK kinase; MKK, mitogen activating kinase kinase.

Not only the N-terminus is important for the cleavage of MAPKK, the C-terminus contains a lethal factor interacting region (LFIR), which is required for their proteolysis. (Figure 2-6) Some point mutation in the LFIR of MEK1 (F310, E311, E319, L313 or a triple mutation in FEE) had no effect on the lethal factor cleavage, whereas others (I316, V317, P322, or L324 to alanine) are crucial for the cleavage of MEK1. Those residues were shown to be conserved in all MAPKK. [60]

	290	310	326	336
MEK1	RTPGRPLSSYGMDSRPPMAIFELLDY	IVNEPP	PKLPS---	GVFSLEF
MEK2	RPPGRPVS GHGMDSRPAMAIFELLDY	IVNEPP	PKLPN---	GVFTPDF
MKK3	-----	FQQLKQ	VVEEPS	PQLPA---DRFSPEF
MKK4	-----	FDQLTQ	VVKGDP	PQLSNSEEREFSPSF
MKK5	-----	LQLLQC	IVDEDS	PVLPV---GEFSEPF
MKK6	-----	FQQLKQ	VVEEPS	PQLPA---DKFSAEF
MKK7	-----	FEVLTK	VLQEEP	PLLPG--HMGFSGDF

Figure 2-6: Lethal factor interacting region.

The binding site of lethal factor with MAPKK displayed with their respective amino acid sequence. Adapted from [60]. Abbreviation: MEK, mitogen activating ERK kinase; MKK, mitogen activating kinase kinase.

Lethal factor shares structural similarities with the N-terminus of edema factor. [61] These regions are important for PA binding. [62] Compared to lethal toxin, edema toxin has a ten times lower mortality rate in rats. However, it was observed that edema toxin can sensitize resistant macrophages and mice strains (DBA/2J) to lethal toxin lysis. Therefore, edema and lethal toxin act synergistically to enhance the fatality. [63]

Lethal toxin is believed to be the most important key player in the anthrax infection. This was indicated by the comparison of *B. anthracis* infected and lethal toxin injected mice since they have similar phenotypes (shock, hypotension, death, and dyspnea). Another supporting fact is the 1000 fold reduction in mortality when LF-deficient strains were analyzed against wild-type strains. [64] Interestingly, lethal toxin does not cause cell death in all cells or mice strains. They are categorized into more susceptible or resistant types (Table 2-1).

Susceptible Cell Lines	Susceptible Macrophages	Resistant Macrophages
J774A.1 (BALB/c monocyte macrophage), RAW 264.7 (BALB/c monocyte macrophage)	129/J, BALB/cJ, C3H/HeJ, C57L/J, CBA/J, FVB/NJ, LP/J, MRL/MpJ, NZB/BinJ, SWR/J, CAST/EiJ, NON/LtJ, NZO/HILtJ	AKR/J, C57BL/6J, I/LnJ, PL/J, DBA/2J, SM/J, SPRET/Ei, IC-21, A/J, NOD/LtJ, SJL/J, 129S1/SvImJ

Table 2-1: Resistant and susceptible macrophage cell lines or mouse strains.

The death of susceptible macrophages starts with an increase in ion permeability (K^+ , Rb^+ , Ca^{2+} , Cr^{2+} , Cl^- , SO_4^{2-}) in the first 45 minutes. Conversion of ATP and the release of superoxide followed 15 minutes later. Shortly after, morphological changes are visual and cell lysis is initiated by loss of membrane integrity. [65]

LT abolishes also the MAPK pathway, which leads to decrease of inflammatory responses, through the reduction of cytokine (IL6), chemoattractant (IL8, RANTES) and enzyme (iNOS) expression. Like ET, LT influences the oxidative burst of polymorphonuclear cells. In addition, in human dendritic cells, apoptosis will be induced and pro-inflammatory cytokines as well as surface activation markers are suppressed (TNF α , IL1b, IL6, IL12, IL10, CD40, CD80, CD86). The elimination of dendritic cells prevent the initiation of the adaptive immunity. T-cell activation is dependent on the MAPK pathway. Therefore, cytokine production/upregulation of surface markers and transcription factors are reduced.

Not only is the T-cell activation impaired, but also their proliferation. B-cells show the same growth inhibition in addition to a lower antibody production (IgM and IgG). [13]

2.1.2 Anthrax Receptors TEM8 and CMG2

As mentioned above, two receptors are known to bind PA, the tumor endothelial marker 8 (TEM8) and capillary morphogenesis gene 2 (CMG2).

The physiological function of TEM8 is not well understood. It was shown to be upregulated in endothelial cells, in the colorectal tumors and vasculature in mouse embryos. The TEM8 receptor is expressed on a wide range of tissues, such as lungs, intestines, heart brain, skeletal muscles and pancreas. [66] TEM8 was discovered in a genetic approach as an anthrax receptor which binds protective antigen. Chinese hamster ovary cells (CHO-K1) were chemically challenged to undergo random mutagenesis and the cDNA of resistant cells were isolated to identify the PA receptor. [30]

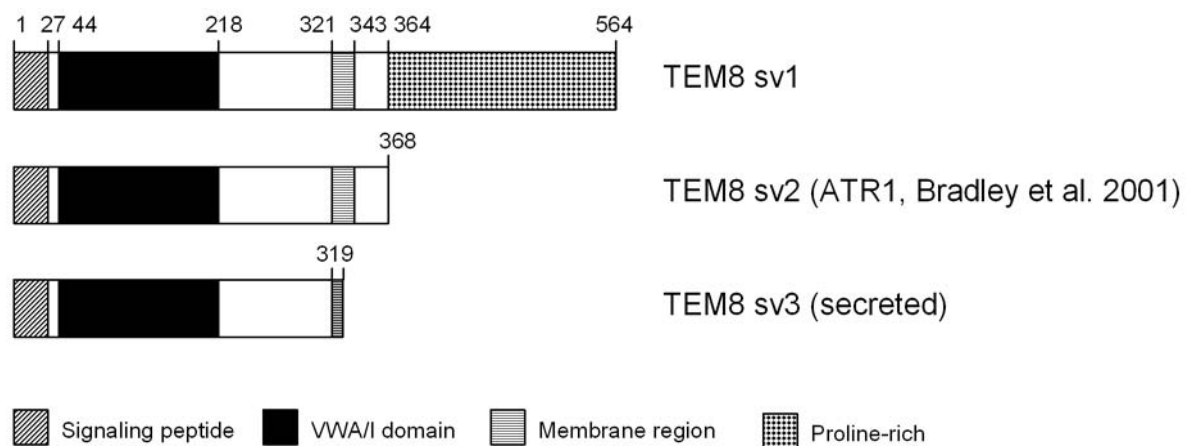


Figure 2-7: Alternative splice variants of the TEM8 receptor.

Splice variants ordered by amino acid size and different domains shown with unique color coding. (sv1 - GenBank accession no.: NP_115584, sv2 - GenBank accession no.: NP_444262, sv3 - GenBank accession no.: NP_060623). Adapted from [67]. Abbreviations: ATR1, Anthrax toxin receptor; sv, splice variant; TEM8, tumor endothelial marker 8; VWA/I Willebrand Factor type A /integrin inserted domain I.

So far, there are three alternative splice variants described. (Figure 2-7) [68] The first 2 variants (sv1 and sv2) function as an anthrax receptor. They contain type I membrane proteins and share distinct homology in their sequence beside the C-terminus tail. On the other hand, the sv3 version is predicted to be secreted due to the absence of a membrane domain. TEM8 sv1 is the original protein found in endothelial cells and with 564 amino acids the longest transcript. Besides the predicted signaling peptide, the extracellular region and the transmembrane domain, it has a 221 amino acid proline-rich C-terminal tail. TEM8 sv2 was identified by Bradley in 2001 as the first known anthrax receptor. [68] It has a length of 368 amino acids containing a shorter C-terminal end than sv1.

The extracellular side between residues 44 and 216 contains a van Willebrand Factor type A (VWA) domain. This motif seems to be important for PA binding, since the D50A mutation was unable to internalize PA. [69] The VWA domain is a well characterized interaction site of the extracellular matrix. It contains a metal ion-dependent adhesion site (MIDAS motif; DXDXS...T...D, with X being any amino acid) for ligand-interactions, which is conserved in both anthrax receptors. The C-

terminus consists of an acidic cluster (EESEE; sv1 residues 360-368 and sv2 360-364), which was also found on the cytoplasmic tail of a furin protease. Therefore, it might provide an interaction between the receptor and the protease to cleave the PA20 subunit required for pore formation. [30]

CMG2³⁸⁶ was identified in human umbilical vein endothelial cells (HUVECs) undergoing capillary formation in vitro. Since its expression is restricted to the endoplasmic reticulum it was excluded as an anthrax receptor, which has to be expressed on the cell surface. [70] However, an alternative splice variant was identified as another anthrax receptor by overexpression with a green fluorescence tag in CHO-R1.1 cells followed by a cytotoxic assay. [71] This CMG2 form was also expressed in a variety of tissues, for example placenta, heart, lungs, liver, small intestine, colon, spleen, kidney, skeletal muscle and peripheral blood leukocytes, but not in brain and thymus.

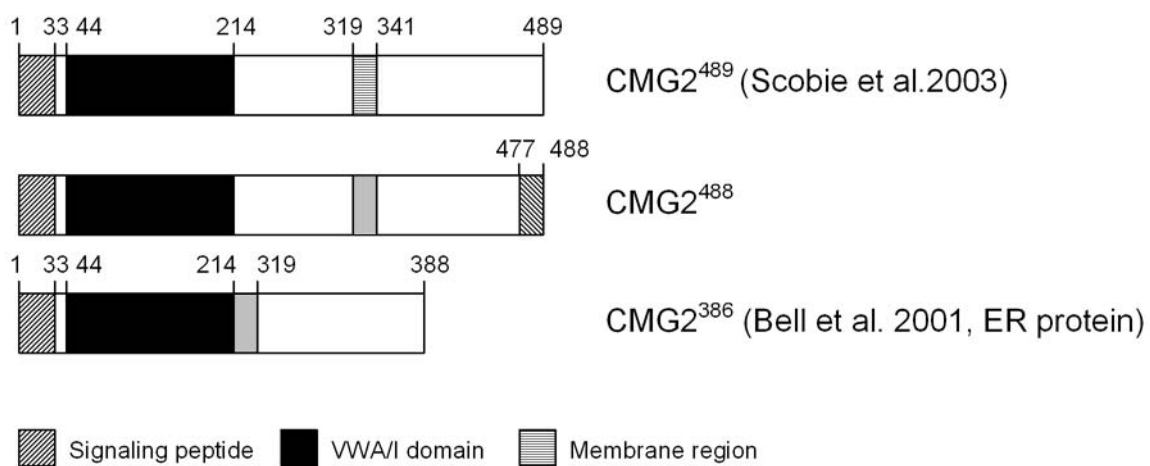


Figure 2-8: The splice variants of the CMG2 receptor.

Splice variants ordered by amino acid size and different domains shown with unique color coding. (CMG2⁴⁸⁹- GenBank accession no.: AY233452, CMG2⁴⁸⁸- GenBank accession no.: BAC03731, CMG2³⁸⁶- GenBank accession no.: AAK77222). Adapted from [67]. Abbreviations: CMG2, capillary morphogenesis gene 2; ER, endoplasmic reticulum; VWA/I Willebrand Factor type A /integrin inserted domain I.

TEM8 and CMG2 share a 40% overall homology. The VWA/I domain is 60% conserved and contains the MIDAS motif. Another similarity is the cluster of acidic residues (EEEEEE; CMG2⁴⁸⁸ and ⁴⁸⁹ residues 362-366, and CMG2³⁸⁶ residues 259-263). [67] CMG⁴⁸⁹ and ⁴⁸⁸ differ in the 12 amino acids at the C-terminus, which match those of CMG³⁸⁶. (Figure 2-8) Therefore, it is believed that 488 and 489 bind protective antigen. The C-terminus is not important for either binding or internalization of PA.

In 2006 it was shown that both receptors need a coreceptor. [72, 73] However, a different group proved that the low density lipoprotein receptor-related proteins 5 and 6 (LRP5 or LRP6) are not important for the uptake of the toxins. [74]

2.1.3 Anthrax Toxin Cycle

Protective antigen, lethal factor and edema factor are non-toxic by themselves since pore formation of PA is required to bind and internalize lethal factor and edema factor, which results in lethal toxin (PA+LF=LT) and edema toxin (PA+EF=ET). (Figure 2-9) The requirement of PA was proven by a study, which introduced LF by

osmotic lysis of pinosomes into cells causing no lethal toxin reaction. [75] The engulfment of the toxin complex occurs by a clathrin-dependent endocytosis and inserts into early endosomes integrated in the membrane of intraluminal vesicles. [76] Edema factor and lethal factor translocate inside the vesicles and are transported by multivesicular bodies to the late endosomes. The acidification in the endosomes leads to a conformational change of the PA pore and unfolds LF and EF. This is required for their translocation through the pore in the cytoplasm after the fusion of the intramural vesicles with the membrane of the endosomes take place. [77, 78]

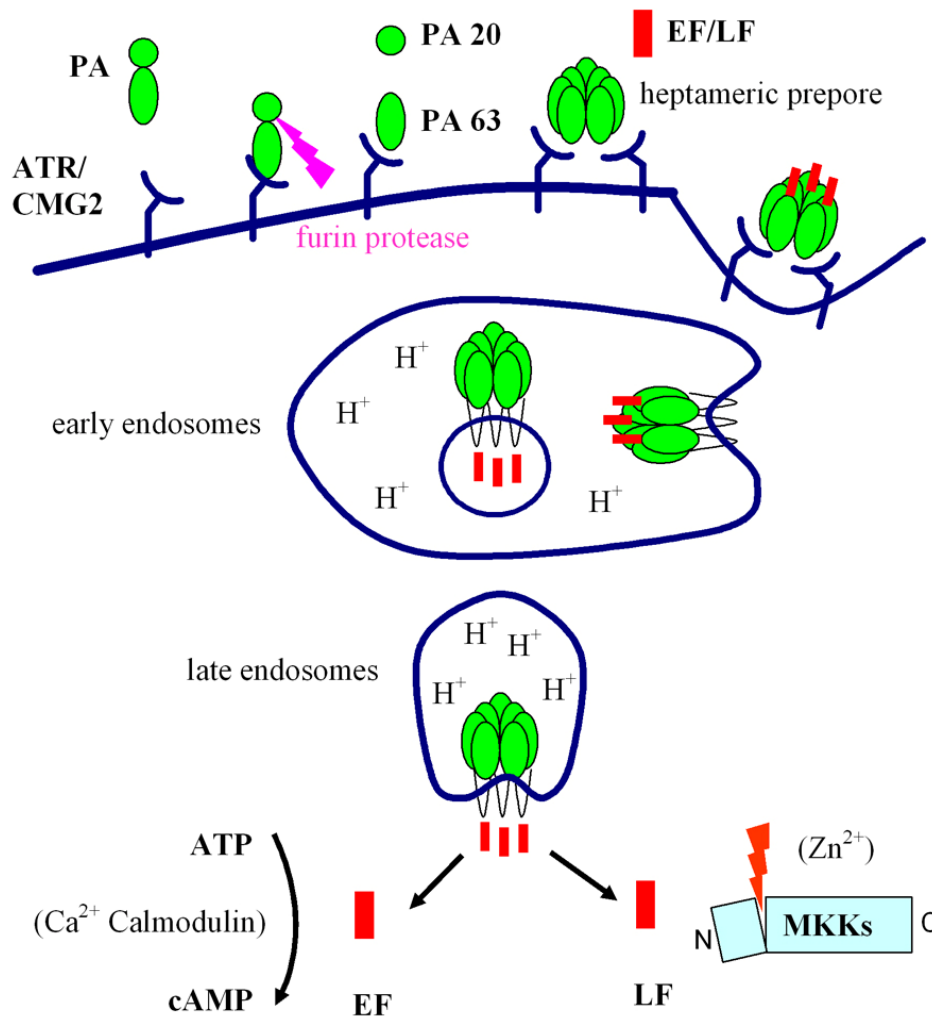


Figure 2-9: Anthrax toxin cycle.

Protective antigen binds to anthrax receptor and forms a prepore after furin cleavage. Bound EF and LF is internalized and released in the cytosol upon pH change, where an increase the cAMP levels or cleavage of MKK occurs. Abbreviation: ATP, adenosine triphosphate; ATR, anthrax toxin receptor; Ca²⁺, Calcium ion; CMG2, capillary morphogenesis gene 2; cAMP, cyclic adenosine monophosphate; H⁺, hydrogen ion; EF, edema factor; LF, lethal factor; MKK, mitogen-activated protein kinase ; PA, protective antigen, Zn²⁺, zinc ion.

2.2 Bacteria and Toxin Interaction with the Epithelium

The epithelial cell barrier is important for protection against external insults. It regulates the transport of molecules and defends the body from infection. Many

invasion mechanisms of pathogens have been described. In general, bacteria are phagocytosed by innate immune cells, such as macrophages or dendritic cells, and destroyed. However, many bacteria are able to interact with cells or secrete toxins to modulate the immune response and escape. Mostly junction and/or cytoskeletal alterations are induced by the bacteria to enter the host. For example, the *Bacteroides fragilis* toxin, which is like LT a zinc- dependent metalloprotease toxin, destroys junctions of polarized intestinal epithelial cells in dose dependent manner. [79]

2.2.1 Lethal Toxin Influence on Junctions and Adhesion

LT was shown to cause endothelial barrier dysfunction in primary human lung microvascular endothelial cells. [80] After 24 hours a drop of transepithelial resistance (TEER) up to 40% compared to the untreated cells, was measured. The resistance increased to 70% after 72 hours. The resistance alteration was accompanied by a change of permeability, which increased by 50%. Morphological changes of the cytoskeleton and adherens junctions (VE-cadherin) were studied by immunofluorescence. Lethal toxin treated cells showed a decrease of F-actin in the cell periphery, whereas the cell body displayed increased stress fibers. Also, the monolayer changed to a more elongated fibroblast-like shape. Monolayer density was slightly lower after 72 hours, but this cannot be the only reason for the TEER increase. Cell death disrupts the integrity of the cell layer and can cause increased permeability. However, only 2.5% and 7% of cells were apoptotic after 48 hours and 72 hours, respectively. [80]

Inhibition of MKK1/2 and JNK decreased the resistance similar to LT, whereas p38 increased the resistance. This showed that the MAPK pathways are partially involved in resistance and permeability alterations. When Warfel et al. used a combination of all three inhibitors, no permeability alteration was seen and the cells did not display the same morphological changes in IF compared to LT treatment. [80]

2.2.2 General Knowledge about Junctions and Adhesions

Epithelial cells have to be polarized and form tight bond, in order to become a very tight barrier. Cell junctions as well as cell-cell and cell-matrix adhesions provide the connections required for layer strength, rigidity, integrity, molecule transport, cell communication and defense.

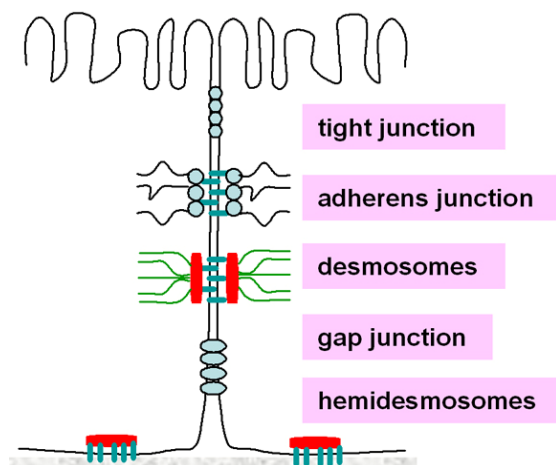


Figure 2-10: Overview of the junction complex.
Adapted from [81].

Four major classes of junctions were described: tight junctions, gap junctions, adherens junctions and desmosomes. (Figure 2-10) Tight junctions are located basolateral right below the apical cell surface. Through their sealing features, they separate apical from basolateral fluids, which is important for the epithelial cell integrity and transport of ions, nutrition and molecules. It also blocks the diffusion of membrane proteins and glycolipids. The major integral membrane proteins present in the junction structure are occludin and claudin. However, many proteins are known to connect junctions with the cytoskeleton, such as vinculin, cortactin, α -actinin and WASP. [82]

Adherens junctions are cell-cell connections to support the cell shape and are localized right under the tight junctions. E-cadherin is associated with actin and myosin through the adaptor protein α - and β -catenin. They are regulated by GTPases, PI3K and the Arp2/3 complex. [82]

Desmosomes were found in adhesion plaques, which are associated with intermediate filaments. Desmoglein and desmocollin are transmembrane linker proteins connecting proteins in the plaques, such as plakoglobin. They are important for maintaining the tissue homeostasis and strength. [82, 83] Gap junctions are intercellular cylindrical channels formed by the transmembrane protein connexin. This channel allows the exchange of ions (e.g. Ca^{2+} , cAMP) and small molecules between cells. Therefore, they control the metabolic activity of cell-cell interactions. [82]

Epithelial cells are linked basal to extracellular matrix proteins. Integrins are the major class of cell-matrix adhesion molecules. They form heterodimers out of α and β subunits. Epithelial cells express a wide range of both of them ($\alpha 1\beta 1$, $\alpha 2\beta 1$, $\alpha 3\beta 1$, $\alpha 5\beta 1$, $\alpha 6\beta 1$, $\alpha 9\beta 1$, $\alpha 6\beta 4$, $\alpha v\beta 5$, $\alpha v\beta 6$). [84] Most common ligands are fibronectin, laminin and collagen. Talin and α -actinin regulate integrin activation, focal adhesion formation, recruitment of proteins to the focal adhesion complex and form a bridge between the integrins and the cytoskeleton. [85]

Focal adhesions are sites connecting the actin cytoskeleton with integrin and matrix proteins. They are distinct by location, size and composition. The front of migrating cells contains mostly small focal adhesion, which are controlled by Rac and Cdc42, followed by elongated attachments regulated by Rho. They are connected to the actin cytoskeleton, located on the end of stress fibers. A variety of focal adhesion proteins are known, such as Src, FAK, cortactin, paxillin and vinculin. Tyrosine phosphorylation is a key event to regulate the dynamics of adhesion molecules. This occurs through Src and FAK. FAK is a tyrosine kinase, which is activated by autophosphorylation at tyrosine 397 (p-Y397). Src becomes stimulated by binding on p-Y397 and causes increased FAK activation and interaction with other proteins (Ras-MAPK pathway) by phosphorylating sites such as Y576, Y577, Y861 and Y925. The importance of FAK on migration was shown in FAK knockout cells leading to an increase of focal adhesion and defect in migration. [85] Active Src is not only important for FAK activation but also binds through a proline-rich domain to the adhesion adapter protein paxillin and phosphorylates it at Tyr31 and Tyr118. Paxillin is connected to the cell membrane, or directly to $\beta 1$ integrin, and can either enhance or decrease motility. [85]

2.2.3 Lethal Toxin Influence on the Cytoskeleton

Proteomic analysis of a macrophage cell line (J774A.1) exposed to LT revealed alteration of cytoskeletal proteins, stress responses and energy generation. In detail,

the expression of tubulin-β2 and γ-actin were decreased, whereas vimentin, a protein of the intermediary family, was increased. [86]

The effect of lethal toxin on the cytoskeleton was shown mainly in neutrophils where it paralyzes actin-based motility. LT impaired the fMLP stimulation of chemokinesis by more than 60% and enabled chemotaxis induced by chemoattractants. Migration requires active dynamics of the cytoskeleton. A lower filamentous actin content after lethal toxin treatment was caused by a reduction of Hsp27 phosphorylation. Cleavage of MKK3/6 led to a p38 activation defect, which reduced the phosphorylation of Hsp27. The reduced activity of Hsp27 results in the release of sequestered actin monomers, which altered the assembly of actin filaments. [87, 88] This could be the reason for the impaired phagocytosis after LT treatment. [89]

2.2.4 General Overview of the Cytoskeleton

The cytoskeleton provides a filamentous network in the cytoplasm shaping the cell and facilitates movements. The main structural elements are microtubules, microfilaments (actin filaments) and intermediate filaments. (Figure 2-11)

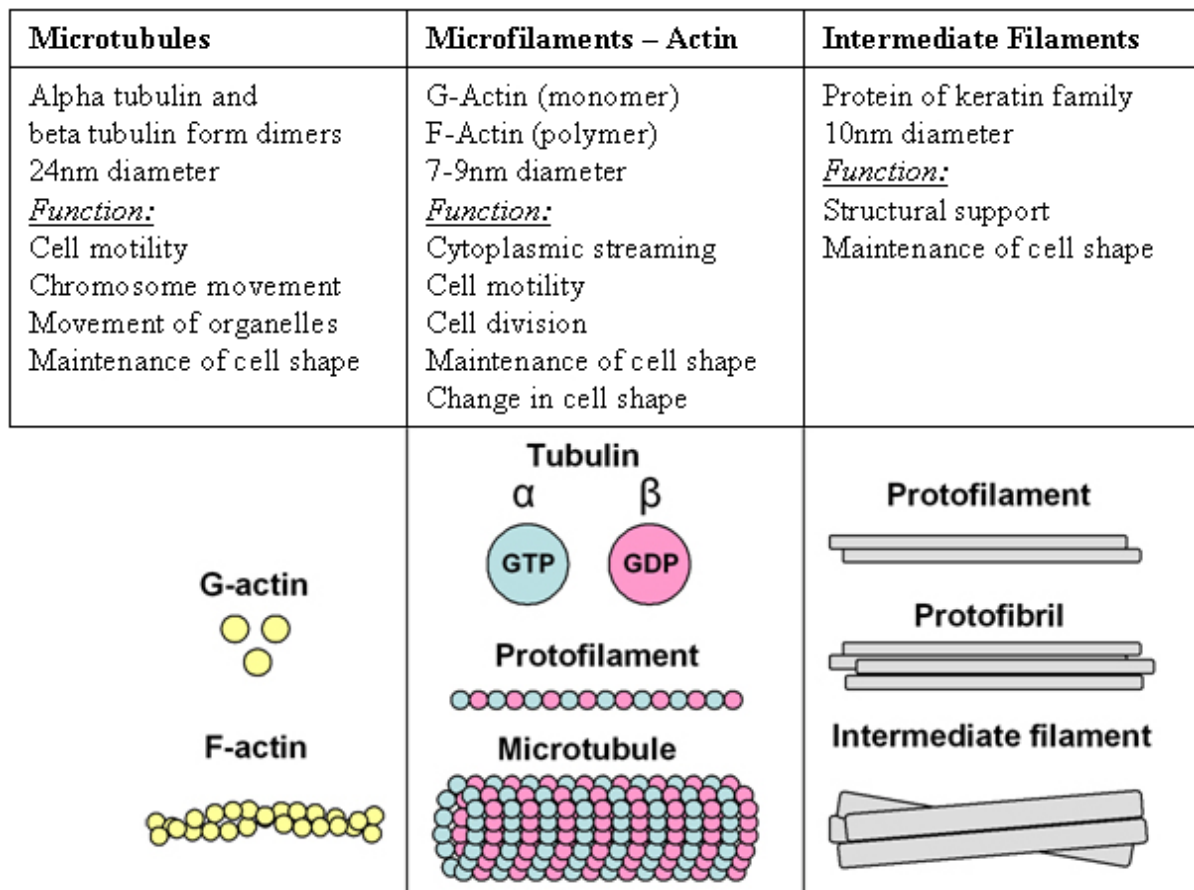


Figure 2-11: Cytoskeletal polymers.

Three different types of filaments are described with their structure and function. Adapted from [90] and [82]. Abbreviation: G-actin, globular actin; F-actin, filamentous actin; nm, nanometer.

The smallest components of the cytoskeleton are the microfilaments. Monomer G-actin (G = globular) forms double helical strands, called F-actin (F = filamentous), which twist around themselves to construct microfilaments. [90] Filamentous actin can shape distinct structures, such as stress fibers. To elongate in the direction of

protrusion, thin actin sheets (lamellipodia) and filopodia (finger-like protrusions) are developed by migrating cells. [91] The polymerization and depolymerization of actin on the leading edge is shown in **Figure 2-12**. They influence motility, cytoplasmic movements, cell shape, muscle contraction and cell division by producing the cleavage furrow.

The actin cytoskeleton can be disrupted by inhibitors, which provide a tool for studying actin polymerization/depolymerization. For example, cytochalasin B binds to the barbed ends and blocks its assembly. Latrunculin inhibits the formation of F-actin by binding G-actin. F-actin is stabilized by phalloidin to abolish depolarization.

Microtubules contribute to the cell shape, polarity, organelle position, vesicle transport, cell division (mitotic spindle), centriole organization and motility. They are located throughout the cell and indispensable player for structural components, such as cilia, centrioles and mitotic spindle.

A variety of tubulin inhibitors are known to interfere with cell polarity. High concentrations of colchicine lead to depolarization of microtubules. Animal cells treated with lower concentration of colchicine block the microtubule rearrangement. This leads to the synchronization of cells in the metaphase. Nocodazole is also used for metaphase synchronization by promoting microtubule depolymerization. Taxol inhibits microtubule dynamics by binding on tubulin sites leading to the stabilization of microtubules. [82] Furthermore, post-translational modifications of tubulin can influence the motility. **Table 2-2** shows the most important alterations and their function.

Tubulin Modification	Comment	Function
Acetylation/ deacetylation	Only tubulin; marker for stable microtubules	Regulation of cell motility, binding of MAPs to microtubule
Tyrosination/ detyrosination	Reversible	Crosstalk to intermediate filaments; differentiation
Generation of $\Delta 2$ -tubulin	Only tubulin; marker for stable microtubules	Removing tubulin from tyrosination cycle; marking microtubule for polyglycylation
Polyglutamylaton	α - and β -tubulin; multiple glutamylation sites possible, up to 20 side-chain residues	Centriole maturation and stability; flagellar and ciliary motility; regulation of interaction with MAPs
Polyglycylation	α - and β -tubulin; multiple glutamylation sites possible, up to 30-40 side-chain residues	Ciliary motility, cytokinesis
Palmitoylation	Demonstrated for budding yeast α tubulin on residues 376	Positioning of astral microtubules in budding yeast
Phosphorylation	Better established for β -tubulin on Ser441/444	Neuronal differentiation

Table 2-2: Posttranslational modification of tubulin.

Shown are different modifications of tubulin with their function. Adapted from [92]. Abbreviation: MAP, Microtubules associated protein; Ser, serine;

Intermediate filaments are, in contrast to the other filaments, a more permanent and stable component. Therefore, they fix the position of organelles and cell shapes even if high mechanical stress occurs. [90]

Cytoskeleton formation and cell polarization (ability to form a front and a back) are crucial for cell locomotion. The motility is initiated by the formation of a wide protrusion (lamellipodia) at the cell front through microfilament assembly on the leading edge. This actin network is cross-linked for stabilization and new focal adhesions connect the membrane with the extracellular matrix to anchor the protrusions. Afterwards the cytosol flows towards the front and the rear starts to contract. Upon disruption of the breakage of focal contacts, the tail moves forward.

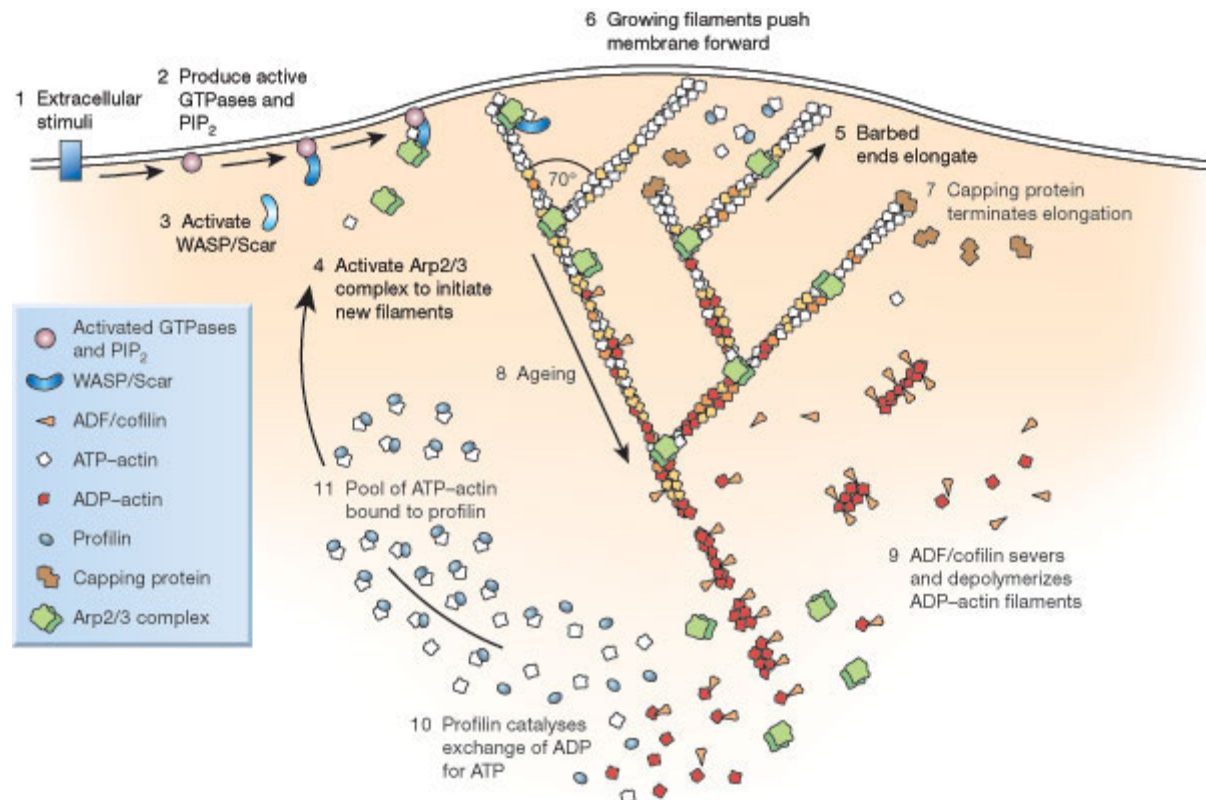


Figure 2-12: Mechanism of actin turnover from [93].

Polymerization of actin with important key players. Abbreviation: ADF, actin depolymerization factor; ADP, adenosine diphosphate; Arp2/3, actin related protein 2/3; ATP, adenosine triphosphate; PIP₂, phosphatidylinositol bisphosphate; Scar, suppressor of cAMP receptor; WASP, Wiscott Aldrich syndrome protein.

The directed migration (chemotaxis) towards a chemotactic gradient needs a defined mechanism of actin polymerization. (Figure 2-12) After stimulation of cell surface receptors (tyrosine kinase receptors) intracellular signaling proteins such as Ras family members are activated. This causes the initiation of cytoskeletal rearrangement to induce directed motility. Active GTPases stimulate WASP and proteins activating the seven protein complex called Arp2/3. This complex initiates the actin filament growth from an F-actin branch, by adding profilin bound ATP-G-actin. CapZ and other capping proteins restrict the barbed ends by preventing the addition or exchange of actin subunits through filament growth is stopped. The length of actin filaments is also controlled by actin-depolymerization factors, such as gelsolin/ADF and cofilin. Actin-binding protein profilin promotes the exchange of dissociated ADP-G-actin to ATP and refills the G-actin content used for assembly. The microfilament growth process can be increased by the hydrolysis of PIP₂ through phospholipase C (PLC). This increases actin turnover by inducing the

release of profilin, cofilin and gelsolin from the membrane. [93] Furthermore, cortactin promotes actin polymerization which is important for lamellipodia formation. It interacts with the Arp2/3 complex and is a known substrate of Src. [94, 95] These mentioned key players for polarization, protrusion and adhesion formation are summarized in **Figure 2-13**.

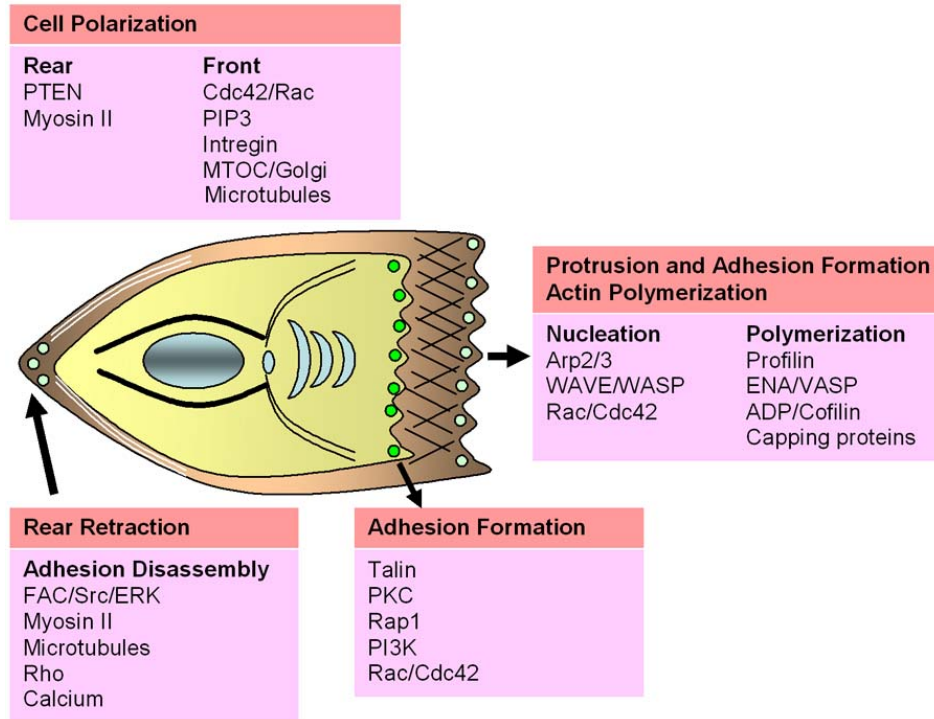


Figure 2-13: Cell migration key players.

Shown are the most important proteins involved in polarization, adhesion, protrusion formation and retraction of the tail. Adapted from [94]. Abbreviation: see list in appendix.

2.2.4.1 Rho-Family GTPase Regulation of the Cytoskeleton

The Rho-family GTPases are one of the most important key regulators of the cytoskeleton. They are small monomeric proteins. Activation occurs indirectly by receptor tyrosine kinases, which dimerize after ligand binding and autophosphorylate their cytosolic tyrosine residues. The exchange of GDP to GTP terminates their activity. GTPases are widely distributed in eukaryotic cells. Only few show tissue specific expression, such as Rab3b in neuronal and Rab17 in epithelial cells. They are localized in the cytosol or at membranes, due to interactions of their post-translational modification with lipids. [91]

All members have different functions. The Ras family regulates gene expression, whereas the Rab and Sar1/Arf families influence intracellular vesicle trafficking. The Ran family changes the nucleo-cytoplasmic transport and arranges the microtubule organization during cell cycle progression. The Rho family regulates gene expression and cytoskeletal rearrangements. Structural comparison of all families reveals a 30-50% homology and shows a specific side for the interaction with GDP and GTP. Since the exchange of GDP to GTP is extremely slow, guanine nucleotide exchange factors (GEF) are used to support this process. GTPase-activating proteins (GAP) regulate the hydrolysis of GTP.

The role of Rho, Rac and Cdc42 was identified by injection of their active forms in fibroblasts. Rho causes stress fiber formation. Rac induces lamellipodia and Cdc42 promotes filopodia. [96] Furthermore, Rho/Rac/Cdc42 are involved in cell growth, development, membrane trafficking, axon guidance and extension. **Figure 2-14** shows the downstream effectors of Rho, Rac and Cdc42 and their involvement in the cytoskeleton reorganization.

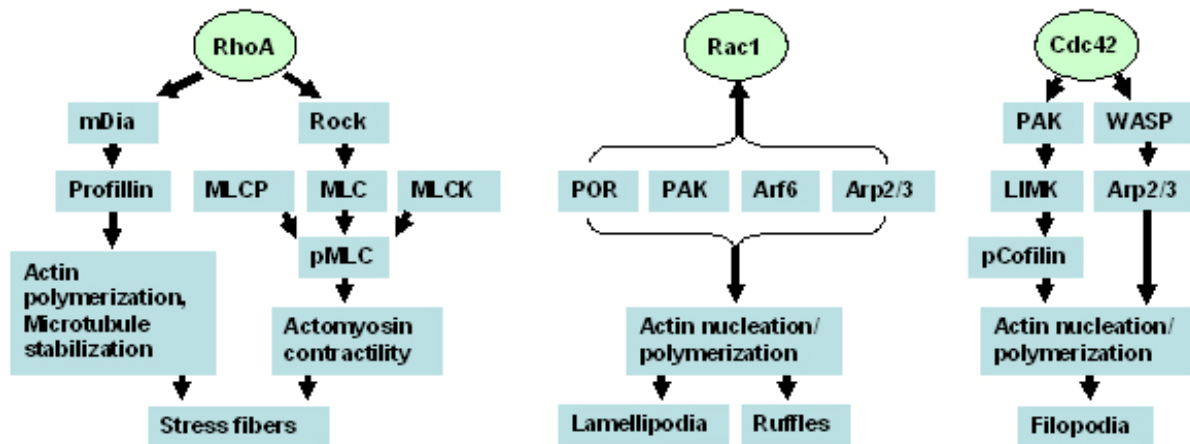


Figure 2-14: Signaling cascade of Rho, Rac and Cdc42 and their influence on the cytoskeleton. Cytoskeletal rearrangements caused by GTPases and their downstream effectors. Picture adapted from [91, 97]. Abbreviation: see appendix.

Wound closure of epithelial cells requires normal levels of Rac and Rho expression in addition to intact microtubules. Activation and inhibition of RhoA or the expression of dominant active Rac1 abolished wound closure. Furthermore, expression of Rac1wt leads to RhoA upregulation, junction disruption and wound closure defects. The inhibition of ROCK (Rho-kinase) stimulates wound closure by increasing Rac1 activity, reducing actin stress fibers and focal contacts. [98]

Cdc42 is an important key player for migration, proliferation, apoptosis and cell polarity. Its localization and connection with the cytoskeleton was explored by FRET analysis. Cdc42 promotes the growth of fine cell extensions, called filopodia. Inhibitor studies with nocodazole and cytochalasin D concluded that Cdc42 interacts with microtubules to regulate vesicle trafficking and adhesion complexes formation. [99] The loss of Cdc42 leads to defects in wound closure, establishment of polarity, migration toward a serum gradient and adhesion to fibronectin. Interestingly, Cdc42 seems to enable the G1/S transition and plays a role in cell cycle regulation. [100]

The Rho family is also involved in the activation of the MAPK pathway. Rac and Cdc42 regulate the activation of p38 MAPK and Jun NH₂-terminal kinase (JNK), whereas Ras proteins and Cdc42 control the activation of the ERK pathway (p42/p44). [91]

2.2.4.2 MAPK Pathway Targets the Cytoskeleton

The only known substrates for LT are MAPKK. They influence inflammation, cell growth, differentiation and apoptosis, but also cytoskeletal changes.

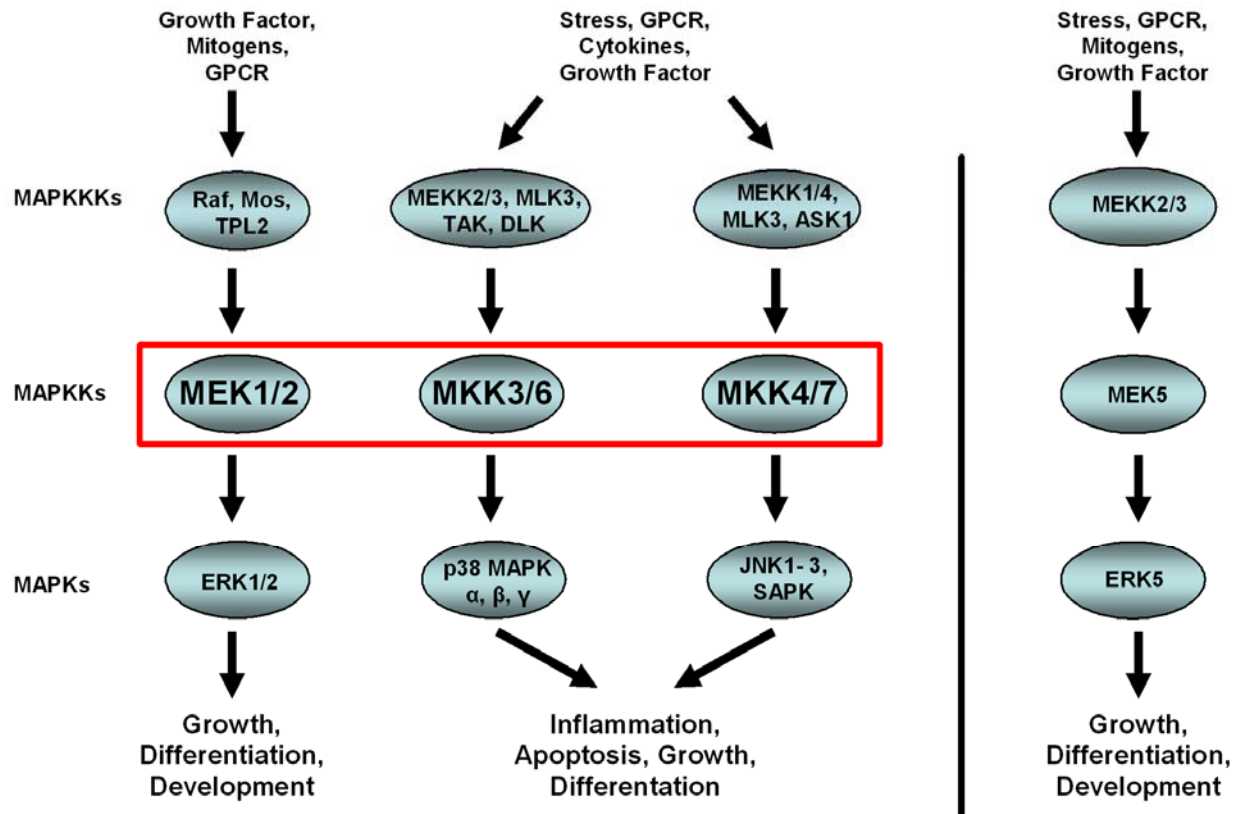


Figure 2-15: MAPK pathway.

Cleavage of the N-terminus of MAPKK by LT affects ERK, p38 and JNK signaling, whereas MEK5 is not altered. Adapted from [101]. Abbreviation: see appendix.

In general the MAPK pathway is activated by extracellular signals stimulating receptor tyrosine kinases or G-protein coupled receptors, which activate MAPKKK through the phosphorylation of threonine and/or serine. (Figure 2-15) MAPKKK induce phosphorylation of MAPKK followed by the downstream signaling to MAPK (ERK = Thr₁₈₃-Glu-Tyr₁₈₅ motif, p38 = Thr-Ala-Tyr motif and JNK = Thr-Pro-Tyr motif). MAPKs can translocate into the nucleus to induce transcription. For their activation dual phosphorylation is required, causing the exposure of threonine and tyrosine. This conformational change allows ATP to bind to the catalytic site. It was also shown, that the ERK, p38 and JNK pathway alter cell migration through rearrangements of the cytoskeleton.

In detail, the ERK pathway is initiated by growth factors stimulating Ras and Raf. (Figure 2-16) Consequently, MEK1 and 2 are activated through phosphorylation of Ser217 and Ser221. [102-106] ERK exists in two isoforms, called p44 (ERK1) and p42 (ERK2), which are both activated by threonine and tyrosine phosphorylation. Studies conducted with dominant negative MEK1 diminished motility, whereas active MEK1 promoted migration. The decrease of ERK by specific inhibitors, such as U0126 and PD98059 or by a dominant negative ERK mutation, inhibits cell migration of various cell types after growth factor stimulation. [107]

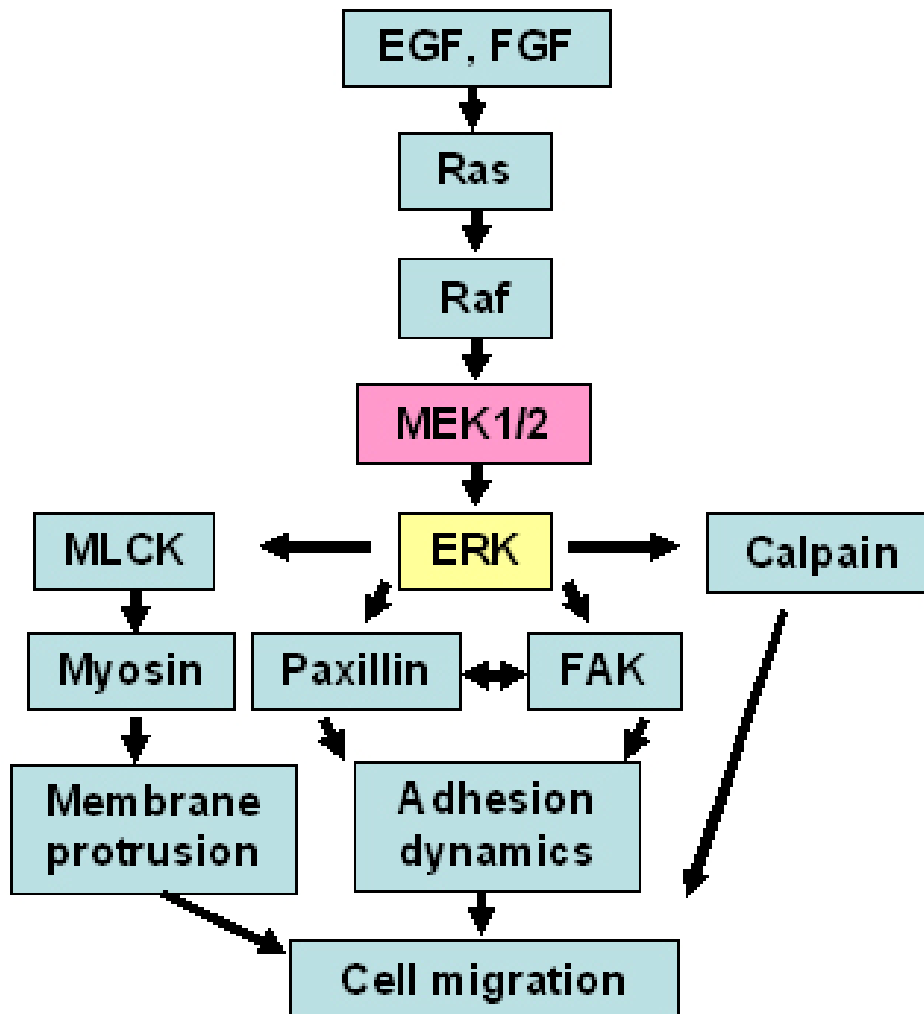


Figure 2-16: ERK signaling pathway causes motility changes.

Shown are the MEK1/2 pathway and its upstream and downstream cytoskeletal effectors. Adapted from [108]. Abbreviation: see appendix.

Some of the ERK substrates affect actin dynamics, adhesion molecules and cell motility. (Figure 2-16) The myosin light chain kinase (MLCK) induces membrane protrusion at the front of polarized cells and influences adhesion maturation. [109, 110] Calpain is phosphorylated at Ser50 by ERK. This is required for cell migration by promoting detachment in the end of the cell shown by mutation analysis. [111] FAK and paxillin are also involved in the adhesion dynamics. They control the focal contacts and connect them to cytoskeletal proteins, respectively. ERK phosphorylates FAK at a variety of tyrosine residues, but the phosphorylation at Ser 910 causes the disruption of the FAK-paxillin interaction. [112]

The proteins involved in activation of p38 and downstream cytoskeletal signaling are shown in Figure 2-17. The decrease of p38 activity by specific inhibitors or expression of a dominant negative mutant causes, in a variety of cells, defects in cell motility. [113, 114]

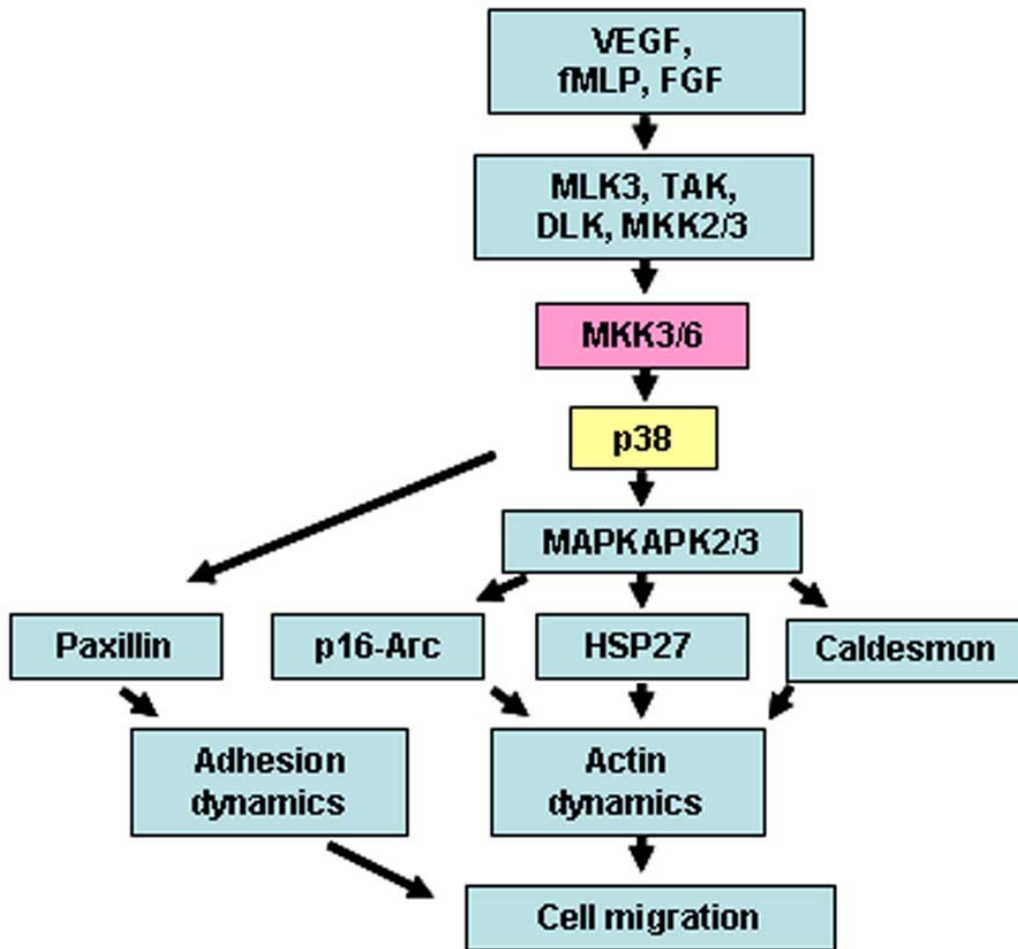


Figure 2-17: p38 signaling pathway causes motility changes.

Proteins of the MKK3/6 cascade influencing cell migration are displayed. Adapted from [108]. Abbreviation: see appendix.

p38 regulates adhesion dynamics by phosphorylating the focal adhesion protein paxillin at serine 83. [115] Caldesmon does not affect focal connections. It regulates the formation of podosomes. It also stabilizes actin filaments by inhibiting the Arp2/3 complex. When phosphorylation by p38 and cdc2 kinase occurs, these described effects are inhibited. [116]

MAPK-activating protein kinase 2/3 (MAPKAPK2/3) stimulates p16-Arc and the heat shock protein 27 (Hsp27) after being activated by p38. Phosphorylated Hsp27 controls actin polymerization, induces stress fibers and is involved in endothelial cell migration. [117-119] p16-Arc, a subunit of the Arp2/3 complex, which influences actin rearrangement, might regulate the speed of migration. [120, 121]

The JNK pathway is initiated by growth factors and influences proteins important for cell migration and also focal adhesion, such as Rac, FAK and Src. Proteins of the cytoskeleton and those involved in migration are controlled through downstream phosphorylation, especially of the threonine and tyrosine motif of JNK. [108] The importance of the JNK pathway in cell migration and cytoskeletal rearrangement was demonstrated with different approaches. (Figure 2-18) The upstream kinase MEKK1 recognizes microtubule integrity and regulates epithelial cell and fibroblast migration. This was observed in MEKK1 (-/-) mice, which are also defective in eyelid closure. [122]

Activation of JNK and expression of constitutively active MKK4 was associated with faster motility in human lung adenocarcinoma cell line A549. [123, 124] The reduction of JNK activity through inhibitors on the other hand or expression of the constitutive-negative mutant (JNK1AF) impaired this motility increase. [125, 126] JNK also needs to be activated to perform proper wound healing in fibroblasts. [125]

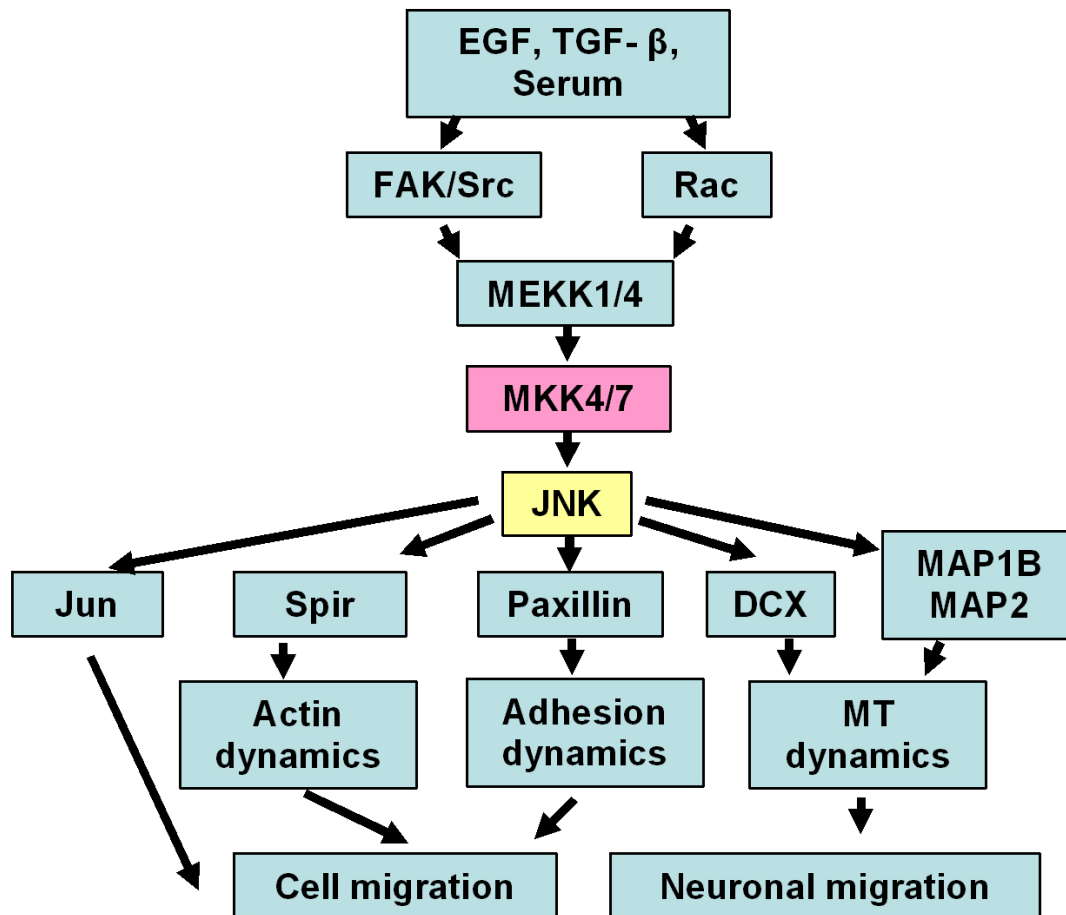


Figure 2-18: JNK signaling pathway causes motility changes.

Actin, adhesion and microtubule dynamics changed by proteins of the MKK4/7 pathway are shown. Adapted from [108]. Abbreviation: see appendix.

Figure 2-18 demonstrates JNK interacting/activating proteins and their possible influence on the cytoskeleton and migration. Jun is a component of the activator protein 1 (AP-1) transcription factor. The phosphorylation at Ser63 and Ser73 of Jun is crucial for cell migration. [125] JNK phosphorylates paxillin at Ser178. Point mutation S178A cannot be phosphorylated anymore and causes migration defect. Overexpression of S178A leads to focal adhesion and stress fiber formation in rat bladder carcinoma cells. Spir is a WASP family member which regulates actin rearrangement causing F-actin clustering. [127]

DCX is associated with neuronal migration, which is inhibited, when JNK mediated phosphorylation of Thr331 and Ser334 does not occur. This microtubule associated protein regulates stabilization of microtubules through phosphorylation. [128] Furthermore, MAP1B and MAP2 are hyperphosphorylated in JNK $-/-$ mice causing defects in microtubule assembly and binding. [129]

2.3 Lethal Toxin Induced Cell Death in Murine Cells

Interactions between LT and murine cells generally lead to cell death. The uptake of *Bacillus anthracis* spores in the lungs occurs through alveolar macrophages [130], dendritic cells [131] and epithelial cells [132]. Engulfment of the spores causes germination inside the macrophage to the vegetative form, which is released after necrosis [133-136] and/or apoptosis [137] of macrophages. Toxin accumulation and rapid bacteria multiplication lead to sepsis and shock. Understanding the death mechanisms would assist in identifying therapeutic targets.

Lethal toxin can cause death after intravenous injection in a variety of susceptible mice and rats strains, such as BALB/c and Fisher rats. (Table 2-1) Interestingly, there are also resistant macrophages which do not lyse after lethal toxin treatment. Genetic studies identified an Ltx1 region at chromosome 11 to be responsible. Kif1C, a kinesin-like motor protein, is located in this region but was excluded because resistant NOD and SJL mice carry the Kif1C allele. Further studies identified Nalp1b as the key player. There are 3 different forms of Nalp1 expressed: Nalp1a, Nalp1b and Nalp1c. Analysis of 18 mouse strains showed that almost all of them carry all three forms. However, 129S1 mice do only express Nalp1b and are susceptible to LT. Further sequencing of the Nalp1b cDNA classified five polymorphic alleles. Resistant strains carry allele 2, 3 or 4, whereas susceptible strains such as 129S1 only have allele 1. These findings suggest that the expression of allele 1 of Nalp1b is important for the susceptibility. This agrees with most of the strains except one strain. The susceptible strain (CAST/EiJ) does not carry the allele 1; instead it displays a 13 residue substitution in allele 5. [138, 139]

Nalp1 is a member of the NOD-like receptor family (NLR) and part of the inflammasome, which controls innate immunity and inflammation. [140, 141] In susceptible mouse macrophage cell lines, RAW264.7 and J774A.1, it has been shown previously that lethal toxin induces the release of IL-1 β and IL-18 through caspase-1 activation. [142] However, to this date it is unknown how the process is possibly initiated by the inflammasome (a multiprotein complex) which is known to be a caspase-1 activator. Nalp1b interacts with the ASC domain (apoptosis-associated speck-like protein containing a CARD) of pro-caspase-1 leading to oligomerization of caspase-1 and autoactivation. [143, 144] How the interaction of lethal toxin and Nalp1b occurs and if it is a proteolytic target is also unknown.

If activation of caspase-1 were solely responsible for the cytotoxicity, caspase-1 inhibitors should prevent cytolysis. Unfortunately, inhibitors (Ac-YVAD-CMK and Z-WEHD-FMK) which covalently bind to the active site of the p10/p20 tetrameric form of active caspase-1 did not reduce cell death significantly and intermediate levels of IL-1 β maturation were detected. Also, IL-1 β neutralizing antibodies could not protect macrophages against LT lysis. Furthermore, caspase activation and therefore IL-1 β production are late events occurring after 50-75 minutes followed by cell death at 85-90 minutes. The MKK cleavage takes place at 20-40 minutes. This suggests that the late cytokine response is not the reason for cell lysis. [145, 146]

Table 2-3 lists inhibitors, which prevent or inhibit the lysis of macrophages after LT treatment. ROS, mitochondria, proteasome and acidification of late endosomes are required for the cytotoxicity of lethal toxin.

Inhibitor	Effect
Oxidants: Beta-mercaptoethanol, dithiothriitol, ethyl alcohol dimethylsulfoxide	Blocks cytolysis by inhibiting oxidative burst [147]
Proteasome inhibitors: MG132, lactacystein, ALLN, epoxomycin	Inhibition of cytotoxicity [148]
Protease inhibitor: Bestatin, chloromethylketones of leucine and phenylalanine EDTA, amino acid hydroxamates, zinc metalloprotease inhibitor ZINCOV	Prevent lethal toxin induced lysis of J774A.1 cells [53] Abolishes all <i>in vitro</i> catalytic function [149]
Vacuolar ATPase pump inhibitor: Concanamycin A, bafilomycin A1, B1, C1, D	Inhibition of acidification of late endosomes, lower cytotoxicity [150]
Protein Phosphatase Calyculin (serine/threonine)	Prevents MEK1 cleavage, by enhanced phosphorylation and inhibits cell death by 78% in J774.1 cells (pretreatment) [151]
Lethal factor inhibitor: EGCG N-Oleoyldopamine Hydroxamate, (2R)-2-[(4-fluoro-3-methylphenyl)sulfonylamino]-N-hydroxy-2-(tetrahydro-2H-pyran-4-yl)acetamide quinoline-containing compounds rhodamine derivates catechol aminoglycosides mixed-type inhibitors	anti-oxidant polyphenol of green tea [152] [153] inhibits LF protease activity [154] [155] [156] [157] [158] [159-163]

Table 2-3: Inhibitors for lethal toxin induced cytotoxicity.

The proteasome controls the levels of regulatory proteins which are important in many cellular processes, such as transcription, cell cycle and apoptosis. The proteasome activity was not affected by LT treatment in macrophages after one hour. However, the inhibition of the proteasome by specific inhibitors such as MG132, ALLN and lactacystin prevented lysis of Raw 264.7 when added at the same time with LT. The MAPKK cleavage still occurred, which indicates that the downstream events are not responsible for apoptosis, instead an unknown substrate might be involved. [148] Another hypothesis suggests that toxin-induced resistant macrophages have a decreased proteasome activity. [164] Furthermore, caspase-1 activation is also controlled by the proteasome. Its activity was diminished after addition of proteasome inhibitors. [165]

Mitochondria dysfunction and membrane perturbation are critical events in induced cytolysis. Lethal toxin leads to swelling of mitochondria accompanied with mitochondrial impairment, shown by decreased mitochondrial membrane potentials and succinate dehydrogenase (SDH) activity in murine J774A.1 macrophages. Two mitochondrial proteins, called Bcl-2/adenovirus E1B 19-kDa interacting protein 3

(Bnip3) and Bnip3-like (Bnip3L; also known as Nip3-like protein X) were downregulated in LT resistant bone marrow-derived macrophages from C57BL6 mice. In toxin-induced susceptible Raw 264.7 macrophages this might be partially mediated through the inhibition of the p38 pathway. [166, 167]

The involvement of p38 in apoptosis was identified by Michael Karin's group. Reconstitution of non-cleavable MKK6 mutants in murine macrophages protected cells from apoptosis induced by lethal toxin treatment. [168] Decreased p38 activity affects NF- κ B target genes, which have association with cell death regulation, causing the activation of apoptosis.

Not all cell types undergo fast apoptosis or necrosis after LT treatment. However, cell proliferation and differentiation were inhibited in B and T lymphocytes [169-171] and in melanocytes [172]. Cell cycle arrest in G₀-G₁ phase was induced via downregulation of cyclin D1/D2 and checkpoint kinase 1 (Chk1) in U-937 cells. Interestingly, THP1 cells could overcome this cell cycle arrest by activation of PI3-K and AKT. [173]

2.3.1 Cytotoxicity Comparison Between Mouse and Human

Human cells seem to be more resistant against lethal toxin induced cytotoxicity than mouse macrophages, which undergo cell death in as early as 2 hours. Human lung epithelial cells and microvascular endothelial cells showed only a very modest increase in cell death after 18 hours. [174] Endothelial cells were treated for up to 72 hours with lethal toxin and evaluated for early and late apoptosis/necrosis. After 24 hours no indication of cell death was found, but after 48 hours a 2% increase of apoptotic cells was detected. This amount increased to 7% at 72 hours and correlated with slightly elevated PI stain, which was only increased by 5%. [80] A different study of human umbilical vein endothelial cells (HUVEC) showed 25% apoptotic nuclei after 18 hours, a 40% decrease in cell viability after 24 hours and 80% after 48 hours. Similar results were obtained by using an inhibitor of MEK1/2 (PD98059). [175]

Innate immune cells, such as human peripheral blood mononuclear cells (lymphocytes and monocytes), were resistant to lysis in the presence of LT for 15-24 hours. However, activated monocytes (IFN- γ for 48 hours) treated with LT showed a slight increase of early apoptosis. Nucleosomal fragmentation was also slightly higher after treatment. [176] Human monocytic cell lines U-937, HL-60 and THP-1 were only susceptible to LT induced cell death when differentiated into a macrophage-like state. [177]

In the human T cell line, Jurkat E6.1 lethal toxin did not decrease the cell proliferation. [178] Whereas murine CD4⁺ T cells derived from Balb/c mice showed a proliferation inhibition after 24 hours lethal toxin treatment. [179]

In addition, lethal toxin induced MAPKK cleavage was shown to inhibit tumor growth in renal cell carcinoma (RCC). Those tumor cells have a higher expression of MKK1 and ERK2. Since lethal toxin leads to a reduction of ERK2 activation by MKK1 cleavage, it inhibits tumor vasculature without affecting cell death and cell cycle progression after 72 hours. [180] Similar effects were detected in murine endothelial cells expressing a human herpes virus protein-coupled receptor (vGPCR-SVEC) causing Kaposi's sarcoma. Lethal toxin blocked cell proliferation and the release of endothelial growth factors. [181] LT causes in human endothelial cells (HUVEC) a 20% reduction in proliferation. [180] In this case, the use of LT in cancer therapeutics would be only possible, if treatments can be directed locally on the tumor without damaging normal tissue.

2.3.2 Clinical Symptoms and Treatment of Inhalational Anthrax

Inhalational anthrax symptoms are similar to those of a common flu. For example, fever, nonproductive cough and chest discomfort are early symptoms of the infection, which often leads to false diagnosis. (Table 2-4)

Symptoms	N=10
Fever, chills	10
Fatigue, malaise, lethargy	10
<u>Cough</u>	9
Nausea or vomiting	9
Dyspnea	8
Sweats, often drenching	7
<u>Chest discomfort or pleuritic pain</u>	7

Table 2-4: Symptoms of 10 Inhalational anthrax cases between October-November of 2001.

Adapted from [11]. Abbreviation: N, number of cases.

Chest radiographs illustrate a widened mediastinum, which occurs through internal bleeding and an increase of pleura fluid. [182] Furthermore, patients showed inflammation, hemorrhage, and lesions in the mediastinum, mediastinal lymph nodes, bronchi, lungs and central nervous system. [13, 183] This leads to short breath, strident cough, pulmonary edema and skin discoloration, caused by poor blood oxygenation.

As of now, only very few prevention and treatment options are available. The protective antigen-based anthrax vaccine is a series of 6 shots in 18 months followed by annual boosters. This vaccine is only available for those people being at a higher risk of exposure such as soldiers.

Antibiotics such as ampicillin, amoxicillin, chloramphenicol, ciprofloxacin, doxycycline, gatifloxacin, levofloxacin and penicillin are effective against *B. anthracis*. The Centers for Disease Control and Prevention (CDC) recommend treatment with 400-500mg ciprofloxacin and 100mg doxycycline in combination with one more antibiotics for at least 60 days. It is important to understand that antibiotics do not destroy the spores. After the antibiotic treatment is completed, a new infection may occur, if spores were able to escape the immune defense system to germinate into bacteria. Other studies showed that antibodies against protective antigen were effective in preventing death, such as ETI-2004 or AVP-21D9. [184, 185]

Most treatments are antibiotic treatments for longer periods of time. This still does not ensure protection. Only recently, a new vaccine-antitoxin combination was discovered, which has not been introduced into clinical trials. This vaccine is based on the expression of the von Willebrand A domain of the CMG-2 receptor on the surface of an insect virus (flock house virus of the family Nodaviridae) coated with protective antigen. Fisher 344 rats were completely protected when immunized 4 weeks prior to lethal toxin challenge (intravenous), and had no intoxication symptoms such as respiratory distress or hypoxia. [186]

3 AIM OF THE WORK

The goal of my work has been understanding mechanisms in the late pathogenesis of an inhalational anthrax infection. This knowledge would assist in generating drug targets to cure one of the deadliest forms of anthrax, characterized by a mortality rate of 95-99%. After inhalation of the spores, phagocytosis by alveolar macrophages and dendritic cells takes place. While migrating to the regional lymph nodes, germination occurs and the bacteria are released by cell lysis. Fast replication and toxin secretion (lethal toxin and edema toxin) influence the behavior of cells and their defense mechanism in the body, ultimately leading to septic shock-like death.

As of now, many studies aiming at elucidating inhalational anthrax effects were performed in mice or mouse cells/cell lines. However, there seems to be a significant difference between the responses of murine cells compared to human cells in susceptibility and reactions. Therefore, I am focusing mostly on human derived cells in my study.

The lung is an immediate target affected by anthrax infection. This is the place where in the beginning bacterial growth and toxin secretion occurs and from where the infection spreads. Later stages of infection are characterized by shortness of breath and respiratory distress, all contributing to ultimate body failure.

Inhalational anthrax is a fast progressing disease. Since the first symptoms are very similar to a common flu, the disease is frequently misdiagnosed. Fast detection methods and antibiotic treatments have been developed. However, they are only effective if given at early times. Therefore, it is crucial to understand cellular signaling events triggered by anthrax infection in late progression to develop powerful medical approaches for death prevention.

Currently, only two studies determined the effect of anthrax toxins on lung microvascular and epithelial cells. They identified permeability changes and a more resistant effect on lethal toxin induced cytotoxicity compared to murine cells.

My goal was it to study the effect of one of the anthrax toxins, lethal toxin, on the human respiratory epithelium. To define key mechanism, human primary lung epithelial cells were grown under normal tissue culture conditions. For more physiological significance, a fully differentiated, polarized three-dimensional airway system was established. During the process of maturation of the 3D-layer an increased formation of junctions and secretion of mucus was observed. This model epithelium responds to stimulation and was capable of rapid wound healing after injury. Consequently, we wanted to define different mechanisms/behaviors between mouse and human cells. In this regard, we determined possible viability, junction and motility alterations.

4 MATERIAL AND METHODS

4.1 Chemicals and Reagents

Ammonium persulfate	Sigma-Aldrich Co, St. Louis, MO
Aprotinin	Sigma-Aldrich Co, St. Louis, MO
Bovine serum albumin	Sigma-Aldrich Co, St. Louis, MO
Bromphenolblue	Sigma-Aldrich Co, St. Louis, MO
BSA, Fatty acid free, low endotoxin	Sigma-Aldrich Co, St. Louis, MO
Collagenase D	Roche, Basel, Switzerland
Collagene (human placenta Type VI)	Sigma-Aldrich Co, St. Louis, MO
DAPI	Sigma-Aldrich Co, St. Louis, MO
Dexamethasone	EMD Biosciences, San Diego, CA
Diethyl pyrocarbonate	Sigma-Aldrich Co, St. Louis, MO
Dimethyl sulfoxide	Sigma-Aldrich Co, St. Louis, MO
dNTP	Promega, Madison, WI
Edema factor	List Biological Laboratories, CA
Ethanol	Aaper Alcohol Co, Shelbyville, KY
Ethidiumbromide	Sigma-Aldrich Co, St. Louis, MO
Ethylenediaminetetraacetic acid	Sigma-Aldrich Co, St. Louis, MO
Fibronectin (human plasma)	Sigma-Aldrich Co, St. Louis, MO
FITC-albumin	Sigma-Aldrich Co, St. Louis, MO
Fluoromount G	Southern Biotech, Birmingham, AL
Glacial acetic acid	Fisher Scientific, Hampton, NH
Glycerol	Sigma-Aldrich Co, St. Louis, MO
Glycine	J.T. Baker, Phillipsburg, NJ
Goat serum	Gibco Invitrogen, Carlsbad, CA
Keratinocyte growth factor	Cell Sciences, Canton, MA
Leupeptin	Sigma-Aldrich Co, St. Louis, MO
Lipofectamine 2000	Invitrogen, Carlsbad, CA
Lipofectamine Plus	Invitrogen, Carlsbad, CA
Lipofectamine Reagent	Invitrogen, Carlsbad, CA
MAPKKide (o-ABZ/DNP)	List Biological Laboratories, Inc
Methanol	Fisher Scientific, Hampton, NH
MTT	Sigma-Aldrich Co, St. Louis, MO
N,N,N',N'-tetramethylethylene diamine	Sigma-Aldrich Co, St. Louis, MO
Na-Cholate	Sigma-Aldrich Co, St. Louis, MO
Nocodazole	Sigma-Aldrich Co, St. Louis, MO
Nonidet P-40	EMD Biosciences, San Diego, CA
Paraformaldehyde	Electron Microscopy Sciences, PA
Phenylmethylsulphonyl fluoride	Sigma-Aldrich Co, St. Louis, MO
Phosphatidylserine	Millipore, Billerica, MA
Polybrene/Hexadimethrine bromide	Sigma-Aldrich Co, St. Louis, MO
Poly-L lysine	Sigma-Aldrich Co, St. Louis, MO
Polyoxyethylene-sorbitan-monolaurate	Sigma-Aldrich Co, St. Louis, MO
Ponceau's S	Fisher Scientific, Hampton, NH
Propidium iodide	Sigma-Aldrich Co, St. Louis, MO
Sae Kem LE agarose	Chembrex Bio Science, ME
Saponin	Sigma-Aldrich Co, St. Louis, MO
Scintillation fluid: Filter Count	Perkin Elmer Instruments, Wellesley, MA

Sodium azide	Sigma-Aldrich Co, St. Louis, MO
Sodium chloride	Fisher Scientific, Hampton, NH
Sodium dodecyl sulfate	Sigma-Aldrich Co, St. Louis, MO
Sodium hydroxide	Sigma-Aldrich Co, St. Louis, MO
Taq-Polymerase	New England Biolabs, Ipswich, MA
TO-PRO-3 iodide (642/661)	Invitrogen, Carlsbad, CA
Trans-Blot, pure nitrocellulose	BioRadLaboratories, Hercules, CA
Tris base	EMD Biosciences, San Diego, CA
Triton X-100	Sigma-Aldrich Co, St. Louis, MO
β-mercaptoethanol	Sigma-Aldrich Co, St. Louis, MO

4.1.1 Kits

BCA™ Protein Assay Reagent A + B	Pierce, Rockford, IL
CytoTox-ONE	Promega, Madison, WI
Endofree Plasmid Maxi Kit	Qiagen, Valencia, CA
FluoReporter® Mini-biotin-XX Protein Labeling	Invitrogen, Carlsbad, CA
In Situ Cell Death Detection Kit, Fluorescein	Roche, Basel, Switzerland
QIAfilter Plasmid Maxi Kit	Qiagen, Valencia, CA
QIAprep Spin Miniprep Kit	Qiagen, Valencia, CA
QIAshredder	Qiagen, Valencia, CA
RNeasy Mini Kit	Qiagen, Valencia, CA
SuperScript™ II Reverse Transcriptase	Invitrogen, Carlsbad, CA

4.1.2 Inhibitors

Inhibitor	Inhibition of	Final Conc.	Company
Aprotinin	serin protease	10μM	Sigma-Aldrich Co
Bafilomycin A1	vacuolar H ⁺ -ATPase inhibitor	50nM	Sigma-Aldrich Co
CCCP	mitochondrial potential	100μM	Sigma-Aldrich Co
Chloroquine	lysosome	100μM	Sigma-Aldrich Co
Cytocholasin B	actin polymerization	1μg/ml	Sigma-Aldrich Co
EGCG	LF inhibitor	10μM	EMD Biosciences
Epoxomicin	proteasome	1μM	EMD Biosciences
JNKII	JNK inhibition	2.5-5μM	EMD Biosciences
Latrunculin A	actin polymerization	2μg/ml	BIOMOL
Leupeptin	serin/cysteine prot.	10μM	EMD Biosciences
MG132	proteasome/lysosome	10μM	EMD Biosciences
Nocodazole	tubulin polymerization	10nM	Sigma-Aldrich Co
PMSF	serin/cysteine prot.	1mM	Sigma-Aldrich Co
Oligomycin	mitochondrial potential	2.5μg/ml	Sigma-Aldrich Co
SB203580	p38	10μM	EMD Biosciences
SB202190	p38	10μM	EMD Biosciences
Sodium orthovanadate	tyrosine protease	100μM	Sigma-Aldrich Co
Sodiumfluoride	protease	1mM	Sigma-Aldrich Co
U0126	MEK1/2	5μM	EMD Biosciences

4.1.3 Molecular Weight Markers

100bp DNA Ladder	NEB Biolabs, Beverly, MA
Benchmark™ Pre-Stained protein ladder	Invitrogen, Carlsbad, CA
PageRuler™ Prestained protein	Fermentas, Hanover, MD

4.1.4 Radioisotopes

[³H]-Thymidine (1mCi/ml)
Trans ³⁵S Label (10mCi/ml)

MP Biomedical, Solon, OH
MP Biomedical, Solon, OH

4.1.5 Buffers

Antibody diluents	50ml 5g 15ml 1ml add 500ml	10x TBS BSA goat serum Tween-20 dH ₂ O
Blocking buffer (Western Blot)	50ml 15g 50ml 50ul add 500ml	10x TBS BSA goat serum 20% NaN ₃ dH ₂ O
Blocking buffer (IF)	5% 1% in	BSA human serum PBS
2.5M CaCl ₂	36.76g 100 ml	CaCl ₂ dH ₂ O
DEPC – H ₂ O	200ul add 100ml	DEPC ddH ₂ O
2X HBS	281mM 100mM 1.5mM	NaCl HEPES Na ₂ HPO ₄ Adjust pH to 7.12
FACS staining buffer	5% in	FCS PBS
4x Laemmli Buffer	40ml 20ml 40ml 4ml pinch	0.5M Tris-HCl, pH6.8 glycerol 10% SDS beta-mercaptoethanol bromophenolblue
Ponceau's S	0.5g 1ml 100ml	Ponceau S Acetic acid H ₂ O
RIPA buffer	150mM 50mM 0.5% 1% 0.1% in ddH ₂ O	NaCl Tris-HCl, pH7.4 Sodiumcholate NP-40 SDS

10x SDS running buffer	30 g 140 g 10 g add 1000ml	Tris base Glycine SDS ddH ₂ O
50x TAE	242g 57.1ml 100ml add 1000ml	Tris base glacial acetic acids 0.5M EDTA, pH8 ddH ₂ O
10x TBS	0.2M 1.4M in dH ₂ O	Tris Base NaCl
10x TBST	0.2M 1.4M 0.5%	Tris Base NaCl Tween-20 pH7.5 in dH ₂ O
1xTE	10mM 1mM	Tris-HCl pH7.5 EDTA in dH ₂ O, sterile filtered
10x Transfer Buffer	250mM 1.92M	Tris Base Glycine in dH ₂ O
1x Transfer Buffer	10% 20% 70%	10x transfer buffer Methanol dH ₂ O

4.1.6 Antibodies

Antibody	Dilution	Isotype	Vendor
Alexa Fluor 488	1:500	Goat	Invitrogen
Alexa Fluor 568	1:500	Rabbit	Invitrogen
Alexa Fluor 594	1:500	Donkey	Invitrogen
Cdc42 Hs (P1)	1:1000	Rabbit	Santa Cruz
Cofilin	1:250	Rabbit	Cytoskeleton
Cofilin (alpha)	1:1000	Mouse	Jim Bamberg
Cortactin (p80/85 clone 4F11)	1:1000	Mouse	Millipore
Cyclin B1 (H-433)	1:2000	Rabbit	Santa Cruz
Cyclin D1 (Ab2)	1:1000	Mouse	EMD Biosciences
DMIA alpha –Tubulin	1:750	Mouse	Sigma
Donkey anti rabbit HRP	1:10000	Donkey	Promega
Donkey anti goat HRP	1:5000	Donkey	Santa Cruz
E-Cadherin	1:1000	Mouse	BD Transduction Labs
E-Cadherin	1:1000	Rabbit	Invitrogen
GDI Ab Rab	1:5000	Rabbit	Selfmade
GEFH1	1:1000	Rabbit	Gary Bokoch
Gelsolin (Clone GS-2C4)	1:1000	Mouse	Sigma

GFP serum A-6455 lot:71C1-2	1:5000	Rabbit	Invitrogen
GM130	1:1000	Mouse	BD Transduction Labs
Goat anti mouse HRP	1:10000	Goat	Southern Biotech
Goat anti rabbit HRP	1:10000	Goat	Southern Biotech
HA – high Affinity	1:1000	Rat	Roche
HA-probe (Y-11)	1:1000	Rabbit	Santa Cruz
His-Probe (H-15)	1:1000	Rabbit	Santa Cruz
6-His	1:1000	Mouse	BAbCO
I κ B- α (C-21)	1:1000	Rabbit	Santa Cruz
LMP2	1:4000	Rabbit	Biomol
LMP7	1:4000	Rabbit	Biomol
MEK-1 (C-18)	1:1000	Rabbit	Santa Cruz
MEK-1 (N-term)	1:1000	Rabbit	Millipore
MEK-2	1:2500	Mouse	BD Transduction Labs
MEK-2 (C-16)	1:1000	Rabbit	Santa Cruz
MEK-3 (C-19)	1:1000	Rabbit	Santa Cruz
MEK4 (C-20)	1:1000	Rabbit	Santa Cruz
MEK4 (K-18)	1:1000	Rabbit	Santa Cruz
MKK6	1:1000	Rabbit	Biologend
MEK7 (C19)	1:1000	Goat	Santa Cruz
MEK7 (ab18565)	1:1000	Rabbit	Abcam
MUC5AC (Clone 45M1)	1:1000	Mouse	Neomarker
p38 MAPK	1:1000	Mouse	Cell Signaling Tech.
p44/42 MAP kinase	1:2000	Rabbit	Cell Signaling Tech.
P53 (sc-6243)	1:1000	Rabbit	Santa Cruz
PARP (H-250)	1:1000	Rabbit	Santa Cruz
Paxillin	1:10000	Mouse	BD transduction lab
Peroxidase Goat anti mouse Ab	1:5000	Goat	EMD Biosciences
phospho FAK [pY ³⁹⁷]	1:1000	Rabbit	Biosource
phospho p38 (Thr180/Thr182)	1:1000	Mouse	Cell Signaling Tech.
phospho p44/42	1:1000	Rabbit	Cell Signaling Tech.
phospho Src	1:1000	Rabbit	Cell Signaling Tech.
phospho cofilin #4317	1:400	Rabbit	Jim Bamberg
phospho paxillin [pY ¹¹⁸]	1:600	Rabbit	Biosource
Phosphotyrosine	1:40	Mouse	Millipore
pSAPK/JNK (Thr183/Thr185)	1:1000	Rabbit	Cell Signaling Tech.
Rac1 (#R56220, lot3)	1:1000	Mouse	BD Transduction Labs
RhoA (26C4)	1:1000	Mouse	Santa Cruz
Rhodamine phalloidin	1:200		Invitrogen
Rock 1 (H85)	1:1000	Rabbit	Santa Cruz
SAPK/JNK (56G8)	1:1000	Rabbit	Cell Signaling Tech.
Streptavidin HRP conjugated	1:10000		Invitrogen
TIAM-1 (C-16)	1:2000	Rabbit	Santa Cruz
Tubulin, Acetylated #T6793	1:1000	Mouse	Sigma
Tubulin-Alpha (B512)	1:1000	Mouse	Sigma
Vinculin (alpha)	1:1000	Mouse	Sigma
ZO-1	1:1000	Mouse	Invitrogen
ZO-1	1:1000	Rabbit	Invitrogen

Table 4-1: Antibody List.

Used antibodies with concentration, isotype and where it was purchased.

4.1.7 Primers

Name	Sequence (5'→ 3')	Length	Annealing Temperature
β-actin for β-actin rev	TGACGGGGTCACCCACACTGTGCCCA CTAGAAGCATTGCGGTGGACGATGG	661bp	60°C 18 cycles
ATR for ATR rev	CCAGGAGGAGACACTTACATG TGAGTGGATGATGCCTTGC	302bp	50°C
BD-1 for BD-1 rev	CTCTGTCAGCTCAGCCTC CTTGCAGCACTTGGCCTTCCC	272bp	66°C
BD-2 for BD-2 rev	CCAGCCATCAGCCATGAGGGT GGAGCCCTTTCTGAATCCGCA	254bp	66°C
Calveolin-1 for Calveolin-1 rev	TCAACCGCGACCCTAAACACC TGAAATAGCTCAGAAGAGACAT	562bp	60°C
CMG2 for CMG2 rev	CCTTTGATCTCTACTTCGTCC GCTGTGACAATTAATGATCCT	810bp	50°C
MUC5AC for MUC5AC rev	TCCGGCCTCATCTTCTCC ACTTGGGCACTGGTGCTG	662bp	55°C
MEK2 for MEK2 rev	CGTACCTCCGAGAGAAGCAC GAAGGTGTGGTTTGTGAGCA	560bp	60°C
MKK3 for MKK3 rev	TTGGACAGGTCAGCAGACAG TCCAGAGCACTCACCTCCTT	539bp	53°C
RhoA for RhoA rev	GCCATCCGGAAGAACTG TTCCCACGTCTAGCTTGC	548bp	60°C
RhoB for RhoB rev	CATCCGCAAGAAGCTGG TCATAGCACCTTGCAGCAG	583bp	60°C
RhoC for RhoC rev	ATGGCTGCAATCCGAAAG TCAGAGAATGGGACAGCC	583bp	60°C
SP-A for SP-A rev	GAGAGATGGTATCAAAGGAG GGTACCAGTTGGTGTAGTT	499bp	58°C
SP-B for SP-B rev	TTCTGGTGCCAAAGCCTGGA CAGGCCTGGTGCATTGCC	836bp	58°C

Table 4-2: Primer list.

4.2 Technical Equipment

1024 confocal microscope	Bio Rad, Hercules, CA
5810R Eppendorf	Brinkman Instruments Inc., Westbury, NY
AB104 Scale	Mettler Toledo, Switzerland
AccuBlock Digital Dry Bath	Labnet International Inc, Edison, NJ
ACCUMET AB15 pH meter	Fisher Scientific, Hampton, NH
Alphaimager 2200	Alpha Innotech, San Leandro, CA

Autoclave Amsco Scientific Series	STERIS Corporation, Mentor, Ohio
AXIOSKOP Microscope	Zeiss, Goettingen, Germany
Beckman GS-6KR	Beckman Coulter, Fullerton, CA
Beckman J2-HC	Beckman Coulter, Fullerton, CA
Biological Safety Cabinets	NUAIRE, Plymouth, MN
BioRad Power Pac 1000	Bio Rad, Hercules, CA
Bio-Rad (Zeiss) MRC1024 LSCM	Bio Rad, Hercules, CA
Eppendorf Centrifuge 5810R	Eppendorf AG, Hamburg, Germany
EVOM	World Precision Instruments, Sarasota, FL
FACSCalibur	BD Biosciences, San Jose, CA
Fisher Stirring Hotplate	Fisher Scientific, Hampton, NH
Fisher Vortex Genie	Fisher Scientific, Hampton, NH
Incubator, NAPCO CO ₂	Fisher Scientific, Hampton, NH
IsoTemp215 waterbath	Fisher Scientific, Hampton, NH
Leica EM FC6 low temp attachment	Leica, Wetzlar, Germany
Leica EM KMR2 Glass Knife maker	Leica, Wetzlar, Germany
Leica EM UC62b Ultramicrotome	Leica, Wetzlar, Germany
LS55 Chemiluminescence Photometer	Perkin Elmer Instruments, Wellesley, MA
Microfuge 22R Centrifuge	Beckman Coulter, Fullerton, CA
Microplate Luminometer LB 96 V	EG + G Berthold, Bad Wildbach, Germany
NanoDrop® ND-1000 Spectrophotometer	NanoDrop Technologies, Wilmington, DE
Nikon Eclipse TE2000-U	Nikon, Melville, NY
Olympus IX70 Microscope	Olympus, Center Valley, PA
Optima Ultracentrifuge	Beckman Coulter, Fullerton, CA
PB3002 Scale	Mettler Toledo, Switzerland
PCR Express	ThermoHybaid, Heidelberg, Germany
Philips CM100 Electronmicroscope	Philips, New York, NY
Power Pac 200	Bio Rad, Hercules, CA
Protein Bio Rad Mini Protein II Cell	Amersham Bioscience, Uppsala, Sweden
PS 500 XT DC Power Supply	Hoefer Scientific Instruments, CA
Reichert Ultracut E Ultramicrotome	Reichert, Depew, NY
Rocker Platform	Bellco Glass, INC Vineland, NJ
SRX-101A Medical film processor	Konica Minolta, Wayne, NJ
Steri-Cult200 Incubator	Thermo Forma Scientific, Waltham, MA
STX2 Electrode	World Precision Instruments, Sarasota, FL
UV/Visible Spectrometer Ultraspec 3000	Pharmacia Biotech, Cambridge, UK
VERSAmax Microplatereader	Molecular Devices, Sunnyvale, CA
Vortex Genie 2	Fisher Scientific, Hampton, NH

4.2.1 Computer and Internet Programs

BioRad LaserSharp 2000	Bio Rad, Hercules, CA
BD CellQuest	BD Biosciences, San Rose, CA
EndNote	EndNote, Carlsbad, CA
Flow Jo	Tree Star Inc, Ashland, OR
Imaris5	Bitplane Inc., Saint Paul, MN
ImageJ	NIH, Bethesda, MD
Metamorph7	Molecular Devices Corp., Downingtown, PA
Spectra Alias	Deltasoft/Biometallics, Princeton, NJ
pDRAW32	AcaClone software
Prism 5.0	Cadmus Professional Communication
VectorNTI	Invitrogen, Carlsbad, CA

<http://elm.eu.org/>
http://frodo.wi.mit.edu/cgi-bin/primer3/primer3_www.cgi
<http://prowl.rockefeller.edu/prowl/peptidemap.html>
<http://smart.embl-heidelberg.de/>
<http://www.basic.northwestern.edu/biotools/oligocalc.html>
<http://www.firstmarket.com/cutter/cut2.html>
<http://www.idtDNA.com>
<http://www.ncbi.nlm.nih.gov/>
<http://www.ncbi.nlm.nih.gov/BLAST/Blast.cgi>
<http://www.umass.edu/microbio/rasmol/>

4.3 Cell Culture

Normal human bronchial epithelial cells (NHBE) were obtained from Lonza (Walkersville, MD) and cultured in small airway basal media (SABM) supplemented with 30µg/ml bovine pituitary extract, 0.5µg/ml hydrocortisone, 0.5ng/ml human recombinant epidermal growth factor, 0.5µg/ml epinephrine, 10µg/ml transferrin, 5µg/ml insulin, 0.1ng/ml retinoic acid, 6.5ng/ml triiodothyronine, 50µg/ml gentamicin, 50ng/ml amphotericin-B and 0.5mg/ml bovine serum albumin-fatty acid free (SingleQuots) at 37°C in a 5% CO₂ incubator.

Cell Culture and Splitting: The Reagent Pack (Lonza) provided the solutions required for subculturing NHBE. It contained HEPES buffered saline solution (HEPES-BSS), Trypsin/EDTA, and trypsin neutralizing solution (TNS). HEPES-BSS neutralized the complex proteins in growth medium that may inactivate trypsin during trypsinization. Trypsin/EDTA removes cells from culture vessel surfaces and TNS neutralized this reaction. The cells were counted with a Neubauer haemocytometer and plated at 50-60% confluency.

Seeding for Experiments: Cells of passage 4-6 were grown in supplemented SABM medium for 24-48 hours. The LT stimulations took place after a three hour starvation in media without supplements (SABM or DMEM/BEGM) and were treated mostly with 1µg/ml PA and 1µg/ml LF for 48 hours.

Freezing and Thawing: Cells were cryopreserved to avoid loss by contamination, to minimize genetic changes and to avoid aging. After centrifugation (950rpm, 3min, RT) cells were resuspended in the freezing medium, containing 80% SABM, 10% DMSO and 10% FBS at a concentration of 8-9x10⁵ cells/ml. The cell suspension was transferred to cryovials and placed in a Nalgene freezing container at -80°C providing 1°C/min cooling rate. After 24 hours the cryovials were transferred to liquid nitrogen (-196°C) for long-term storage. The thawing process was done very quickly. The vial was placed in a 37°C water bath for few minutes, complete media was added, cells were centrifuged and reseeded in fresh SABM media with supplements. Afterward the cells were put into a 37°C incubator with 5% CO₂ and 80% humidity until assay was performed.

4.3.1 Polarized Airway System

The air-liquid interface system (ALI) reflects an *in vivo* situation and need to be obtained in order to generate a mucociliary epithelium, since culturing techniques with immersed feeding could not generate this type of airway. [187, 188] Several key factors play an important role on proliferation, differentiation and secretion of mucus in the polarized airway system. Coating of membrane/tissue culture surfaces with collagen or fibronectin enhances the attachment and proliferation of bronchial cells.

The presence of transforming growth factor- β (TGF- β) in serum, which inhibits proliferation of airway cells, led to the use of serum free media. [189] Therefore, culturing the cells in a mixture of hormones and growth factors was developed, containing insulin, transferrin, epidermal growth factor (EGF), hydrocortisone and bovine pituitary extract (BPE) to stimulate the cell growth. Thyroxine hormone (T_3) inhibits mucin synthesis. Vitamin A plays an important role in maintaining the homeostasis of the epithelium, regulating mucus cell differentiation. [190] Another key regulator is calcium, which is not only important for junction formation, but also required for mucus cell function. [191]

For the differentiated lung epithelial model (3D) cells were detached with trypsin and seeded onto inserts with semi-permeable support membranes (Costar Transwell-clear culture insert, polyester, 0.4 μ m pore, Corning Costar) coated with human placenta collagen type VI (15 μ g/cm², Sigma). The differentiation media contained bronchial epithelial basal medium (50% BEBM, 50% DMEM with 4.5g/L D-glucose) supplemented with 200 μ g/ml bovine pituitary extract, 0.5 μ g/ml hydrocortisone, 0.5ng/ml human recombinant epidermal growth factor, 0.5 μ g/ml epinephrine, 10 μ g/ml transferrin, 5 μ g/ml insulin, 1.5 μ g/ml bovine serum albumin fraction V, 6.5ng/ml triiodothyronine, 50 μ g/ml Gentamicin, 50ng/ml Amphotericin-B and 50nM retinoic acid, prepared freshly to induce differentiation. After 2 days in immersed culture conditions, cells were switched to an air-liquid interface for 3-4 weeks. (Figure 4-1) Daily media changes were required.

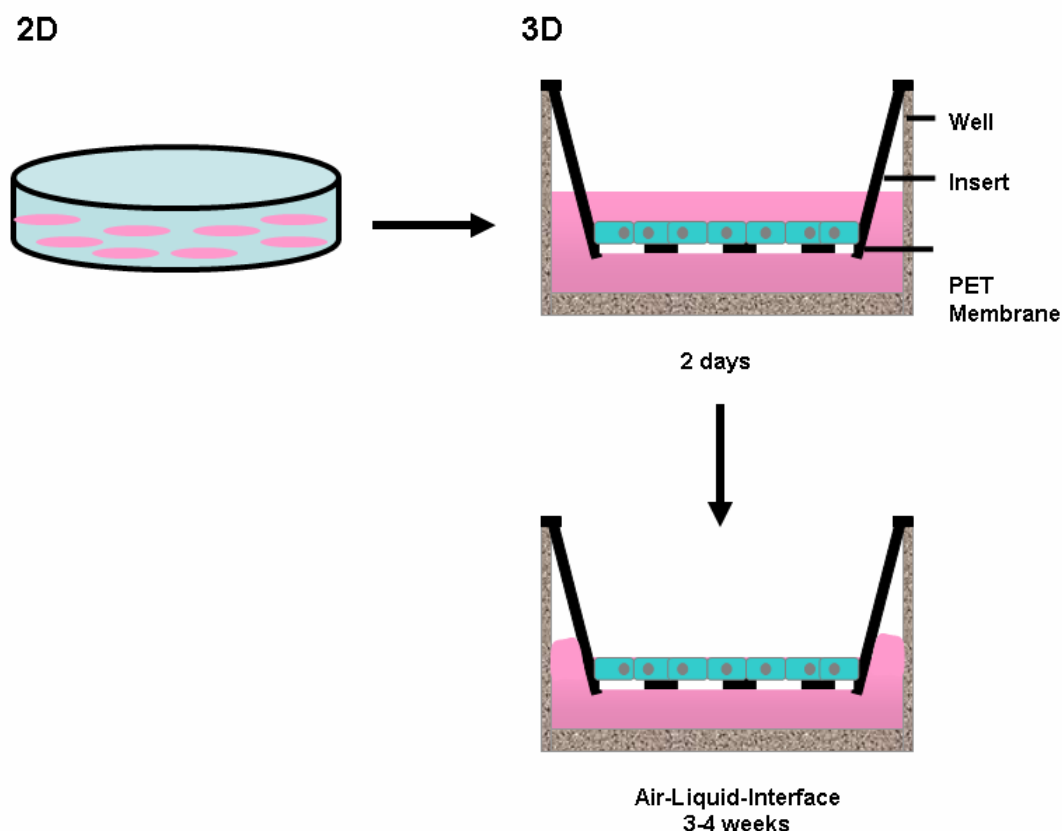


Figure 4-1: Differentiated airway system.

Normal tissue culture plated cells (2D) were trypsinized and plated on an insert (3D) with a porous membrane. After two days in culture the upper liquid phase was removed and the differentiation of an air-liquid interface took place in 3-4 weeks. Abbreviation: 2D, 2 dimensional; 3D, 3 dimensional; PET, polyester.

4.3.2 Culturing of Murine Macrophages

For some cytotoxicity and MAPKK cleavage assays, we used a lethal toxin susceptible murine macrophage cell line Raw 264.7. This leukemic monocytic macrophage cell line was derived from the mouse strain BALB/c. The cells were fed with DMEM high glucose media containing 10% FBS and 1% HEPES and were subcultured by gentle scraping using a cell lifter. The cells were grown to 100% confluency at 37°C and 5% carbon dioxide. We plated 4×10^4 cells in a 96-well plate for MTT assays and 1×10^6 cells in a 6-well plate for protein lysates.

4.4 Gene Expression

RNA Isolation: Ribonucleic acid (RNA) acts as messenger between DNA and proteins. Upon the transcription from DNA to RNA by an enzyme called RNA polymerase, the RNA leaves the nucleus and moves to the ribosomes. That is where the translation to proteins occurs. Isolation of RNA is one of the steps to look at gene expression, next to generating cDNA and amplifying the gene of interest.

After lysis of cells with β -mercaptoethanol containing RLT buffer (supplied in the kit), the solution was applied to the QIAshredder (Qiagen) which reduces viscosity caused by cellular components and cell debris. Ethanol was added to provide ideal binding conditions. The lysates were loaded onto the columns of the RNeasy Mini Kit, washed with wash buffer and eluted in 30-50 μ l water.

Quantification of RNA and DNA Concentrations: RNA and DNA concentration were determined in a Nonodrop spectrophotometer by measuring the absorbance. The concentration was calculated with following formula.

$$\text{DNA concentration } (\mu\text{g}/\mu\text{l}) = \frac{A_{260} * 50 * \text{dilution factor}}{1000}$$

$$\text{RNA concentration } (\mu\text{g}/\mu\text{l}) = \frac{A_{260} * 30 * \text{dilution factor}}{1000}$$

cDNA Synthesis: Complementary DNA (cDNA) was synthesized from RNA by using SuperScript™ II Reverse Transcriptase (Invitrogen). 2 μ g of total RNA were mixed with 1 μ l Oligo(dT)12-18 primers (500 μ g/ml) and 1 μ l dNTPs (10mM each) with water in a total volume of 12 μ l and heated to 65°C for 5 minutes. 4 μ l 5x first-strand buffer and 2 μ l 0.1M DTT were added and incubated at 42°C for 2 minutes. Afterwards 1 μ l SuperScript™ II RT (200units) was used to start the cDNA synthesis at 42°C for 50 minutes and inactivated by heating at 70°C for 15 minutes. 1 μ l RNaseH (2units/ μ l) was added for 20 minutes at 37°C to catalyze the cleavage of RNA.

4.4.1 Polymerase Chain Reaction (PCR)

Polymerase chain reaction (PCR) is an *in vitro* technique for enzymatic replication of DNA fragments. Primers determine the DNA fragment that is been amplified and can be up to 10kb in length. The process was carried out by a thermal cycler. The double stranded DNA was separated at 95°C, followed by an annealing temperature specific for the primers binding. At the elongation temperature from 72°C the DNA polymerase synthesized a new DNA strand. This process was repeated for up to 35 cycles to generate enough DNA to visualize on an agarose gel.

The following reaction mix was used in all PCRs, whereas the annealing temperatures depended on the primers: (Table 4-2)

Reaction Mix:

10X	PCR Buffer [200 mM Tris-HCl (pH 8.4), 500 mM KCl]	5µl
50mM	MgCl ₂	1.5µl
10mM	dNTP Mix	1µl
10µM	Forward primer	1µl
10µM	Reverse primer	1µl
5U/µl	<i>Taq</i> DNA polymerase	0.4µl
	cDNA from first-strand reaction	2µl
	autoclaved, distilled water	<u>38.1µl</u>
		50ul

Program:

	94°C	-	2min	
	94°C	-	1min	
Annealing Temperature	°C	-	1min	35x cycles
	<u>72°C</u>	-	1min	
	72°C	-	5min	
	4°C	-	hold	

Agarose Gel Electrophoresis: Agarose gel electrophoresis is a method to separate RNA and DNA by size. The negatively charged nucleic acids are moving towards the cathode. The estimation of the size was determined by running a DNA Ladder with known fragment sizes, where smaller fragments migrate faster and vice versa. This method was used to assess the quality of RNA and visualize the PCR products. 1µg of non-degraded RNA showed on a 1% gel the 28S, 18S and 5S ribosomal subunits. When a smear with no defined bands occurred, the RNA was degraded and not used.

5-10µl PCR product were mixed with 0.5-1µl 10x DNA loading dye to apply it on a 1% agarose gel containing ethidium bromide made in 1x TAE. The separation was performed at 100 Volt for approximately 30-60 minutes. Ethidium bromide intercalates in the DNA, fluoresces under UV light and allowed visualization of the PCR products with an Alphaimager 2200.

4.5 Immunoblot

The immunoblot (western blot) is a method to detect proteins. SDS-PAGE gel electrophoresis is used to separate denatured proteins by mass. After transferring the proteins on a membrane (nitrocellulose), detection is possible by incubating the membrane with a specific antibody. A luminescence reporter enzyme (horseradish peroxidase) bound on the secondary antibody allows visualizing the protein band on a photographic film.

Protein Isolation: A detergent-containing lysis buffer (RIPA) with several protease inhibitors (see below) was used to break the lipid barrier surrounding cells by solubilizing proteins and disrupting lipid:lipid, protein:protein and lipid:protein interactions. Before adding the lysis buffer, cells were washed once with 1x PBS. To increase the yield of total protein, the cells in RIPA lysis buffer were incubated at -80°C for at least 30 minutes. Cells were scraped off the tissue culture plate, transferred in a microcentrifuge tube, vortexed and incubated for 15 minutes on ice

to ensure the solubilization of transmembrane proteins. The cell debris was separated from the lysates by centrifuging at 14000rpm for 15 minutes at 4°C and the supernatant was transferred in a new centrifuge tube. Storage of the samples at -80°C minimized protein degradation until the assay was performed.

<i>Protease inhibitor:</i>	10µM Aprotinin	serine protease
	10µM Leupeptin	serine and cysteine protease
	1mM PMSF	serine protease
	100µM Sodium orthovanadate	tyrosine protease

Protein Quantification Assay: The BCA (bicinchoninic acid) protein assay is a method for colorimetric detection and quantification of total amounts of proteins. In the first step, proteins reduce Cu^{2+} to Cu^{1+} in an alkaline solution. Afterwards the BCA forms a complex with the cupric ion, which is blue/violet and absorbs light at 562nm. The absorption can be detected by using a spectra microplate reader with DeltaSoft3 analysis software. The protein concentration of each sample was determined from standard curve of absorbance versus micrograms of protein.

SDS-PAGE Electrophoresis: Polyacrylamide gel electrophoresis (PAGE) was used to separate charged proteins according to physical properties as they are forced through a gel by an electric current. Sodium dodecyl sulfate (SDS) is an anionic detergent that dissolves hydrophobic molecules and covers the protein with many negative charges. Laemmli buffer was added to the lysates. It contains β -mercaptoethanol that linearizes proteins by preventing the reformation of disulfide bonds.

After assembling the gel chamber, the running gel followed by the stacking gel was cast. The percentage of the running gel was between 6 -15% acrylamide, depending on the size of the protein. Higher molecular weight proteins were better separated in lower percentage gels and vice versa.

Running Gel	Percent Acrylamide Gel			
	6%	10%	12%	15%
1.5M TRIS•HCl pH 8.8	5ml	5ml	5ml	5ml
30% Acrylamide/ 0.8% Bisacrylamide	3ml	5ml	6ml	7.5ml
10% SDS	150µl	150µl	150µl	150µl
10% APS	150µl	150µl	150µl	150µl
TEMED	20µl	20µl	20µl	20µl
in H ₂ O	6.3ml	4.3ml	3.3ml	1.8ml

Stacking Gel	3% Acrylamide Gel
	0.5M TRIS•HCl pH 6.8
30% Acrylamide / 0.8% Bisacrylamide	500µl
10% SDS	50µl
10% APS	50µl
TEMED	10µl
in H ₂ O	3.2ml

Protein Transfer: In order to make the proteins accessible to antibody detection, the SDS-PAGE gel was transferred onto a membrane made of nitrocellulose by applying a current (1hr, 0.3A).

Blocking: Blocking of non-specific antibody binding was achieved by placing the membrane in a blocking solution containing bovine serum albumin (BSA), goat serum and sometimes 3% non-fat dry milk for one hour at room temperature. A wash of 5 minutes with TBST followed.

Protein Detection: During the detection process, the membrane was incubated with an antibody for the protein of interest (primary antibody) for 1-3 hours at room temperature or overnight at 4°C. The secondary antibody, detecting the Fc region of the primary antibody, was linked to a reporter enzyme (HRP), which drives a colorimetric or photometric signal.

Protein Analysis: The horseradish peroxidase (HRP)-linked secondary antibody was used in conjunction with an enhanced chemiluminescent agent (ECL). The reaction product generates luminescence in proportion to the amount of protein, which was detected by a photographic film. The amount of ECL and the exposure time depended on the amount of detected protein, usually 1:1 - 1:20 dilutions of the ECL to water and times between 5 seconds and 20 minutes were used.

Membrane Stripping: To gently break the antibody-antigen interaction, stripping buffer (Western Re-Probe from G-Biosciences) was used. The nitrocellulose membrane was washed once for 10 minutes with water, incubated 30 minutes with stripping buffer at room temperature on a shaker and washed 3 times with TBST for 10 minutes. After blocking a different primary antibody can be used for an additional signal on the same membrane.

4.6 Immunocytochemistry and Microscopy

Immunocytochemistry is a powerful method to detect proteins/antigens with fluorescent dyes and visualize their location in the cell with a fluorescence microscope. Immunostaining was performed on cells grown on collagen coated glass coverslips or in inserts. Fixation with 4% paraformaldehyde, methanol or methanol/acetone and permeabilization in 0.5% Triton X-100 in PBS took place for 10 minutes at room temperature. After blocking in 5% BSA and 1% heat-inactivated human serum for one hour, primary antibodies diluted in 2% BSA were used to detect the proteins of interest. The secondary antibody was conjugated with a fluorescence dye, such as FITC, alexa-488 or -568. The nucleus was stained for 10 minutes with 1µg/ml DAPI in PBS and mounted with Fluoromount-G (Southern Biotech) on glass slides. After drying the samples overnight at room temperature, they were examined with a fluorescent microscope. The pictures were analyzed with either ImageJ or Metamorph.

Confocal Microscopy: Confocal microscopes obtain extremely high-quality images with a maximum resolution. Three-dimensional information of cells grown on inserts can be generated. Also, colocalization of signals from different fluorochromes can be reliably studied. The laser scanning confocal microscope 1024 from BioRad has a krypton / argon mixed gas laser that excites at 488nm, 568nm and 647nm. All cells were fixed, mounted and the images were taken with 10x to 100x objective lenses. The analysis was performed with ImageJ or Metamorph.

Live cell Imaging: Live cell imaging had the advantage of capturing processes in real time. A Nikon Eclipse TE2000-U was used to generate movies of LT, infected or

inhibitor treated cells. The cells were plated on collagen coated glass cover slips, grown for two days, starved with SABM media for 3 hours and treated for 24 hours prior to imaging. DIC pictures were taken every thirty seconds or one minute for thirty minutes up to two hours with a 20x objective lens. Metamorph or ImageJ were used to analyze and convert the pictures.

Transmission Electron Microscopy: Transmission electron microscopy (TEM) is an imaging technique whereby a beam of electrons is focused onto a specimen causing an enlarged version to appear on a photographic film. The sample preparation was performed by the microscope core facility at TSRI. 3D differentiated cells were fixed for 60 minutes on ice in 2.5% glutaraldehyde in 0.1M sodium cacodylate buffer (pH7.3) and washed in 0.1M cacodylate buffer 3 times. After treatment with 1% osmium tetroxide in 0.1M cacodylate buffer for 1 hour at room temperature and washing in 0.1M sodium cacodylate buffer, each sample was incubated in 0.5% tannic acid in 0.05M cacodylate for 30 minutes. They were rinsed in 1% Na₂SO₄ in 0.1M cacodylate for 10 minutes and then washed again with 0.1M cacodylate buffer. The cells were dehydrated in graded ethanol 50%, 70%, 90% and 100%. The filter was removed from the inserts, cleared with two changes of propylene oxide for 15 minutes and embedded in Epon/Araldite resin. After polymerization at 60°C for 24 hours, the resin disc of cells was placed on a cleaned glass slide. Using a scalpel blade the specimen was cut into strips and placed in the embedding molds. Thin sections were sliced using a diamond knife and mounted on copper slot grids. They were stained with uranyl acetate and lead citrate and examined on a Philips CM-100 electron microscope. Images were taken photographically using a Kodak film.

4.7 Flow Cytometry

Flow cytometry analysis physical and chemical characteristics of cells in suspension when they pass by a laser beam. It has many applications, such as the quantification of DNA, detection of proteins on the cell surface or in the cytoplasm and sorting a specific cell population.

4.7.1 Determine Cell Cycle Content by Propidium Iodide (PI) Stain

Propidium iodide is a fluorescent dye that intercalates in the DNA and excites at 488nm. PI does not penetrate the cell membrane. Therefore, it was required to trypsinize the cells, fix them overnight with 70% ethanol at 4°C and permeabilize them with 0.25% Triton X-100 for 15 minutes. The cells were washed in PBS twice and resuspended in 25µg/ml PI (Sigma) containing 0.1mg/ml RNase A for 15 minutes at 37°C to remove the double-stranded RNA, since this would be also stained by PI. Nine times more PBS was added and the DNA amount was measured in the FACScalibur. The intensity of the PI signal is directly proportional to DNA content. Cells in G1 phase have single DNA content, whereas cells in G2/M state have a double DNA content. The area between these peaks described cells within S-phase.

4.7.2 Measurement of Mitochondrial Potential

The mitochondrial potential was measured with a fluorometric method using a cationic mitochondrial dye (tetramethyl rhodamine methyl ester - TMRM). [192] Hyperpolarized cells shifts to the right compared with healthy cells, whereas in hypopolarized cells the peak shifts to the left. NHBE cells were treated for 48 hours

with lethal toxin or biotinylated-histidine-tagged lethal toxin (LFhisbio), trypsinized and stained for 15 minutes with 50nM TMRM at 37°C. A membrane depolarization inhibitor CCCP (carbonyl cyanide 3-chlorophenylhydrazone, 100mM) was used as hypopolarization control, whereas incubation with oligomycin (2.5mg/ml) led to hyperpolarization. The cells were counted in a FACScan (FSC/SSC, linear scale, TMRM, log FL2) and analyzed by Flow Jo.

4.8 Lethal Factor Activity Assay

4.8.1 MAPKKide Cleavage Assay

The MAPKKide assay is a FRET (fluorescence resonance energy transfer) based assay to determine the cleavage activity of lethal factor. List Biological Inc developed a fluorescent substrate similar to MAPKK-2, which contains on the N-terminus a fluorophore, o-aminobenzoyl (Abz), that is quenched by the C-terminal attached chromophore, 2,4-dinitrophenyl (Dnp). Upon substrate cleavage by the lethal factor, the N-terminus portion of MAPKK-2 containing Abz can be followed in a fluorometer by excitation with 320nm and an emission wavelength of 420nm. To determine the total amount of fluorophore a standard curve containing an unquenched MAPKKIDE™ (Abz) was diluted in 20mM HEPES, pH8.2 in a range from 0-1µM. Lethal factor or its modified forms (LFhis, LFhisbio, LFbio: 1µg/ml) were added to 1µM MAPKKide (oABZ/Dnp) and measured every two minutes for one hour at an excitation wavelength of 320/20nm and an emission at 440/40nm (75% sensitivity). Each dilution was done in triplicate using 250µl/well.

4.9 Lentivirus Production

Transient Transfection of HEK293Ts for Virus Production: 2x10⁶ HEK293T cells/10ml per poly-L-lysine coated 10cm dish were seeded approximately 24 hours prior to transfection in DMEM high glucose with 5% FBS, HEPES, Glutamax. Plasmid DNAs were prepared in 5ml FACS tubes as follows:

Per 10cm dish: 10µg transfer vector plasmid
 6.5µg GAG/pol plasmid
 3.5µg VSV.G plasmid
 2.5µg pRSV-rev plasmid
 Bring up to a total volume of 450µl with 0.1x TE

50µl 2.5M CaCl₂ and 500µl warm 2X HBS were applied dropwise, while vortexing at full speed. 1ml of the solution was added immediately to the plate of HEK293T cells and swirled to disperse the precipitate. Approximately 16 hours later the media was changed and the cells were further incubated at 37°C and 5% CO₂.

Lentivirus Collection and Concentration: The media was collected after 24 and 48 hours, sterile filtered through a 0.22µm filter and centrifuged in an ultracentrifuge at 19400rpm for 2.2 hours at 4°C. The supernatant was discarded and the pellet resuspended in 5% BSA/PBS. The virus suspension was frozen in small aliquots at -80°C until further use. **Table 4-3** shows all the viruses used in this study.

Name	Vector	Origin	Base Change
CG-WIZ-EGFP	CG-WIZ-EGFP	Dr. Torbett B.	
MEK1 (P8A)	CG-WIZ-EGFP	Dr. Kun-Liang Guan	P=CCC ->A=GCC
MEK2 wt	CG-WIZ-EGFP	Dr. Kun-Liang Guan	
MEK2 (P10A)	CG-WIZ-EGFP	Dr. Kun-Liang Guan	P=CCG ->A=GCG
MKK 3 (I27E)	CG-WIZ-EGFP	Dr. David M.	I=ATA ->A=GAA
MKK 4 (K45Q, L46E, R58Q, F59D)	CG-WIZ-EGFP	Open Biosystems Clone ID 5272439	K=AAG ->Q=CAG R=AGG ->Q=CAG L=TTG -> GAG F=TTT -> D=GAT
MKK 6 (I15A)	CG-WIZ-EGFP	Dr. David M.	I=ATT ->A=GCT
MKK 7 (Q44K, G76A)	CG-WIZ-EGFP	Dr. Han J.	Q=CAG ->K=AAG G=GGG ->A=GCG

Table 4-3: Non-cleavable MKK mutants.

4.10 Cell Viability and Cell Death

4.10.1 MTT Assay for Cell Viability

MTT is a yellow water-soluble tetrazolium dye that is reduced by living cells to a water-insoluble purple formazan. The amount of formazan can be determined by solubilizing it in DMSO and measuring the absorbance at 560nm spectrophotometrically. Comparisons between the spectra of treated and untreated cells can give a relative estimation of cytotoxicity or proliferation. [193]

MTT assays were performed in a 96-well plate according to manufacturer's instructions (Sigma). After or during the treatment, MTT was added to each well at a final concentration of 200-500µg/ml. 0.5-1 hour later, the media was removed, washed twice with PBS and formazan was dissolved in DMSO (Sigma). Absorbance at 560nm was determined for each well using a microplate reader (Bio-Rad).

4.10.2 TUNEL Assay to Determine DNA Strand Breaks

Degradation of nuclear DNA can be examined by the TUNEL assay, which allows *in situ* detection of nicked DNA and DNA breaks. This method is based on the enzymatic labeling within the cell of free 3'-OH groups at the ends of nicked DNA and the blunt ends of broken double-stranded DNA with fluorescein-labeled deoxyuridine. The TUNEL kit from Roche titled *In situ* Cell Death Detection Kit, Fluorescein was used according to manufacturer's instructions. [194, 195]

4.10.3 Phosphatidylserine Exposure

In the early stages of apoptosis changes occur at the cell surface and plasma membrane. One of these plasma membrane alterations is the translocation of phosphatidylserine (PS) from the inner side of the plasma membrane to the outer layer. Therefore, PS becomes exposed at the cell surface. Cells were plated on collagen-coated coverslips and treated for 48 hours with or without lethal toxin. Afterwards, they were incubated with a PS antibody for 20 minutes, fixed with 4% PFA and rinsed quickly with PBS. PS exposed to the cell surface was visualized with the mouse-alexa-488 antibody under a fluorescence microscope.

4.10.4 Caspase Activation

Caspase 3 activation plays a key role in the initiation of cellular events during the early apoptotic processes. It cleaves specific substrates at aspartic acid residues. PARP, a nuclear protein involved in DNA repair, is cleaved from a 116kDa protein, yielding fragments of 85 and 25kDa. Rho-associated coiled-coil protein kinase-1 (ROCK-1, 160kDa) is also a direct cleavage substrate of activated caspase-3, leading to fragments of 130kDa and 30kDa, which can be detected by specific antibodies in immunoblots.

4.10.5 LDH Release Assay

The LDH release assay is a fluorometric method for estimating the number of nonviable cells. LDH is a cytoplasmic enzyme which is measured in a 10-minute coupled enzymatic assay that results in the conversion of resazurin to the fluorescent product, resorufin.

The LDH amount was determined after 48 hours treatment in the bottom media (500µl) of the inserts. The total amount of cells on top of the inserts was measured by the release of LDH through lysis. 100µl lysis buffer was added for 10 minutes. 50µl media were combined with 50µl assay buffer provided by the CytoTox-ONE™ Kit from Promega in a 96-well plate. The plate was shaken for 10 minutes and fluorescence was measured with an excitation wavelength of 560nm and an emission wavelength of 590nm (Ex. 540/35nm, Em. 590/20nm, 30% sensitivity). [196, 197] The percent of cytotoxicity was calculated with following formula:

Percent cytotoxicity =

$$100 \times \frac{(\text{Amount of LDH in Experimental Medium} - \text{Medium Background})}{(\text{Amount of LDH of Lysed Cells} - \text{Medium Background})}$$

4.10.6 Proteasome Activity

The proteolytic activity of proteasomes was measured by a fluorogenic method. Suc-LLVY-AMC (Biomol) is a dye, which fluoresces when chymotryptic activity of the proteasomes is effective. Cells were treated for 1-48 hours with LT or LThisbio. Proteasome inhibitors MG132 or epoxomicin were added for 4 hours to provide positive controls for the reduced activity. The cells were scraped in PBS and centrifuged at 1000rpm for 3 minutes. The cell pellet was lysed in 200µl lysis buffer (50mM Tris HCl, pH 7.5, 250mM sucrose, 5mM MgCl₂, 0.5mM EDTA, freshly added 2mM ATP, 1mM DTT, 0.025% digitonin) and incubated on ice for 5 minutes, followed by a centrifugation at 20000g (19300rpm) for 15 minutes 4°C. After a BCA protein assay of the supernatant, 25µg of the protein extract was incubated with 100µM Suc-LLVY-AMC in 200µl assay buffer (50mM Tris HCl, pH 7.5, 40mM KCl, 5mM MgCl₂, freshly added 0.5mM ATP, 1mM DTT, 0.5mg/ml BSA). The kinetic of the peptide cleavage was measured for 1 hour at 37°C in a spectrofluorimeter at an excitation wavelength of 380nm and emission wavelength of 460nm (320/20;440/40, 50% sensitivity).

4.11 Evaluation of the Polarized Airway System

4.11.1 Epithelium Transepithelial Electrical Resistance

Transepithelial electric resistance (TEER) is a convenient method to evaluate and monitor the growth of epithelial tissue cultures *in vitro*. The tightness of the cellular monolayer is marked by a sharp increase in TEER. The electrical voltohmmeter (EVOM) and the STX2 electrode from World Precision Instruments were used for the resistance measurement. (Figure 4-2) The electrode was sterilized in 70% Ethanol for 15 minutes and equilibrated in SABM media for one minute. The media level inside and outside of the inserts needed to be adjusted to the same level (inserts with membrane area of 0.33cm^2 were added $250\mu\text{l}$ top and $400\mu\text{l}$ to the 0.6ml existing media in the bottom). The resistance measurements were taken 3 times per sample and the average was determined. Afterwards the media was gently removed from the top.

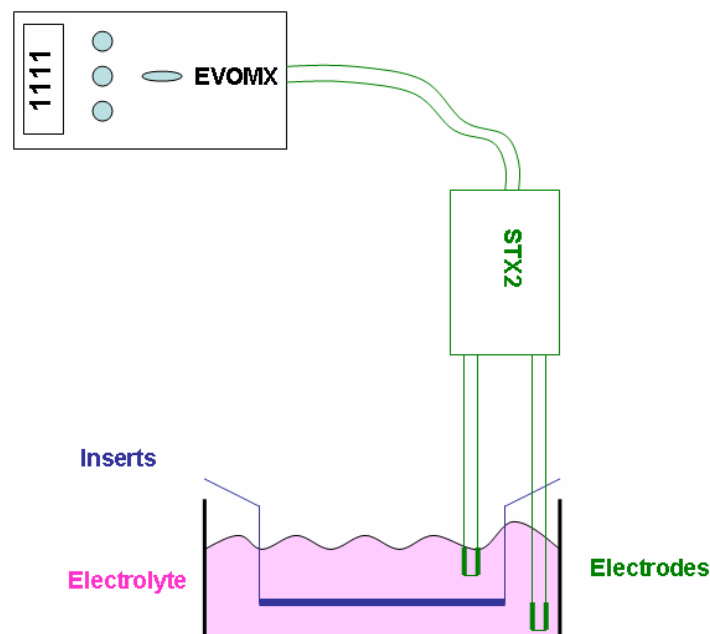


Figure 4-2: Resistance measurement of 3D grown cells with an electrical voltohmmeter.

To evaluate the differentiation of the layers in the polarized system we used an EVOMX to measure the electrical resistance in Ohm/area^2 . Abbreviation: 3D, three dimensional; EVOMX, electrical voltohmmeter X.

4.11.2 Permeability Measurements

The alterations of junction were also measured by permeability changes of the differentiated cell layer in the inserts. A FITC coupled albumin ($100\mu\text{l}$ of $5\text{mg}/\text{ml}$) was applied to the apical side and detected by a fluorometric assay in the basal HBSS ($450\mu\text{l}$) after 2 hours at 37°C with an excitation wavelength of $485/20\text{nm}$ and an emission wavelength of $530/25\text{nm}$ (30% sensitivity). The standard curve equation of $x=y/15.195$ calculates the penetration through the cell layer in μg . By division of 2 hours and surface of the insert (0.33cm^2) the amount of FITC-albumin per hour and surface area ($\mu\text{g}/\text{hr}/\text{cm}^2$) was determined. Cells were always treated with $1\mu\text{g}/\text{ml}$ LT for 48hr in starving media from the basal side. However, KGF ($250\text{ng}/\text{ml}$) and dexamethasone ($10\mu\text{M}$) were preincubated for 1 hour before LT was added.

4.12 Cell Adhesion and Migration

4.12.1 Adhesion Assay

NHBE were plated in 10cm dishes and grown for 2 days. After 3 hours starvation in SABM media, cells were treated with 1µg/ml PA and 1µg/ml LF for 48 hours. 24-well plates were coated with human fibronectin (10µg/ml), poly-L-lysine (100µg/ml), collagen (5µg/ml) or left untreated. The cells were trypsinized, counted and seeded in triplicates on the different coatings. Adherence was allowed to take place for 24 hours. Metabolically active adherent cells were stained with 500µg/ml MTT solution for 30 minutes, washed twice with PBS and dissolved in 120µl DMSO. The absorbance of 100µl DMSO solution was measured spectrophotometrically at 560nm.

4.12.2 Migration Assay in Boyden Chamber

In order to study *in vitro* cell migration, a polycarbonate membrane with a pore size of 8µm was used. The membrane was coated with human fibronectin on both sides. After 3 hours of starvation, cells were LT treated for 48 hours, followed by detachment with trypsin. Cells were plated on the top of the membrane in SABM media without supplements and the migration took place for 21 hours towards SABM media with supplements. Migrating cells to the lower side of the membrane were visualized with actin (rhodamine phalloidin) and nuclear (DAPI) stains by a fluorescence microscope.

4.12.3 Wound Healing Assay

The closure of a scratch in the 3D system was performed by wounding the cell layer with a 10µl pipett tip (cross). The cells were fixed immediately after the wounding as a control or grown for 18-21 hours. After staining of the actin filaments with rhodamine phalloidin, confocal images with a 10x objective lens were taken. ImageJ was used to analyze the width of the scratch. Two different inserts per condition, six to eight images with ten measurements per image were calculated.

4.13 Fractionation

4.13.1 Fractionation of Membrane, Cytosol and Cytoskeleton

NHBE cells were washed with 1xPBS and scraped on ice in fractionation buffer (25mM Tris, pH7.5, containing 2mM EDTA, pH8, 10mM β-mercaptoethanol, 10% Glycerol, 10µg/ml leupeptin, 10µg/ml aprotinin, 1mM phenylmethylsulfonyl fluoride). Cells were sonicated two times 15 seconds using a microprobe sonicator (Microson XL) and the nuclei were removed by centrifugation at 1000xg for 10 minutes. Membranes and cytoskeleton were isolated from the post-nuclear supernatant by centrifugation at 100,000xg for 30 minutes in an Optima TLX ultracentrifuge with a TLA 100.3 rotor (Beckman Instruments Inc., Palo Alto, CA). The pellet (membranes and cytoskeleton) was washed with the fractionation buffer and incubated on ice for 45 minutes in the same buffer including 1% (v/v) Triton X-100. After centrifugation at 100,000xg for 15 minutes the supernatant containing the membrane fraction was removed and the cytoskeletal pellet was washed and sonicated.

4.13.2 Fractionation of Membrane and Cytosol

After washing the cells with 1xPBS, they were harvested in relaxation buffer (100mM KCl, 3mM NaCl, 3.5mM MgCl₂, 1mM EGTA, 10mM HEPES, 0.5mM 1,4-piperazine diethane sulfonic acid, pH7.4) and disrupted by two times 15 seconds of sonication at 4°C using a microprobe sonicator (Microson XL). Unbroken cells and nuclei were pelleted by centrifugation at 1000g for 10 minutes at 4°C. The supernatant was centrifuged at 100,000g for 30 minutes at 4°C in an Optima TLX ultracentrifuge with a TLA 100.3 rotor (Beckman Instruments Inc., Palo Alto, CA). The high-speed supernatant represented the soluble cytosolic fraction. The pellet was washed and resuspended in relaxation buffer by two times sonication.

5 RESULTS

The lung epithelium represents an indispensable barrier between host and environment. Its homeostasis and its role in the gas exchange are indispensable for normal airway function. The exchange of carbon dioxide in the blood to oxygen and its transport to the tissues is essential for cell performance. The secretion of surfactant and mucus lowers the surface tension and traps inhaled small particles, which are removed by the ciliated movements. Lung injury and pulmonary diseases are often caused by an imbalance of pro- and anti-inflammatory responses of the epithelium.

Many pathogens enter the human body through the lungs. In the case of an inhalational anthrax infection, spores were ingested by alveolar macrophages, dendritic cells and lung epithelial cells. [130-132] During the migration of macrophages to the regional lymphnodes the spores develop into the vegetative bacterium. After release of the bacteria in the lymphatic system or blood stream fast replication occurs followed by lethal and edema toxin secretion. In the late stage of anthrax pathogenesis the lungs is characterized by respiratory distress, edema, swelling and extensive bleeding, which leads to septic shock and toxemia/bacteremia to the death. The mechanism of the respiratory distress is not well understood. Therefore, we were investing the effects of one of the toxins – lethal toxin – in primary human lung epithelial cells.

5.1 Characterization of Airway Epithelial Cells

Electron microscopy pictures of normal tissue culture plated NHBE are shown in **Figure 5-1 (A)**. Their cell shape varies from round to oval and because of their mixed cell population the cell size can differ. Nevertheless, they are large flat cells with a large cytoplasm. Not only morphological phenotype changes in those cells were studied, but also a more defined *in situ* system was used. [198] Therefore, we established a fully differentiated, polarized three-dimensional airway model by culturing primary lung epithelial cells on a collagen coated porous polyester transwell membrane (insert). During the process of maturation of the 3D-layer increasing formation of junction complexes and the secretion of mucus and surfactant were observed. Signaling responses to bacterial ligands and cytokines can be investigated and the model is capable of rapid wound healing after injury. The establishment of this airway model system enables us to measure alterations in secretion, permeability, signaling pathways and pathogen interaction. It provides a perfect tool to understand the effect of lethal toxin in the respiratory epithelium. EM cross sections of the three-dimensional polarized lung epithelial system are displayed in **Figure 5-1, B-E**.

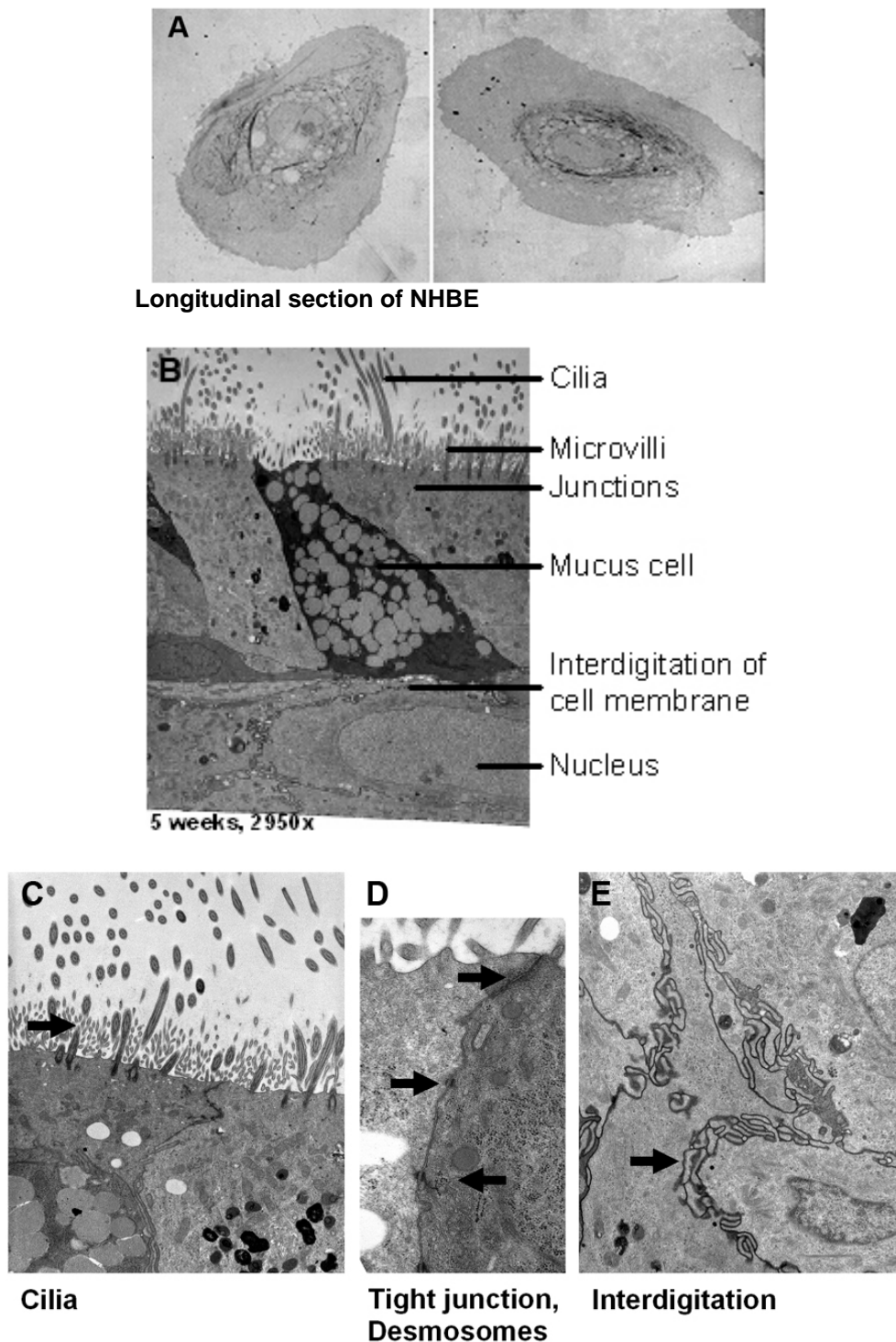


Figure 5-1: Morphology of normal tissue culture treated NHBE and polarized 3D cells in EM.

A) Longitudinal EM sections of tissue culture plated cells stained with uranyl acetate and lead citrate. B) Overview picture shown of a 5 weeks old insert in a cross section. C-E) Higher magnifications display (C) cilia, (D) junctions and (E) interdigitations indicated by arrows.

In **Figure 5-1, B** a 3D layer with several different cell types such as basal, ciliated and mucus/goblet cells were formed in two to three layers. Interdigitations between cells and complex junctions such as tight junctions and desmosomes led to a very dense almost tissue-like structure. (**Figure 5-1, C-E**) The integrity of the cell connection was measured by permeability changes (**Figure 5-6**), which increases with tight

connections and interdigitations. Furthermore, cilia and flagella on the apical side were formed to transport and segregate the secreted mucus. (Figure 5-1, C) The beating of the cilia could be observed under a normal light microscope.

To determine which type of lung cells existed under 2D and 3D culture conditions, we decided to test for markers characteristic for each lung cell type. (Table 12-1) Therefore, we performed a RT-PCR of calveolin-1, a pneumocyte type 1 marker. [199] Human beta defensins 1 and 2 are secreted by lung epithelial cells for antimicrobial protection. [200] Pneumocyte type 2 and Clara cells secrete surfactant A and B, to lower the respiratory surface tension. To distinguish the surfactant secretion between pneumocyte type 2 and Clara cells, we also tested for CC10, a distinct Clara cell marker. (data not shown) Unfortunately without a positive control, we were unable to detect the mRNA expression, which could be due to incorrect PCR conditions or not existing Clara cells.

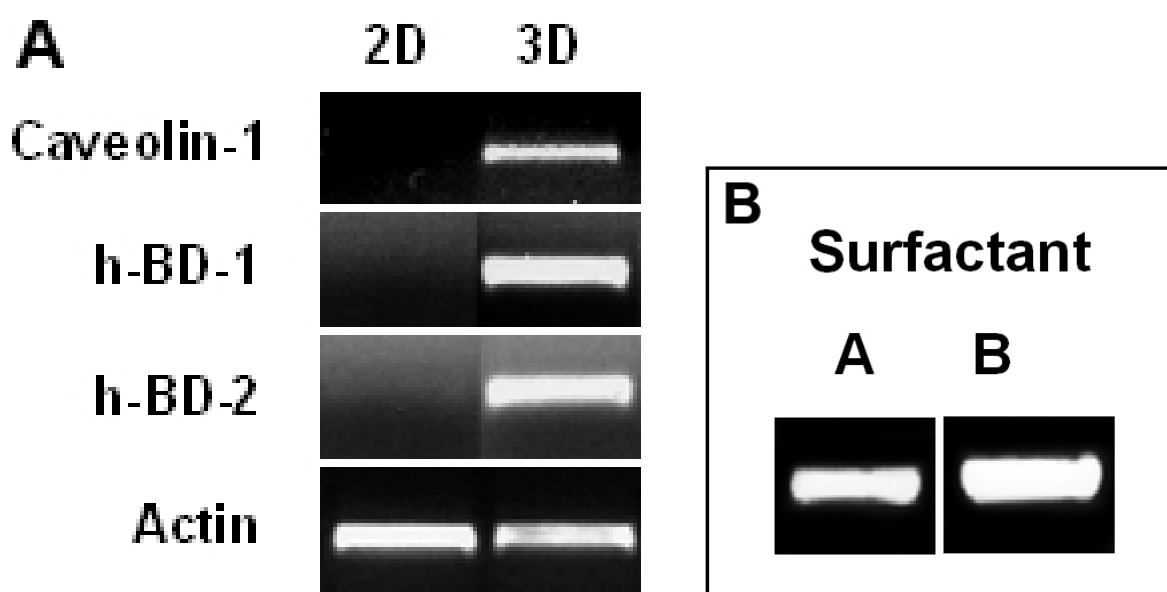


Figure 5-2: Pneumocyte characterization.

A) The mRNA message for calveolin-1, h-BD-1, h-BD-2 of NHBE in normal tissue culture treated cells (2D) and in the 3D system were shown in RT-PCR. Actin was used as loading control. B) Surfactant A and B detected after differentiation in 3D. Abbreviations: 2D, 2 dimensional; 3D, 3 dimensional; h-BD-1, human beta defensin-1; h-BD-2, human beta defensin-2; RT-PCR, reverse transcription – polymerase chain reaction.

Only in the polarized 3D system, NHBE were able to differentiate into pneumocytes. (Figure 5-2, A) The surfactant A and B expression in Figure 5-1, B was also exclusively detected in the 3D system. Tissue culture grown cells contained precursors of a variety of cell types, which under three dimensional conditions develop to define bronchial and lung cells.

After cell differentiation for 7 to 10 days on inserts, mucus production was observed by the secretion of a viscous fluid on the apical side. (Figure 5-3, B) The mucus was mainly generated by goblet cells. The expression time course of one of the mucin proteins (MUC5AC) showed mRNA upregulation between day 2 and 5 of growing cells in the air liquid interface. (Figure 5-3, A) The protein expression was visualized in immunofluorescence by staining with a MUC5AC specific antibody. The tight junctions were used to distinguish cell borders. (Figure 5-3, B)

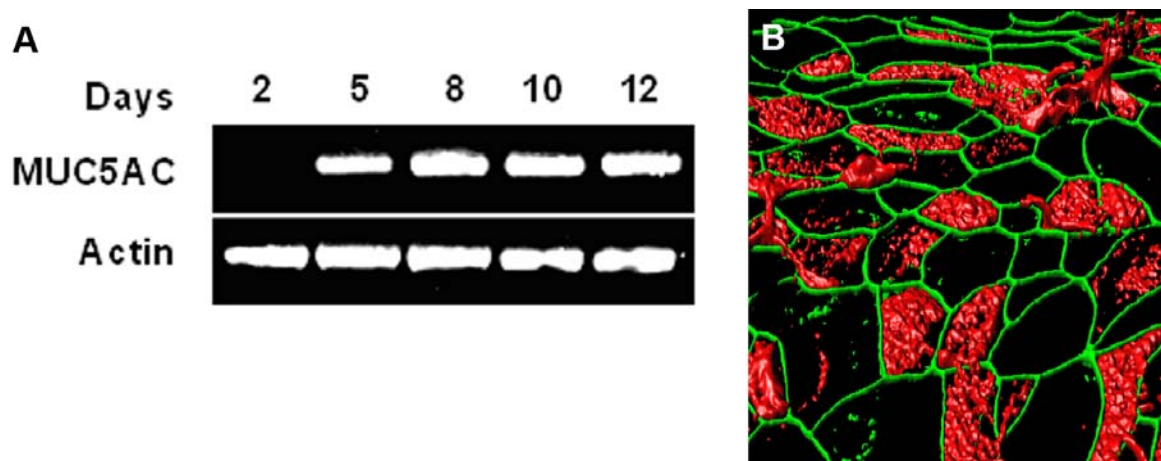


Figure 5-3: mRNA and protein expression of MUC5AC in the 3D system.

A) RT-PCR of a mucin, called MUC5AC, in differentiated NHBE and actin expression were shown at indicated time points. B) Immunofluorescence stain of tight junction (ZO-1, green) and MUC5AC (red) in three weeks old inserts. Abbreviations: MUC5AC, mucin 5AC; RT-PCR, reverse transcription-polymerase chain reaction; ZO-1, zonula occludin-1.

5.1.1 A Model to Study Anthrax Infection

In order to investigate, if NHBE are suitable for this study we looked into the anthrax receptors expression, anthrax toxin receptor (ATR) and capillary morphogenesis gene-2 (CMG2). These receptors are crucial for the uptake of the lethal factor/toxin and edema factor/toxin. Lung epithelial cells were previously described to express ATR and CMG2. In the ciliated epithelial cells of the bronchi the ATR seemed to be particularly abundant. [71, 201]

To confirm the receptor expression in NHBE we performed RT-PCRs and detected mRNAs of ATR and CMG-2. CMG-2 was slightly increased over the ATR message. Actin was used as a housekeeping control gene. Because of the lack of available receptor antibodies, we were unable to test for their protein expression.

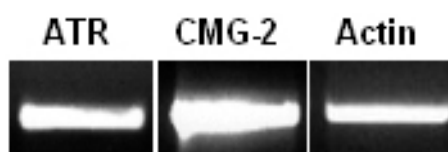


Figure 5-4: Anthrax receptor expression.

NHBE cells expressed both anthrax receptors. Actin was used as loading control. Abbreviations: ATR, anthrax receptor; CMG-2, capillary morphogenesis gene 2.

The receptor expression on the surface can be indirectly proven by MAPKK cleavage. Without the presence of a functional receptor, PA binding cannot occur, lethal factor cannot be internalized and released in the cytoplasm. With the exemption of MEK5, LT cleaves all N-terminal parts of MAPKK (Figure 2-5). This cleavage was visualized by immunoblotting with antibodies raised against the N-terminal part. The loss was detected after 48 hours of LT treatment of cells in 2D and 3D conditions. (Figure 5-5, A, B) Lethal toxin did not influence the mRNA levels of MEK2 or MKK3, which was demonstrated in Figure 5-5, C by RT-PCR. The actin expression was used as equal loading control. Those findings indicate that normal human bronchial epithelial cells have all the requirements to study the LT effects in the respiratory system.

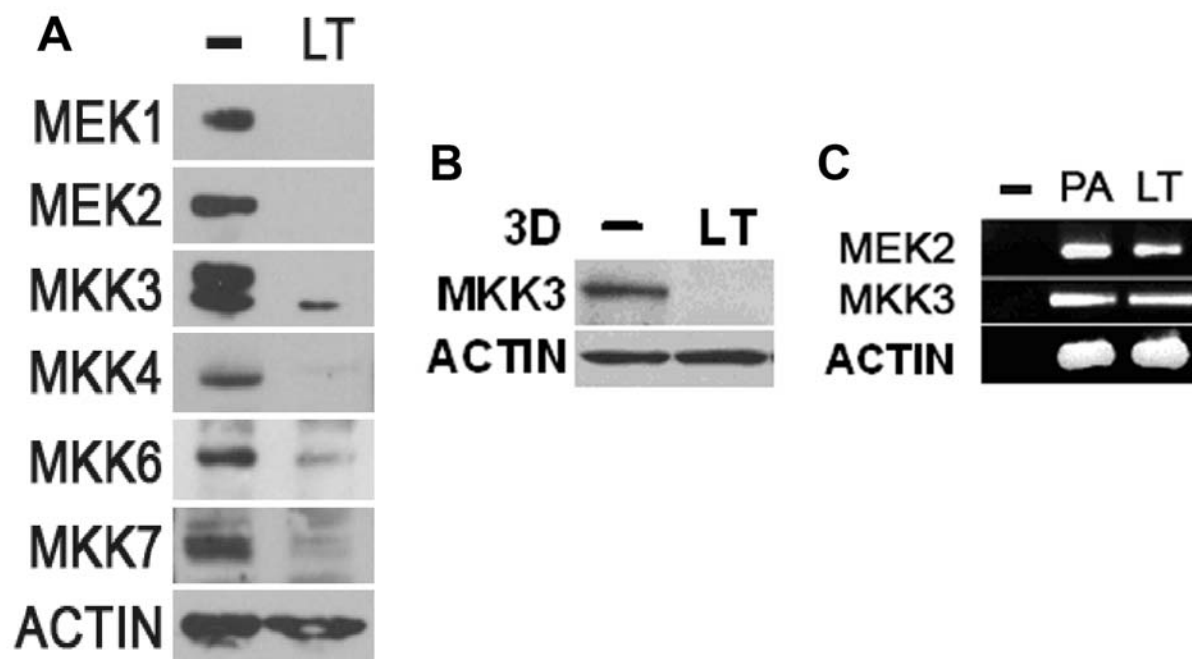


Figure 5-5: Effect of LT treatment on the protein and mRNA levels of MAPKKs.

A) Protein expression of all MAPKK besides MKK5. After lethal toxin cleavage antibodies against MAPKK are unable to detect the protein in 2D. B) The same MKK3 cleavage was observed in three weeks old inserts. C) Gene expression was not affected. The untreated panel did not contain any DNA. Abbreviations: -, untreated; 2D, 2 dimensional; 3D, 3 dimensional; LT, lethal toxin, MEK, mitogen-activated ERK kinase; MKK, mitogen-activated kinase kinase; MAPKK, mitogen-activated protein kinase kinase; PA, protective antigen.

5.2 Junction Changes After LT Treatment

A polarized epithelium has an apical and basolateral side. The junctional complex provides a seal between cells and regulates the diffusion of substances. Cell connections play major roles in cell communication (gap junctions), formation of tissue boundaries, migration and cell shape rearrangements. [202] Therefore, the assembly and turnover of adhesive contacts has to be tightly regulated.

Human lung endothelial cells are located right underneath the epithelium to support the gas exchange. It was shown, that lethal toxin disrupts the barrier function of endothelial cells by decreasing the resistance and increasing permeability. [80]

To compare, if there is a similar effect in lung epithelial cells that could induce respiratory distress, we analyzed junctional changes and evaluated the tightness of the differentiated lung model. We measured a decrease of resistance in NHBE by approximately 75% compared to untreated cells. (Figure 5-6, A) Also, the increase of permeability measured by a fluorescent dye penetrating through the layer after toxin treatment proved the disruption of the cell barrier. (Figure 5-6, B)

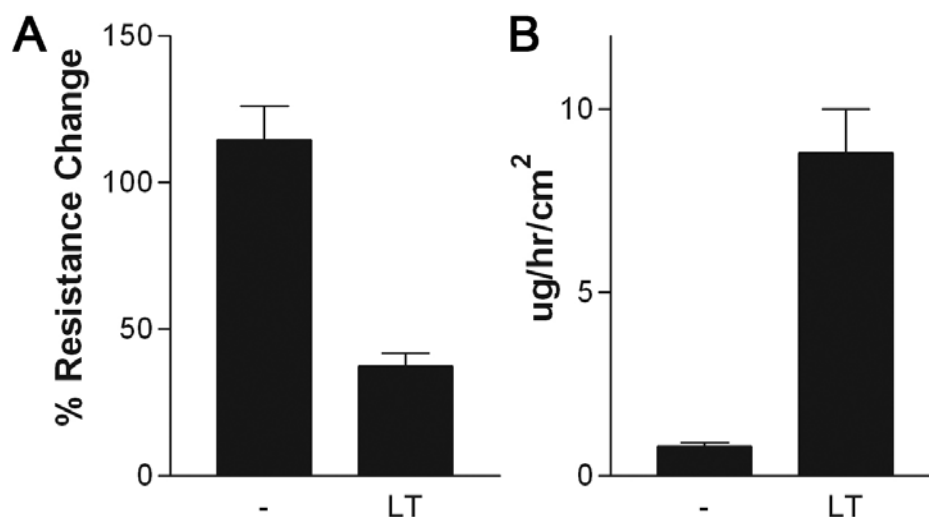


Figure 5-6: Resistance and permeability change.

A) Resistance of NHBE grown for 3 weeks in 3D inserts measured before and after 48 hours of LT treatment. Resistance before treatment was set as 100% and change after 48 hours is shown in % of change. B) Permeability measurements of insert after 48 hours LT (1 μ g/ml) treatment. Abbreviation: %, percent; -, untreated; cm², square centimeter; hr, hours; LT, lethal toxin; ug, microgram.

The increase of permeability and decrease of resistance might be due to viability or junction changes. The death of cells would lower the cell density and damage the integrity of the polarized system. On the other hand, junction disruptions or alteration would lead to a leaky layer.

To test the possibility of cell death occurring during the 48 hours of treatment, we measured the LDH release in the basal media. Cells undergoing death will burst or leak cytosolic LDH in the surrounding media. The release of LDH was compared to the amount of apical cells in the intact layer. In **Figure 5-7** we showed, that untreated as well as LT treated cells had minimal cell death occurring after 48 hours. However, lethal toxin treated cells seemed to have 5% higher LDH levels, compared to the untreated cells. Therefore, the increased toxicity can be partially involved in the resistance changes, but cannot explain the resistance drop of 75% completely.

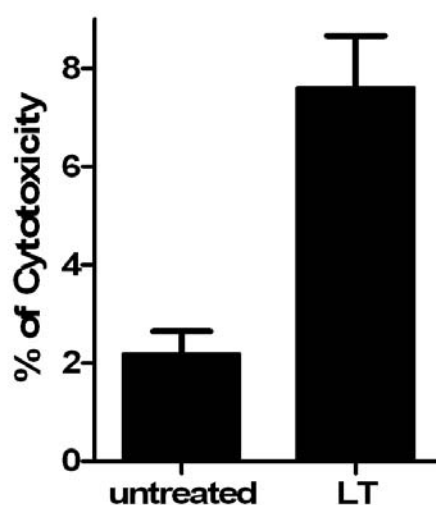


Figure 5-7: LDH release after LT treatment in the 3D system.

The LDH release of apoptotic cells was measured after 48 hours treatment of 3 weeks old inserts. Displayed is the percentage of toxicity compared to the total amount of cell in the top of the cell layer. Abbreviation: LDH, lactate dehydrogenase; LT, lethal toxin; %, percent.

To visualize and understand the leakage of this cell layer through junction alterations, we decided to look for changes by immunofluorescence and electron microscopy. (Figure 5-8, Figure 5-9) The immunofluorescence stain of tight junctions at the apical side in the 3D system suggested the mechanism behind the leaky cell layer. Lethal toxin treated cells showed an increased appearance of disruptions of multicellular junction sites, indicated by the white arrows in Figure 5-8, B. In the kidney epithelial cells (MDCK) these sites were identified as naturally occurring events, when apoptotic cells detach from the cell layer. [203] In an intact cell layer, junctions will be remodeled to form a tight system. This led us believe that both, a slight increase in cell death and a junctional modeling defect play a role in the leakage of the 3D layer.

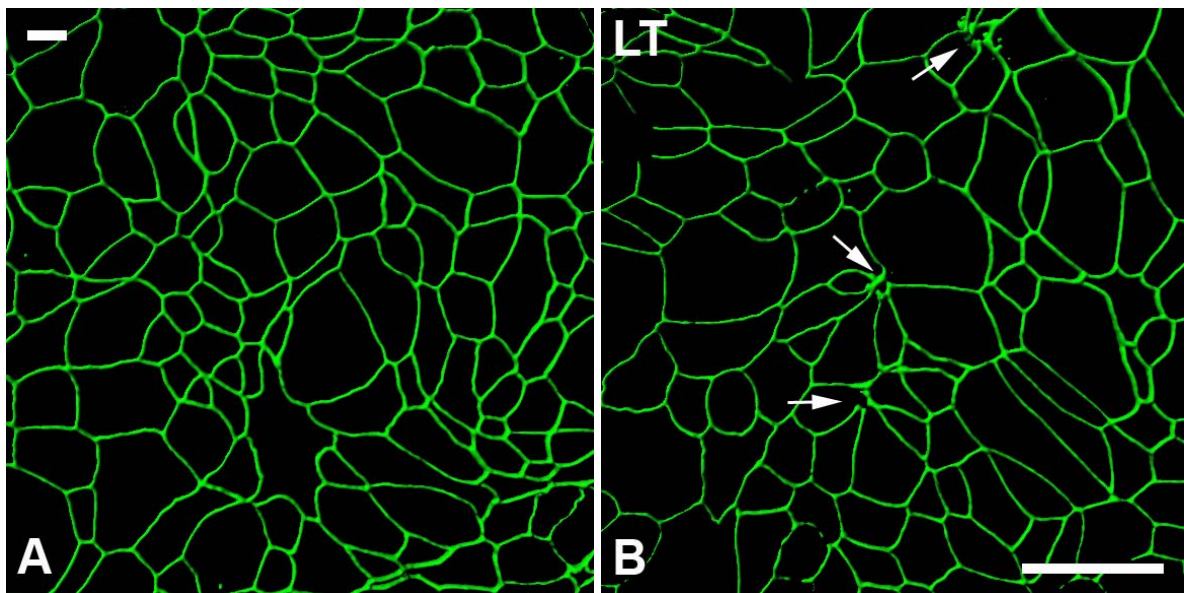


Figure 5-8: Increase of multicellular junction sites after LT treatment at the apical side.

A) Untreated and B) LT treated immunofluorescence images of ZO-1 (green) of 3 weeks old inserts. LT causes disruption of multicellular junction sites indicated with white arrows. A Z-series was performed and the images were afterwards flattened. Scale bar represents 50 μ m. Abbreviations: -, untreated; LT, lethal toxin; ZO-1, zonula occludens -1.

A more dramatic change was observed in electron microscopy cross sections after lethal toxin treatment. (Figure 5-9, B) LT led to the separation of basolateral cell connections and interdigitations, and increased the height of the layer. The apical located tight junctions were mostly intact. Figure 5-9, B shows a very extreme case, some other experiments had milder disruptions. The untreated layer displayed a very tight tissue-like structure with a minimum of two layers. (Figure 5-9, A)

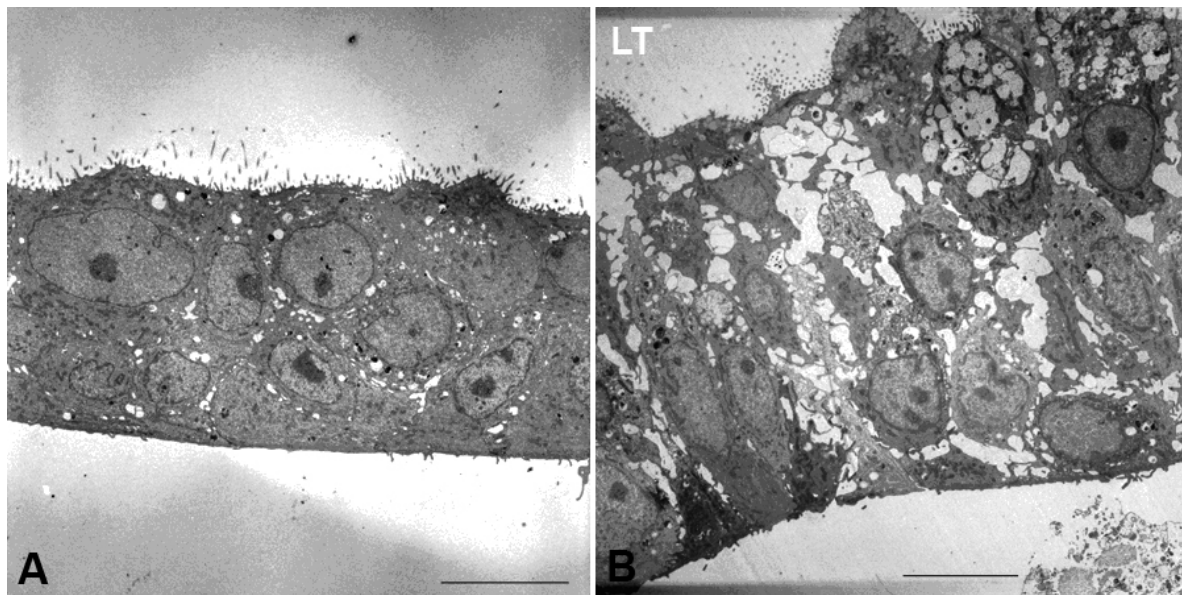


Figure 5-9: Electron microscopy pictures of LT treated, polarized NHBE.

A) EM cross section of 3 weeks old untreated insert. B) Disruptions (white spaces) of the layer after 48 hours of LT treated insert in EM. Scale bar represents 10 μ m. Abbreviation: LT, lethal toxin.

Next to the air liquid culture results, we wanted to compare junction alterations in normal tissue culture plated cells. This could provide a better understanding of molecular mechanism behind the junction complex alterations. Therefore, we stained tight and adherens junctions and evaluated them by immunofluorescence.

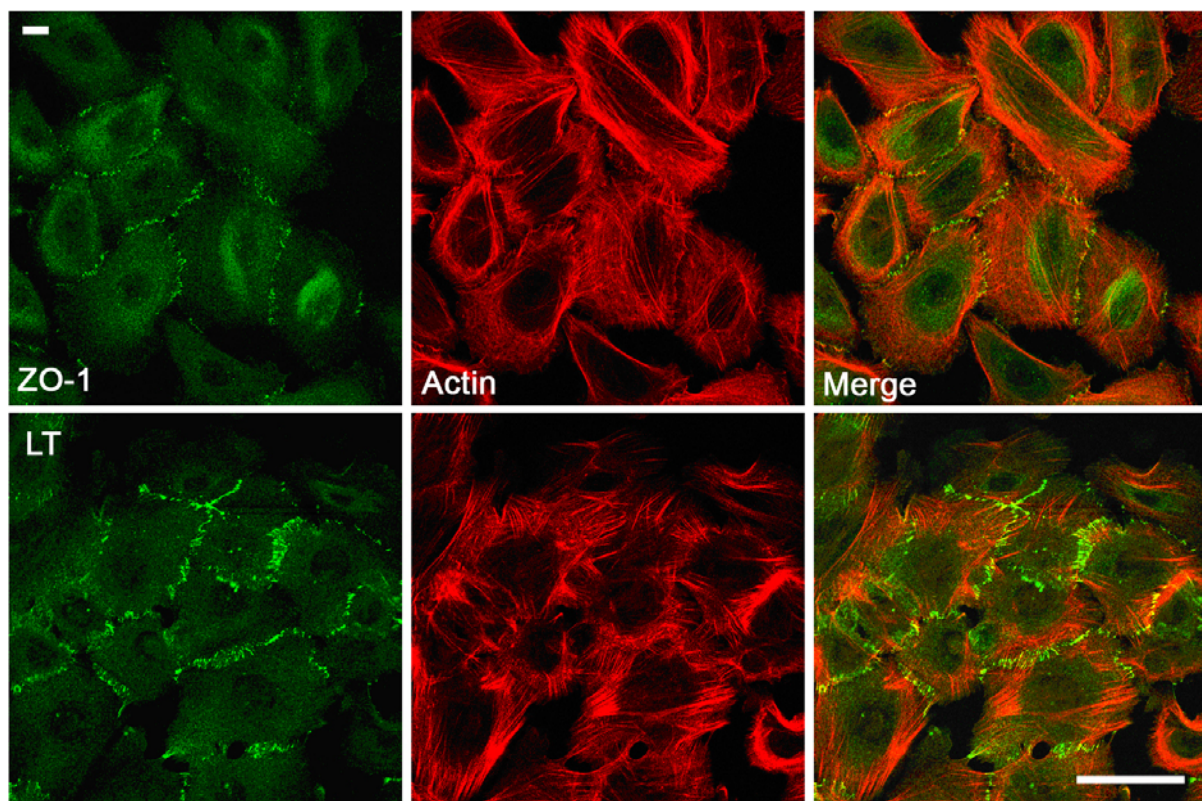


Figure 5-10: Lethal toxin induces tight junction alterations.

IF of ZO-1, a tight junction marker (green), actin (red) and the merged image (red/green). Increased amounts of disturbed ZO-1 seen after LT treatment. Actin was used to define the overall cell structure. Scale bar represents 50 μ m. Abbreviations: -, untreated; LT, lethal toxin; ZO-1, zonula occludens -1.

The tight junction displayed a very diffuse junction phenotype accompanied with an increase in the expression after lethal toxin treatment. (Figure 5-10, ZO-1) This proved that an induced expression of junction proteins did not favor a tighter layer seen in the permeability and resistance changes. There might be incorrect assembly or remodeling of tight junctions occurring.

A similar phenotype was observed with an adherens junction stain (Figure 5-11, E-cadherin) after LT exposure. The junctions showed a diffuse distribution pattern with a wider range and higher amount of cell connection proteins. This alteration also did not lead to an increase in junction tightness, instead a deregulation of the junction complex took place.

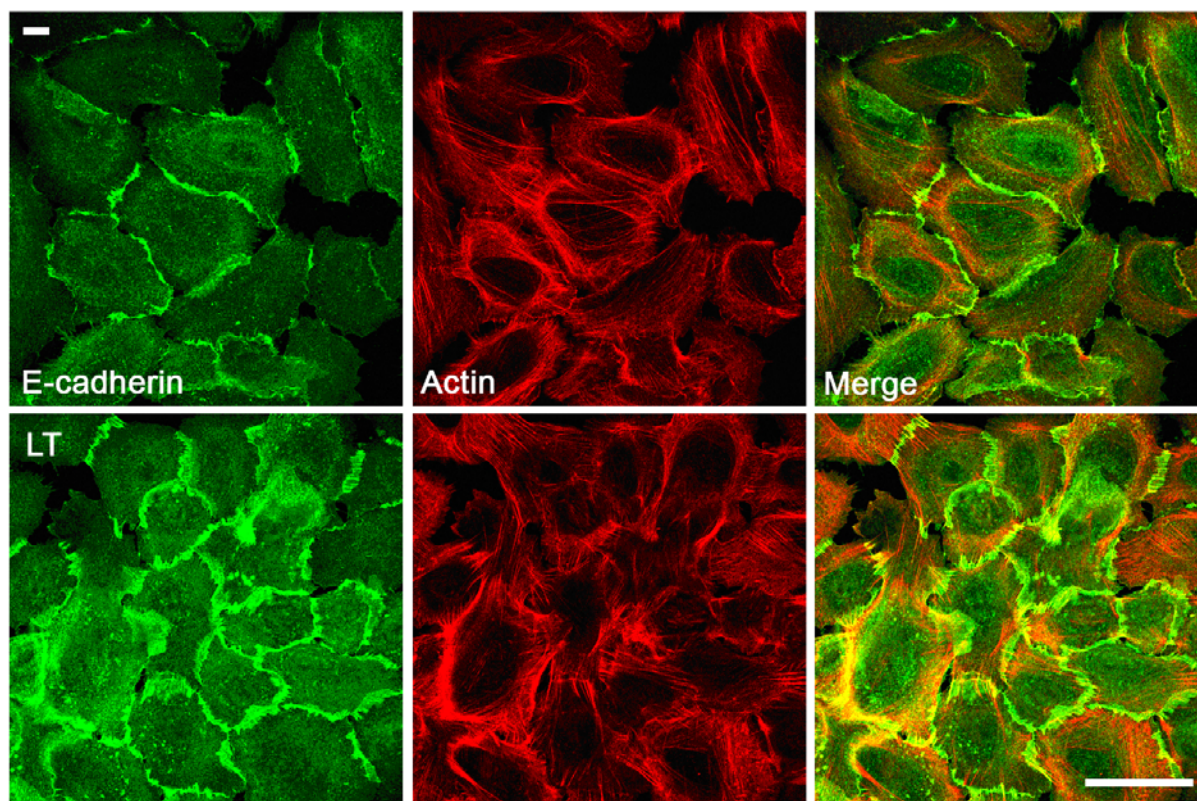


Figure 5-11: A diffuse adherens junction stain occurred after LT treatment.

Immunofluorescence of E-cadherin (green), actin (red) and the merge (red/green). The upper panel showed untreated NHBE whereas the lower panel was LT treated. Lethal toxin increased disrupted adherens junctions. Actin was used to define the overall cell structure. Scale bar represents 50 μ m. Abbreviations: -, untreated; LT, lethal toxin.

The increased levels of protein were also detected by immunoblotting, when cell lysates were fractionated in cytosol, membrane and cytoskeleton. (Figure 5-12) E-cadherin was increased in the membrane and cytoskeleton, whereas ZO-1 showed only an increase in the cytoskeletal fraction. Those results agree with the immunofluorescence pictures where membrane associated junctions and the connection with the cytoskeleton were affected, but no change was observed in the cytosol.

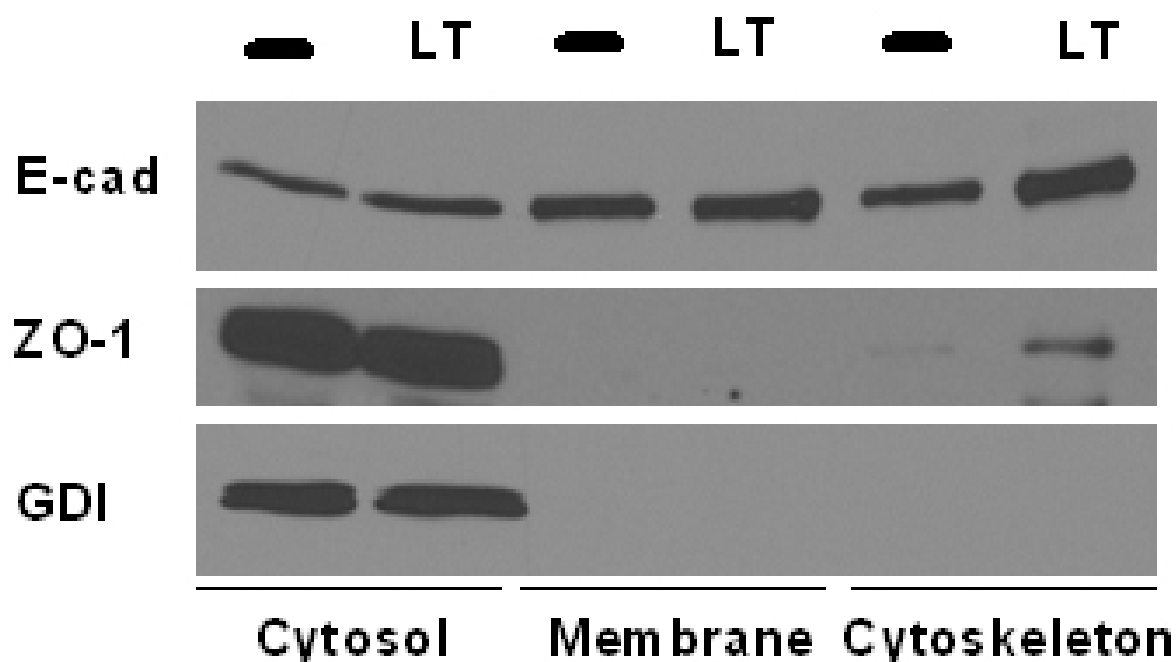


Figure 5-12: Junctional proteins increase in membrane and cytoskeleton after LT exposure. Fractionation of junctional proteins and a cytosolic control (GDI) were displayed. Increased amounts of E-cadherin were found in the membrane and cytoskeletal fraction, after 48 hours of LT treatment. ZO-1 showed only an increase in the cytoskeletal fraction. Abbreviations: -, untreated; LT, Lethal Toxin; E-cad, E-cadherin; ZO-1, zonula occludens -1; GDI, GDP dissociation inhibitor.

5.3 Alteration of the Cytoskeleton After LT Treatment

The cytoskeleton consists of actin, tubulin and intermediate filaments, which control the cell shape and the ability to move. Their rapid assembly and disassembly is tightly regulated by diverse proteins, such as Rho GTPases and generates an efficient recycling mechanism. They also play an important role in chromosome transport during mitosis, cell separation in cytokinesis, organelle location and uptake of pathogens by phagocytosis.

LT disrupts the actin filament assembly leading to impaired polymerization and motility inhibition in neutrophils. [87] This might be due to a downregulation of Hsp27 phosphorylation, which is p38 dependent. p38 inhibitor studies showed a similar effect. [88] In endothelial cells an increase of stress fibers and a reduction in peripheral F-actin was observed, leading to incomplete cell-cell adhesion. [80] Furthermore, the actin cytoskeleton is linked to the cytoplasmic domain of E-cadherin containing interaction proteins such as α - and β -catenin, p120 α -actinin and vinculin. [202] Therefore, we investigated the effect of LT on the cytoskeleton to determine alterations, which could be involved in the deregulations of the junction assembly.

5.3.1 Actin and Tubulin Changes

Actin und microtubule alterations were visualized by immunofluorescence. We observed, when comparing untreated and LT treated cells, increased stress fiber formations and bundle-like tubulin assembly in NHBE cells. Interestingly, lethal toxin caused the growth of many large protrusions/lamellipodia, seen in the tubulin stain in Figure 5-13.

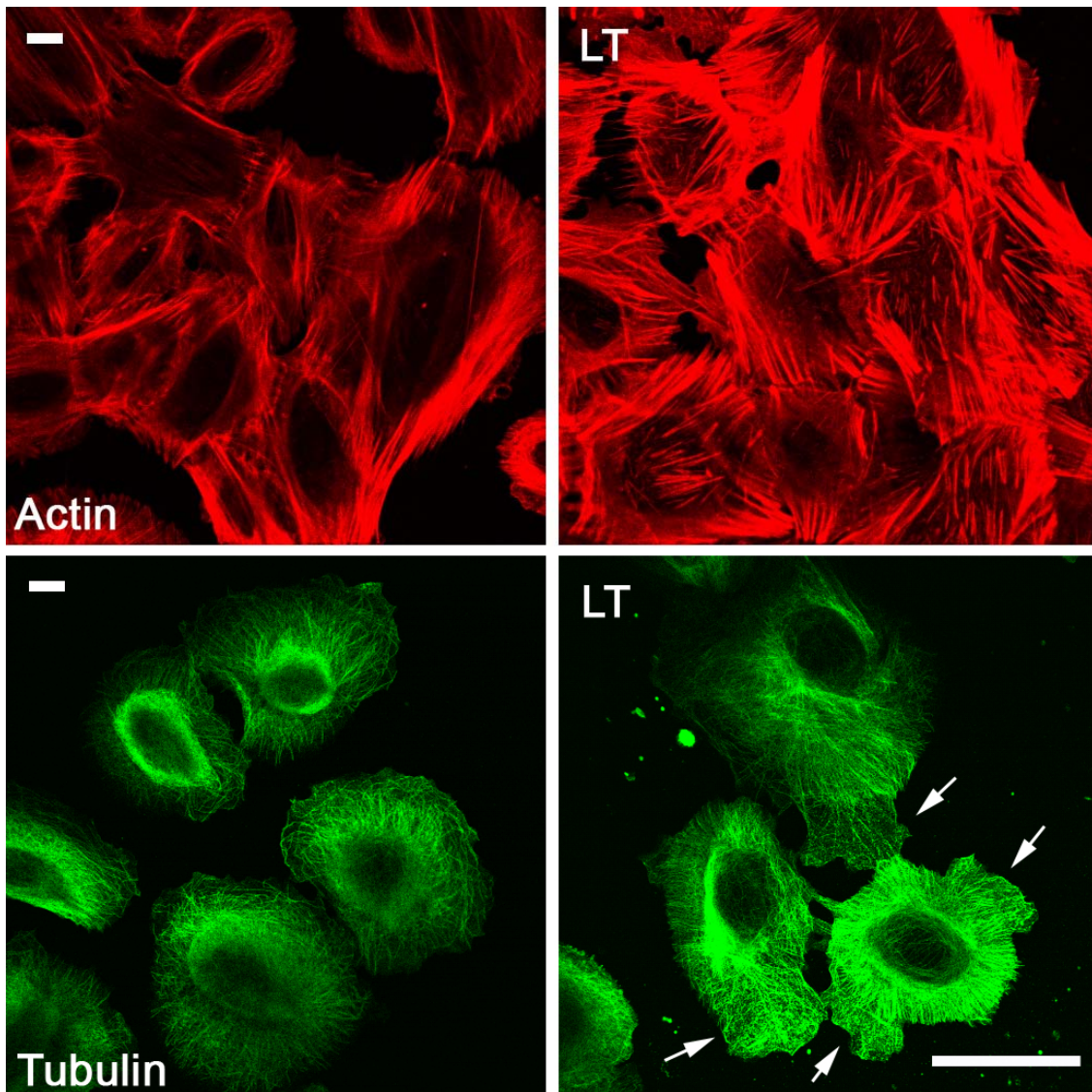


Figure 5-13: Stress fiber and tubulin bundle accumulations after LT treatment.

Immunofluorescence stain of actin (red) and tubulin (green). LT causes severe stress fiber formation and bundle-like tubulin structures. Wide protrusions were observed in the tubulin LT treated cells, which were indicated with arrows. Scale bar represents 50 μ m. Abbreviations: -, untreated; LT, lethal toxin

The stress fiber formations could be caused by an increase of actin assembly or decrease of actin disassembly. Therefore, we tested actin-specific inhibitors, such as latrunculin A, which binds actin subunits and prevents their polymerization. (Figure 5-14, A, B, E) The actin stain revealed more actin filaments left over in the LT treated cells. This is not enough evidence to suggest a slower actin disassembly process, since the amount of actin filament was higher from the beginning on.

The inhibition of actin assembly, using cytochalasin B, caps the plus ends and prevents the growth of actin filaments. (Figure 5-14, C, D, F) The immunofluorescence stain of actin confirmed a similar phenotype with left over actin filaments in the LT exposed cells. Only dotty-like actin structures were displayed in the untreated cells after cytochalasin B treatment.

The quantification of containing actin filaments after latrunculin A treatment was up to 60% increased with LT exposure. (Figure 5-14, E) The amount of positive cells, with almost 100%, was even more dramatically after cytochalasin B. (Figure 5-14, F)

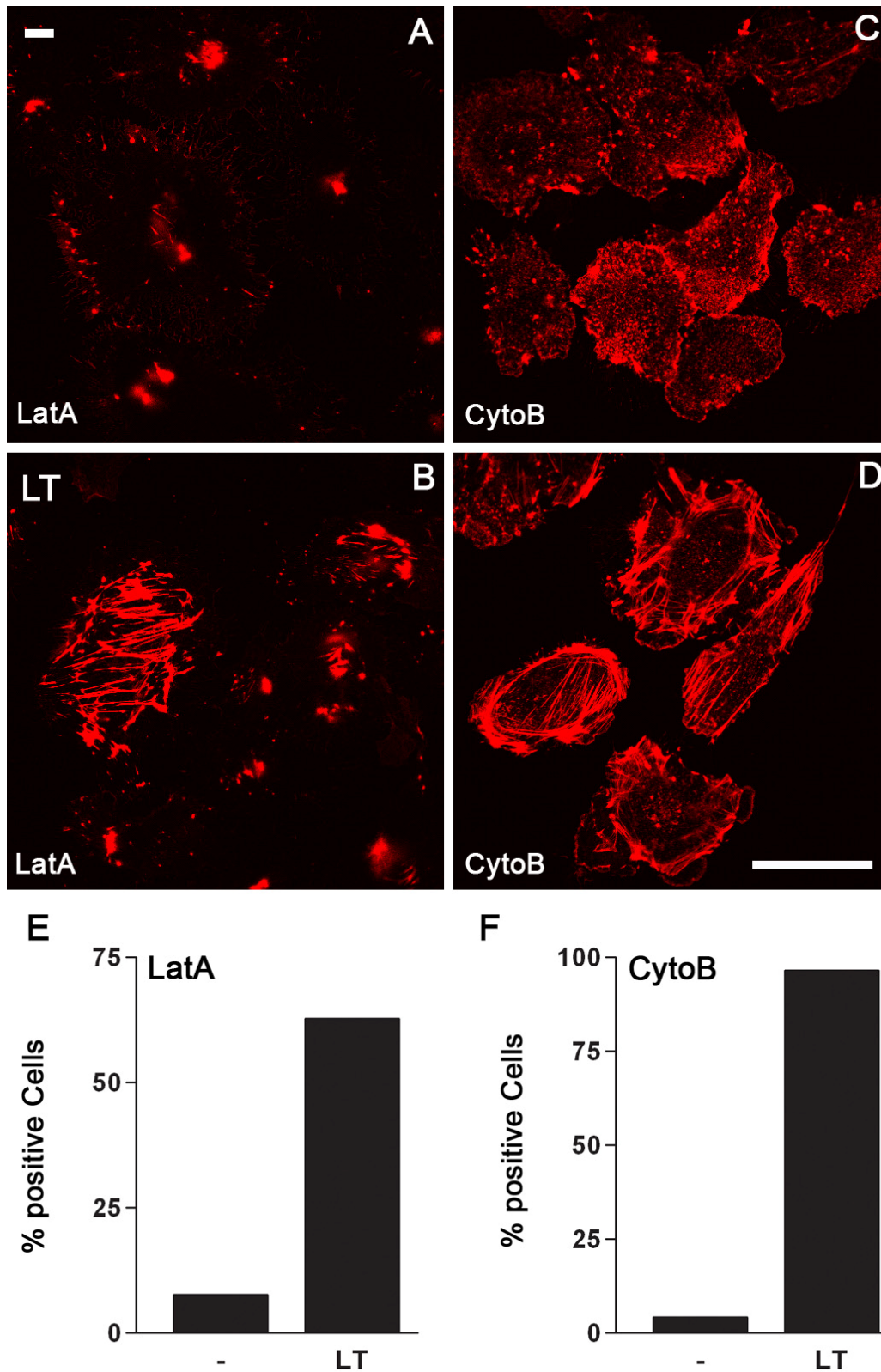


Figure 5-14: Quantification of increased actin filaments after LT treatment and actin polymerization inhibition.

Inhibition of actin polymerization with latrunculin (A, B, E) and cytochalasin B (C, D, F) after LT treatment (B, D) compared to untreated cells (A, C). Quantification shown in % of positive cells with left over actin filaments (red) of 250 cells. Scale bar represents 50 μ m. Abbreviations: -, untreated; CytoB, cytochalasin B, LatA, latrunculin A; LT, lethal toxin.

Residual actin filaments were observed after LT treatment and inhibition of polymerization. To define if it is a defect of actin filament assembly we used a reversible inhibitor to stop polymerization of the actin filaments. A wash-out of the inhibitor followed, which allowed the cell to generate new filaments in 35 minutes. (Figure 5-15) The actin filaments returned to their stress fiber formation, which indicates no defect in the actin growth.

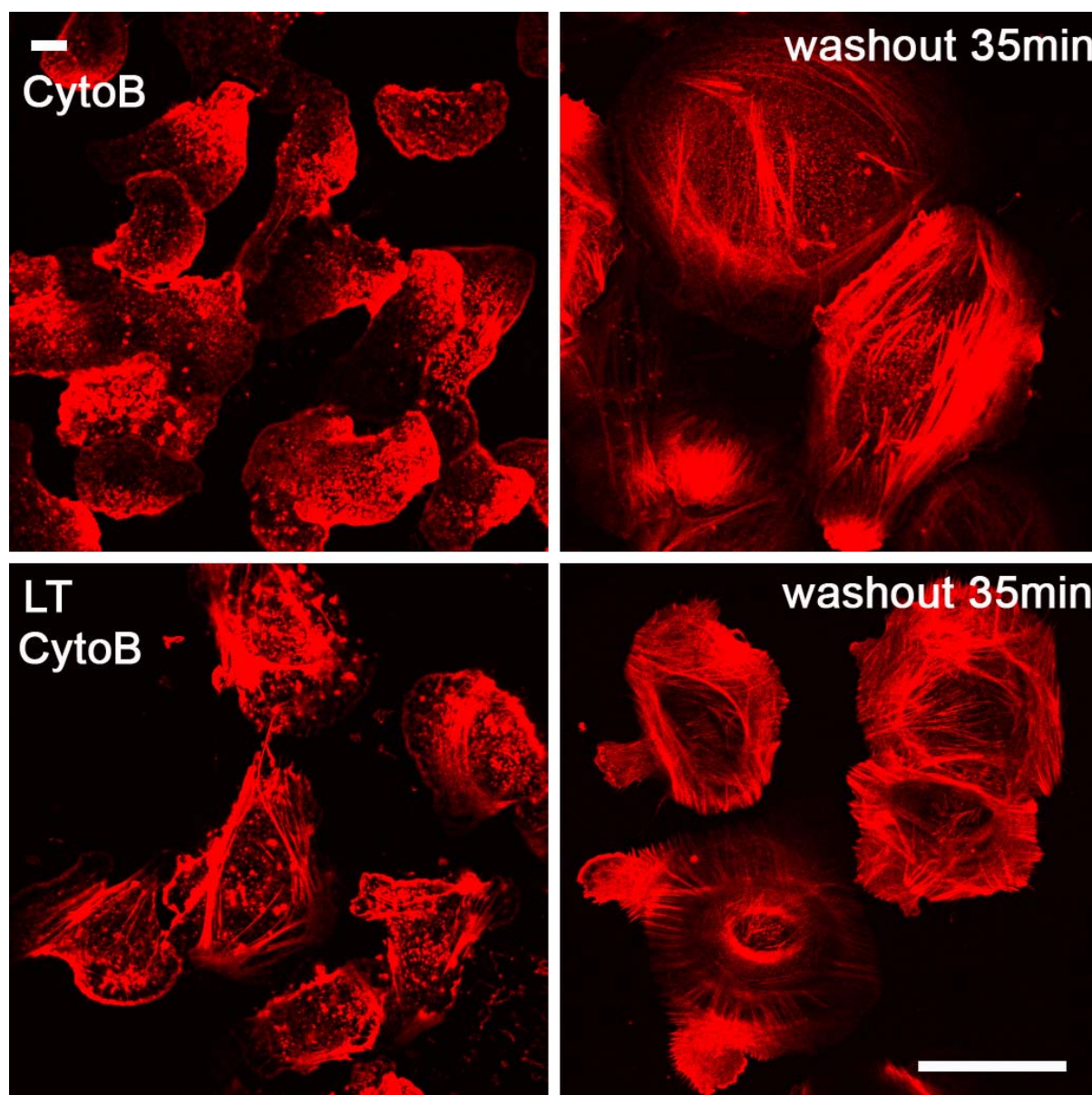


Figure 5-15: Actin assembly is not inhibited after LT treatment.

Immunofluorescence stains of actin (red) after 48 hours LT treatment, 1 hour cytochalasin B and 35 minutes of cytochalasin B wash-out with fresh media, displayed the ability of actin to polymerize. Scale bar represents 50 μ m. Abbreviations: -, untreated; CytoB, cytochalasin B, LatA, latrunculin A; LT, lethal toxin.

By fractionation of cell lysates in cytosol, membrane and cytoskeleton, we were able to detect an increase of actin in the LT treated cytoskeletal fraction. (Figure 5-16) GDI was used as a cytosol marker.

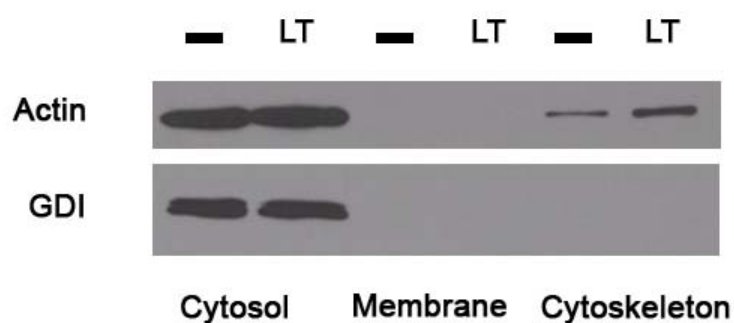


Figure 5-16: Increased actin amounts in cytoskeletal fraction after LT treatment.

Amount of actin and GDI in cytosol, membrane and cytoskeletal fractions after 48 hours LT treatment. GDI was used as a cytosol loading control. Abbreviations: -, untreated; GDI, GDP dissociation inhibitor; LT, lethal toxin.

After LT treatment microtubules showed bundle-like structures, which were directed towards the periphery. (Figure 5-13) Tubulin can be modified by acetylation, tyrosination, polyglutamylation, polyglycylation, palmitoylation and phosphorylation. (Table 2-2) To test, if LT induced changes, leading to loss or increase in tubulin stabilization, we prevented their polymerization with an inhibitor called nocodazole after LT treatment. Acetylation occurs only at α -tubulin and is a marker for their stability. It regulates cell motility and binds microtubule-associated proteins (MAPs) to microtubules.

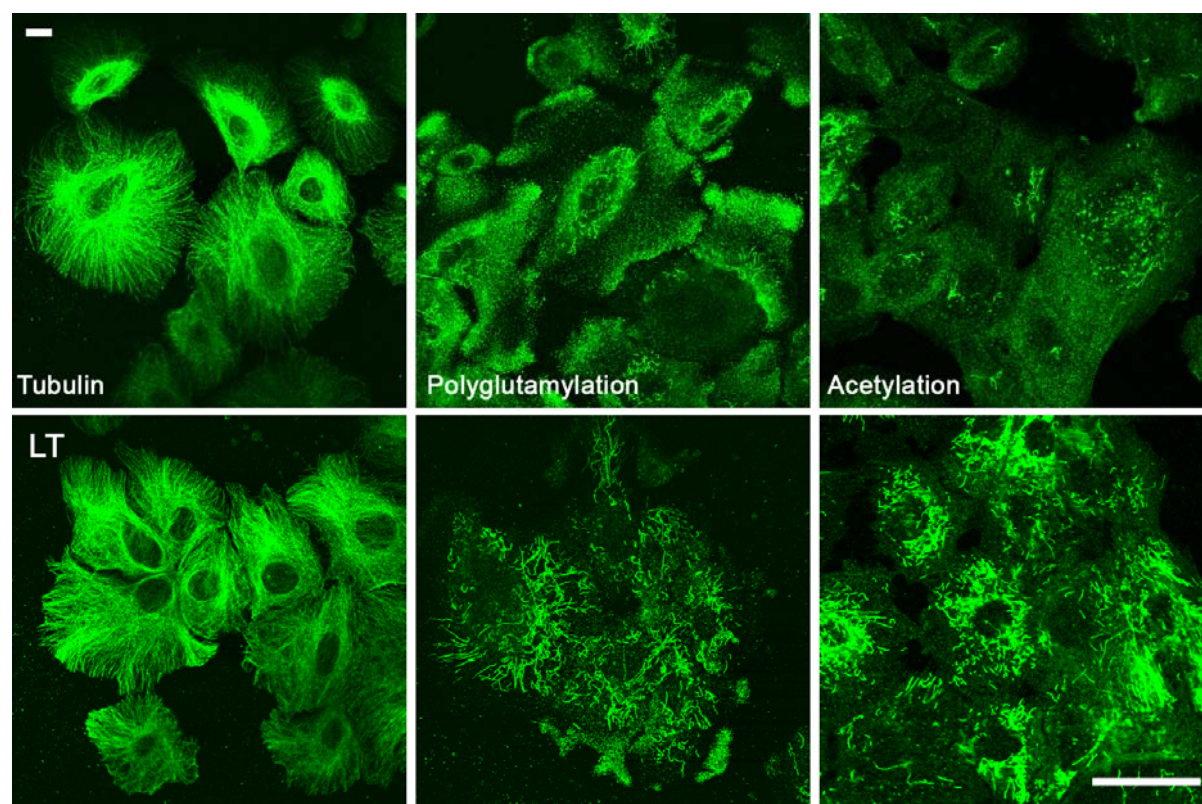


Figure 5-17: Increased tubulin stabilization after LT treatment.

IF stain of tubulin after LT exposure. Polyglutamylation and acetylated tubulin after 48 hours of LT and 1hour nocodazole treatment. Scale bar represents 50µm. Abbreviations: -, untreated; LT, lethal toxin.

Up to 20 side-chain residues of glutamic acid can be added to α - and β -tubulin, which is called polyglutamylation. This stabilizes microtubules and regulates the interaction with MAPs. Using antibodies detecting acetylation and polyglutamylation an increase in microtubule stability was detected in lethal toxin treated cells in IF. (Figure 5-17) Therefore, we showed, that lethal toxin changes the cytoskeleton by increasing the amount of actin filaments and stabilizing microtubules.

5.3.2 Motility Defects

Imbalance in cytoskeletal proteins often causes changes in motility. To migrate, cells need to polarize and extend their protrusions on the front side. Those protrusions can be wide lamellipodia and fine filopodia. By anchoring the cytoskeleton with adhesion molecules to the extracellular matrix, the front will be stabilized, while the disassembly of actin at the rear end takes place, allowing the tail to detach and move forward.

The accumulation of actin stress fibers and stable tubulin could influence the cell shape and motility. Therefore, we performed a wound healing experiment that is also called scratch assay. 21 hours after scratching the cell layer, the ability of wound closure was evaluated by an actin immunofluorescence stain. Figure 5-18 showed the originally scratch (0hr), whereas the next pictures were taken after 21 hours later. At that time, untreated cells and the inactive mutant of LF (E687C) were able to almost completely close the wound. Lethal toxin treated cells did not migrate into the wound, which indicated a defect in cell motility.

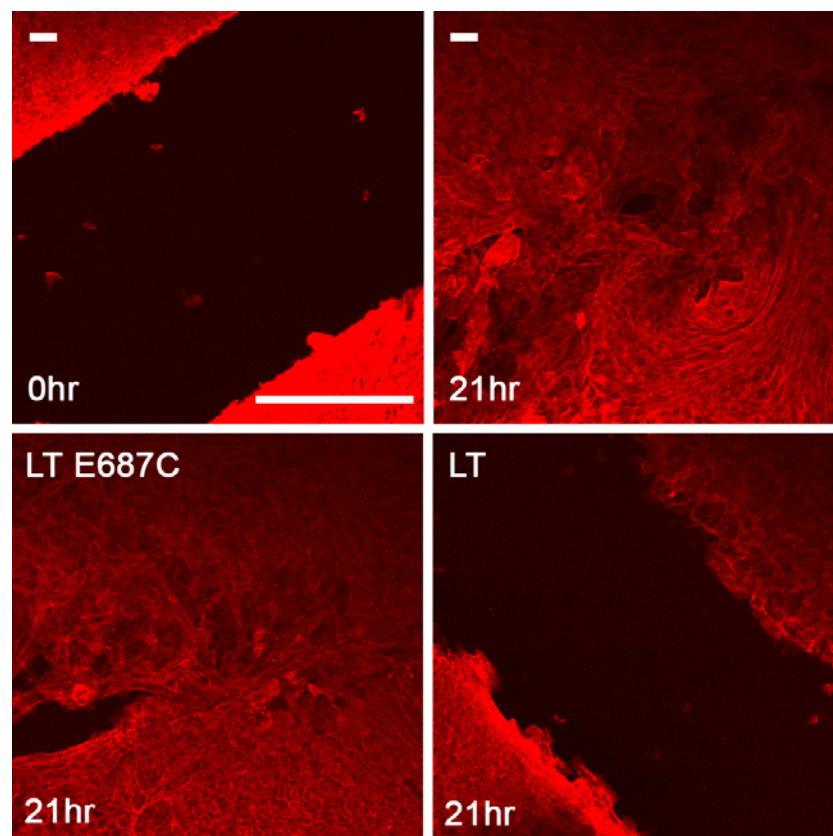


Figure 5-18: Wound healing defect caused by LT.

Scratch of 3D polarized cells right after scratching (0hr) and 21 hours after wounding with visualized with F-actin stain (red). Untreated (-) and the non-proteolytic active LT (E687C) mutant close the wound, whereas LT did not migrate into the scratch. Scale bar represents 100 μ m. Abbreviations: -, untreated; LT, lethal toxin.

We determined, if the directed migration towards a chemical stimulus would allow cell polarization and enhance the motility. Cells migrating through the pores were attracted by chemoattractants, such as EGF to the other side in 21 hours. (Figure 5-19, D-E) To prove similar attachment on the top of the chamber, we stained NHBE after one hour with actin and a nuclear marker (Figure 5-19, A-C). The attachment of cells with no treatment (Figure 5-19, A), LT (Figure 5-19, B) or the inhibition of all downstream MAPK pathways (Figure 5-19, C) showed comparable adherence. In contrast, the migration to the other side towards the stimulus was only achieved by non-treated cells (Figure 5-19, D). Therefore, a defect in chemotaxis and wound healing is caused by lethal toxin treatment.

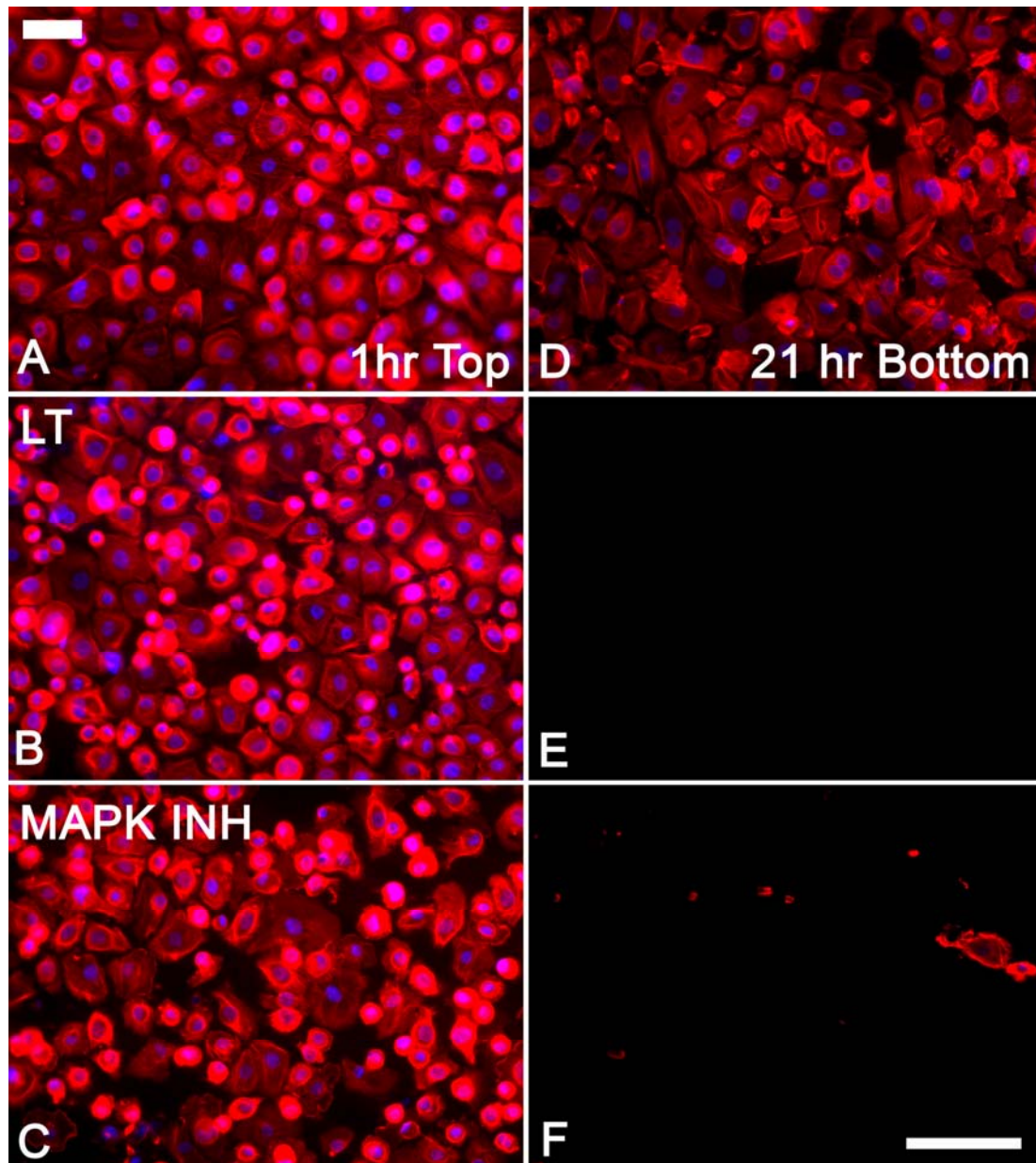


Figure 5-19: Chemotaxis defect of LT and MAPK inhibitors treated cells.

A-C) Similar attachment of different treated cells stained with actin (red) and dapi (blue) after one hour adhesion from the top. D-F) Migrated cells were visualized after 21 hours on the bottom side of the chamber with actin and dapi. D) Untreated cells migrated through the pores. E, F) LT and MAPK inhibited cells could not migrate to the side of stimulation. Scale bar represents 100 μ m. Abbreviations: -, untreated; LT, lethal toxin.

The tubulin stain in **Figure 5-13** revealed the ability to form protrusions after LT exposure. However, cytoskeletal proteins seem to accumulate and defects in migration were observed causing defects in motility. To observe the cells after lethal toxin treatment under live conditions, we performed live cell imaging with a global stimulation of EGF supplemented media. Pictures were taken every minute for up to 2 hours. (**Movie 1**, **Movie 2**) **Figure 5-20** displays one frame of the **Movie 2 (LT treated)**, showing multiple protrusion sides all over the cell edge. The toxin treated cells are unable to polarize in one direction. The **Movie 1, untreated** showed clearly the smooth lamellipodia growth in the untreated cells and their ability to polarize and migrate. LT treated cells extended rapidly undirected protrusions. (**Movie 2**)

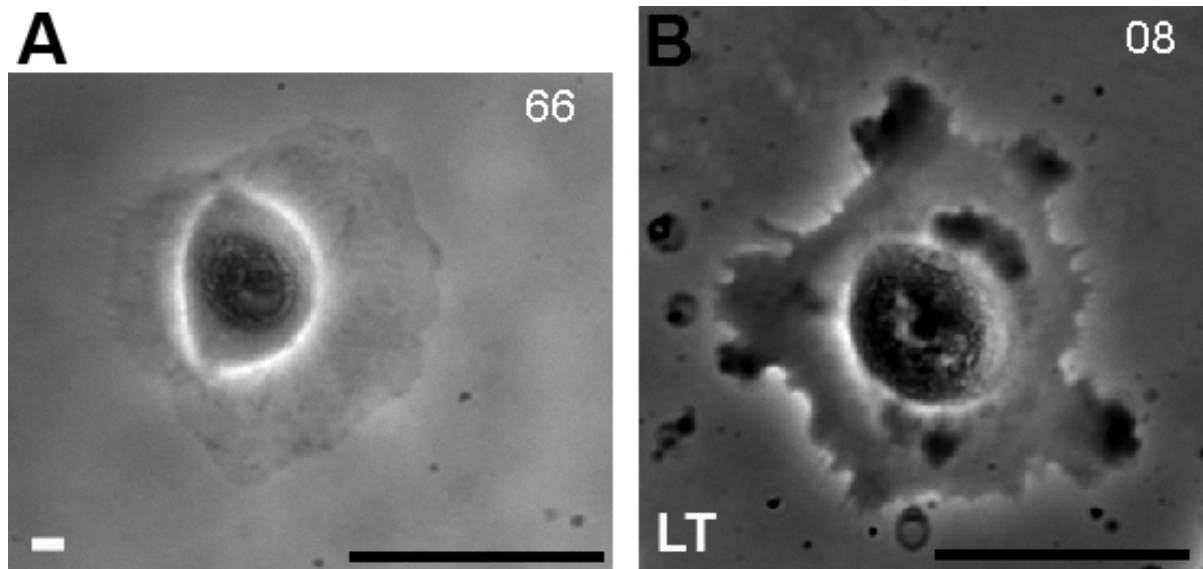


Figure 5-20: Live cell imaging picture.

A) A typical polarized phenotype of a migrating cells after global EGF stimulation, taken from Movie1. B) LT treated cell with many unpolarized protrusion from Movie2. The time frame in minutes of the movie is indicated at the upper hand corner. Scale bar represents 50 μ m. Abbreviation: -, untreated; LT, lethal toxin.

5.3.3 Adhesion Alteration After LT Treatment

Adhesion of cell surface proteins to the extracellular matrix is a crucial factor for cell migration and spreading. Focal adhesions are formed behind the leading edge of moving cells. They assemble a stationary plaque from where the focal adhesions grow. Vinculin, α -actin, talin and paxillin are proteins of the focal adhesion complex. These adhesion molecules are associated also with actin filaments. Immature focal contacts are increased, when microtubules are disrupted with inhibitor such as nacodazole. [204]

The motility change after LT treatment might be caused by adhesion defects to the extracellular matrix. Vinculin is known to play a major role in connecting the integrins or adherens junctions with the cytoskeleton. Therefore, we tested if adhesion molecules are altered and responsible for the motility alteration. First, we performed an immunofluorescence stain for vinculin (**Figure 5-21**), which suggested, that LT treatment partilly enlarged focal contacts.

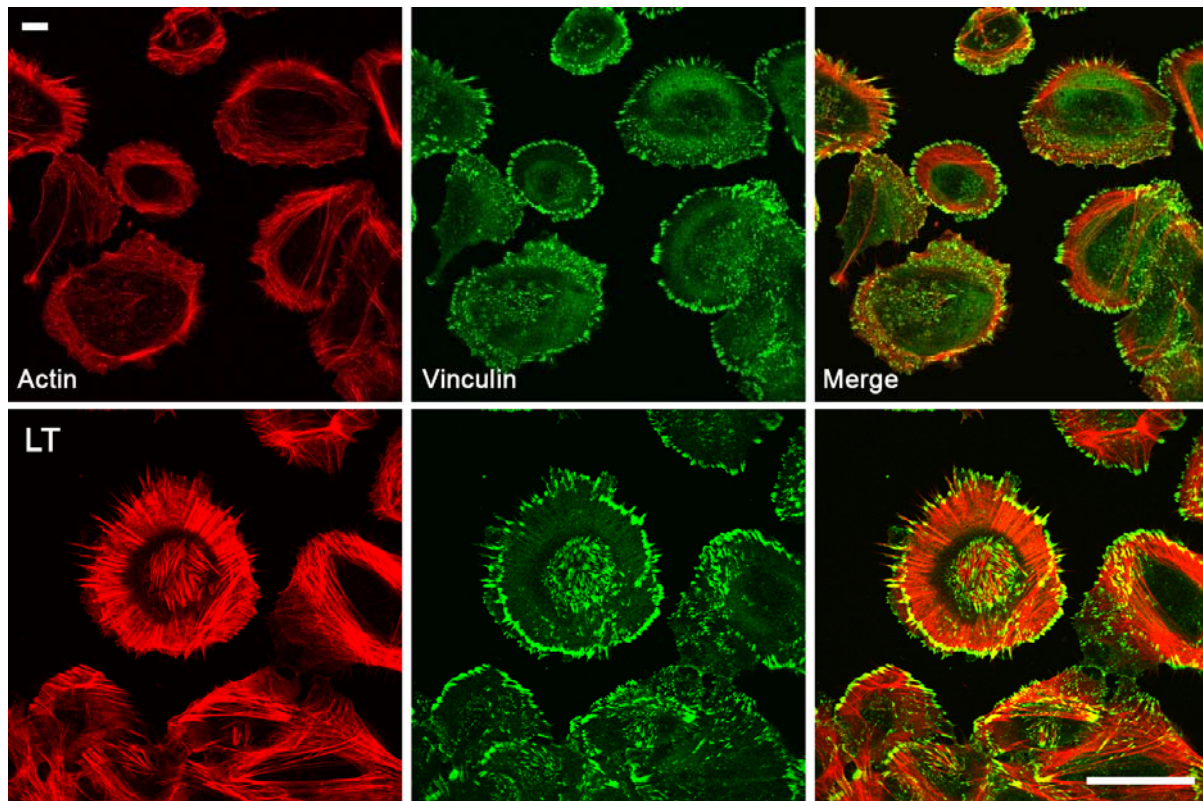


Figure 5-21: Elongation of focal adhesion.

Comparison of untreated and 48 hours LT treated NHBE in immunofluorescence of actin (red), vinculin (green) and merged image. Actin stress fiber formation and slightly elongated focal adhesions were seen after LT treatment. Scale bar represents 50 μ m. Abbreviations: -, untreated; LT, lethal toxin.

Since the IF stain did not show noticeable differences in vinculin formation, we thought that the fractionation of focal adhesion proteins could give a clearer picture of occurring changes. (Figure 5-22) Vinculin is mainly localized at the cell periphery and interacts with the cytoskeleton and the cytosolic part of E-cadherin to promote motility. Paxillin is like vinculin a focal adhesion molecule. It binds to actin and modulates effector molecules such as PAK, PIX and the Rho GTPase family, which are involved in cytoskeletal rearrangement and migration. Those focal adhesion molecules are regulated by phosphorylation through protein tyrosine kinases such as FAK and Src. [205]

Comparison of vinculin and paxillin in the cytosol, membrane and cytoskeleton showed a slight increase in the cytoskeletal fraction. Furthermore, paxillin seem to have a reduced expression in the cytosolic fraction. However, FAK expression was not significantly altered. To prove no cross contamination in the other fractions, GDI was chosen as a cytosolic protein.

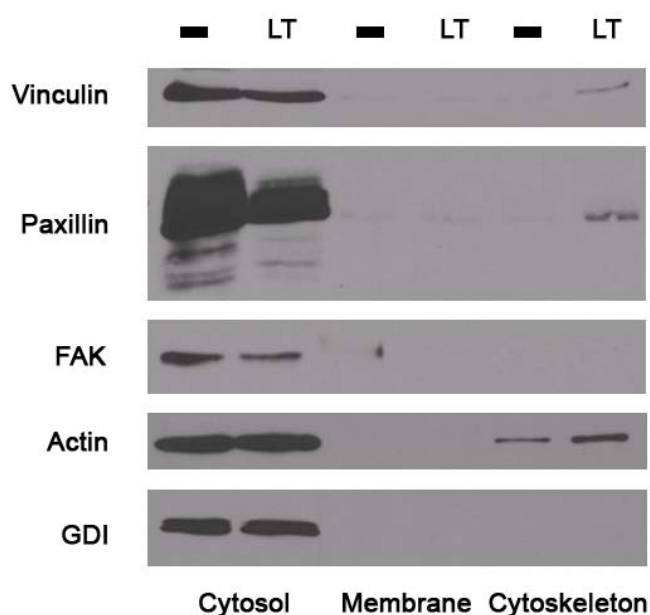


Figure 5-22: Fractionation of adhesion proteins and their regulatory proteins.

The adhesion proteins vinculin and paxillin were increased in the cytoskeletal fraction of NHBE with LT treatment. Paxillin is decreased in the cytosolic fraction. FAK was not altered. GDI was used as a cytosol loading control. Abbreviations: -, untreated; LT, lethal toxin, FAK, focal adhesion kinase, GDI, GDP dissociation inhibitor.

Activation of FAK and paxillin occurs by phosphorylation. N-terminal phosphorylation of paxillin by FAK and Src regulates the downstream effectors CDK, which mediated the gene expression levels of MAPKK. [205] Paxillin has a couple of phosphorylation sites, such as Y31, Y118 and Y181. The phosphorylation Y118 regulates cell-cell adhesions. FAK can be phosphorylated at 8 tyrosine sites, after integrins interact with the extracellular matrix. The FAK phosphorylation site Y397 is a Src binding site and important for EGF stimulated motility. [206]

We tested for phosphorylation of FAK at Y397 and Src at Tyr416 and could not detect any changes. (Figure 5-23, A-B) However, the phosphorylation of paxillin at Y118 seemed to be decreased after LT treatment, but compared to the protein expression not changed. (Figure 5-23, C) The lower expression might be involved in motility defects, since there is less paxillin expressed over all.

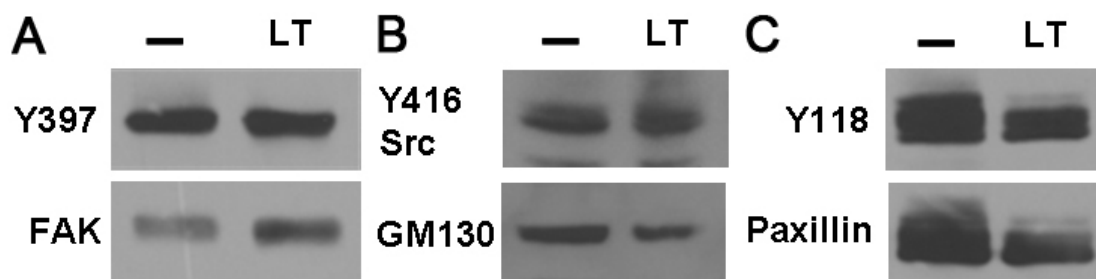


Figure 5-23: Phosphorylation of adhesion proteins are not altered after LT treatment.

A) Expression of total FAK and its Y397 phosphorylation site B) Phosphorylation of Y416 Src are not altered. C) Lower expression of total paxillin and its Y118 phosphorylation site after LT treatment. B) GM130 was used as a loading control for the phosphorylation of Src. Abbreviations: -, untreated; FAK, focal adhesion kinase; LT, lethal toxin; GM130, cis-golgi matrix protein 130kDa.

Because of the focal adhesion increase in paxillin and vinculin as well as the slight decrease in the cytosolic fraction of paxillin, we determined the effect on the actual adhesion process of different coated surfaces. Therefore, we measured only viable, attached cells, which were untreated or LT treated after replating by an MTT assay. Integrin mediated adhesion to fibronectin and collagen was not significantly changed. (Figure 5-24) Instead, cells were unable to adhere to positively charged surfaces such as tc-treated and poly-L-lysine.

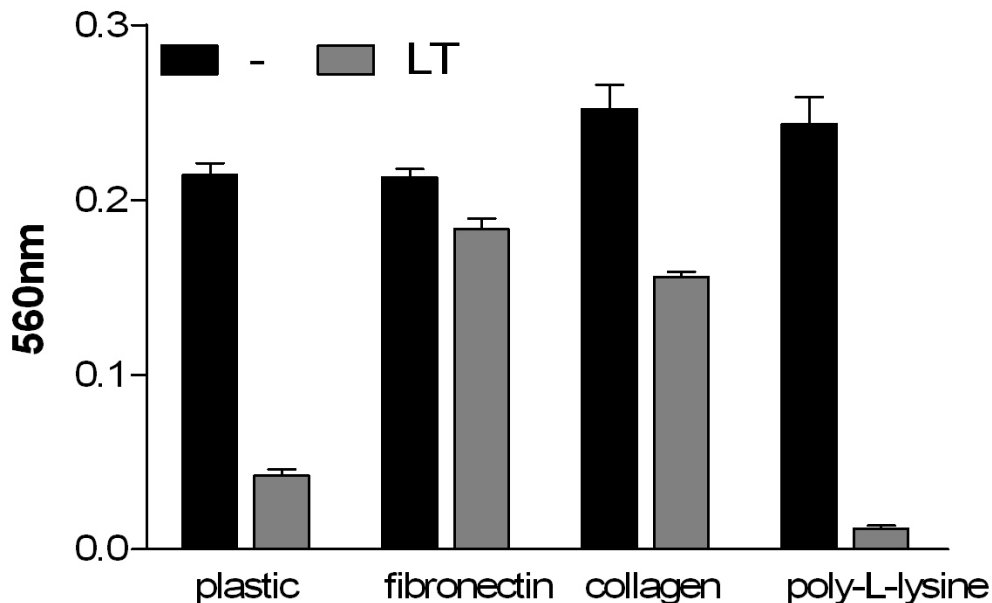


Figure 5-24: Adhesion defect to positive charged surfaces after LT treatment.

Attachment of viable cells (MTT-assay) after replating untreated or 48 hours LT (1 μ g/ml) treated NHBE at indicated surface coated dishes for 21 hours. Abbreviations: -, untreated; LT, lethal toxin; nm, nanometer.

5.3.4 Effector Molecules for Cytoskeleton and Motility Changes

Rho GTPases were shown to induce cytoskeletal rearrangements. The involvement in the regulation of many proteins was studied, such as WASP, which by themselves activate the Arp2/3 complex. The Arp2/3 complex is needed for the initiation of the actin filament formation.

Stress fibers can be caused by an increase of RhoA activity by inducing actin polymerization through mDia signaling and inhibition of actin depolymerization by reducing cofilin activity (RhoA \rightarrow MLCK \rightarrow LIMK \rightarrow cofilin). Measuring mRNA expression did not reveal any changes after LT treatment. (Figure 5-25, A) We were unable to detect any RhoA activity or observed differences of expression in the lysates. (Figure 5-25, B) In addition, we measured protein expression levels of RhoB and C, which were also not altered. (data not shown)

Higher Rac1 activity increases lamellipodia formation. Since LT treatment causes protrusions, it was important to determine, if Rac1 plays a role in this process. The amounts of active Rac-1 were very similar between untreated and LT treatment and therefore, not responsible for the lamellipodia formation. (Figure 5-25, B) NHBE cells did not form filopodia after LT treatment. Cdc42 induces filopodia formation and is involved in cell polarization. The activity of Cdc42 was increased after LT treatment, which might explain why LT treated cells were unable to polarize.

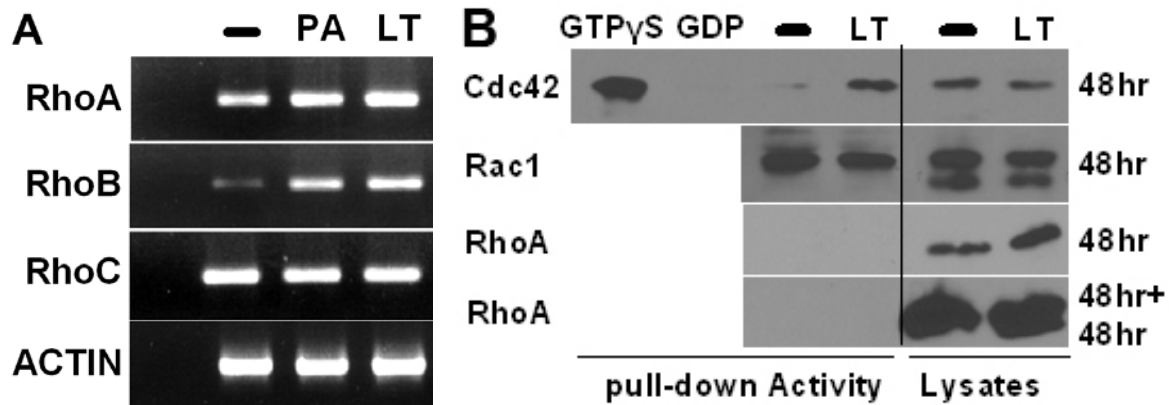


Figure 5-25: RhoGTPase mRNA and protein activity measurements.

A) RT-PCR of RhoA, B and C of untreated, PA and LT treated NHBE. The first lane did not contain any cDNA. Equal loading was defined by actin expression. B) GTPase activity and normal expression levels after 48hr or 48+48hr of LT treatment were displayed. GTPγS bound to Cdc42 was used as positive and inactive GDP bound Cdc42 was used as negative control. [207] Abbreviations: -, untreated; GDP, guanosine diphosphate; GTPγS, guanosine 5'-O-thiotriphosphate; hr, hours; LT, lethal toxin; PA, protective antigen.

Furthermore, we tested other proteins involved in actin formation. mDia acts downstream of RhoA. It increases actin polymerization and stabilizes microtubules. We compared the localization and expression levels in immunofluorescence which was similar between treatments. (data not shown) Cofilin is an actin-depolymerizing factor, which binds actin and promotes the dissociation of the G-actin. It is regulated by phosphorylation. In western blot analysis, we could not detect significant differences in the phosphorylation pattern. (data not shown) In addition, the Arp2/3 complex is a major key regulator of the actin cytoskeleton. Therefore, we examined modifications in immunofluorescence without any clear difference seen. (data not shown)

5.4 Involvement of the MAPK Pathway

MAPKKs can influence the cytoskeleton and are the only known substrates of LT. Since tested proteins involved in the cytoskeletal rearrangement were not the main key player in the motility defect, we decided to compare the inhibition of the MAPK to the LT effects on wound healing. **Figure 5-26** shows, that the inhibition of only the MEK1/2, p38 or JNK pathway by itself induces slight closure of the wound. However, with a combination inhibition of all three MAPK pathways, cells were unable to migrate into the wound. Therefore, the motility defect could be caused by the loss of activation of the downstream effectors by the MAPKK cleavage. The inactive LT (E687C) mutant closed the wound in the same way compared to untreated.

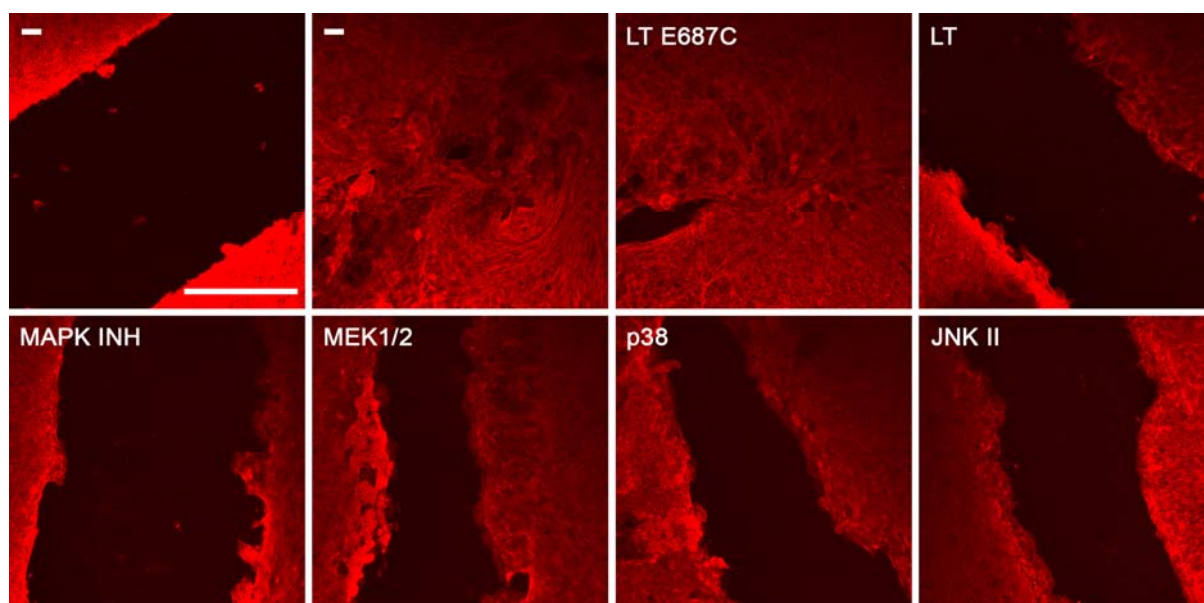


Figure 5-26: MAPK pathways are important for wound healing.

Polarized NHBE treated with LT or inhibitors for 48 hour. Scratch in picture one (upper left), displays original scratch. All other actin stained (red) cell scratches were imaged 21 hours after original scratch. LT and three MAPK inhibitor combinations were defective in wound closure, whereas the single inhibitors MEK1/2, p38 and JNKII partially migrated in the wound. Inactive LT (E687C) behaved like untreated cells. Abbreviation: -, untreated; JNKII, Jun N-terminal kinase II; LT, lethal toxin; MAPK INH, mitogen activated protein kinase inhibitor combination; MEK1/2, mitogen activated ERK kinase.

The quantification of the wound was performed by measuring ten times the wound distance of 4 scratches in two different experiments. A wide wound length indicates the inhibition of migration. (Figure 5-27) The zero time point shows the originally scratch. The three inhibitor combinations have similar motility defects, followed by the JNK inhibition.

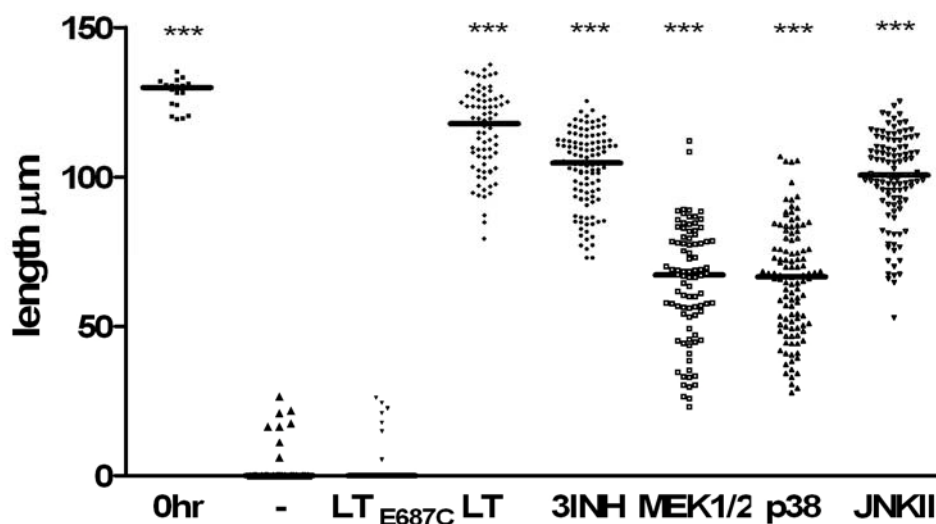


Figure 5-27: Quantification of wound healing defects.

Almost complete closure was shown by untreated and LT (E687C) cells. MEK1/2 and p38 inhibition closed the wound for around 50% compared to untreated. LT, JNK and 3 inhibitor combination were defective in wound healing. The scatter graph indicates the original scratch at 0hr. Abbreviations: -, untreated; JNKII, Jun N-terminal kinase II; 3INH, inhibitor combination of MEK1/2, p38 and JNKII; hr, hours; LT, lethal toxin; MEK1/2, mitogen activated ERK kinase.

We compared the migration behavior of MAPK inhibited cells with LT treated cells to determine if the MAPK pathway is involved in global stimulated motility defects. Therefore, we performed live cell imaging. After 24 hours of inhibition pictures were taken for around 40 minutes with a frame per 30 seconds.

In **Movie 3** untreated cells were able to migrate with smooth protrusion formation. Whereas in **Movie 4** lethal toxin treated cells were not motile and had many disoriented lamellipodia. Inhibition of all three MAPK pathways with a three inhibitor combination confirmed the lethal toxin phenotype shown in **Movie 5**. To distinguish if one of the MAPK pathways, ERK, p38 or JNK had a higher impact in motility changes, we also imaged individual MKK1/2, p38 and JNK II inhibitors, which are shown in the following movies, **Movie 6**, **Movie 7**, **Movie 8**. All of those inhibitors seem to have an increase in protrusion formation. The majority of cells were also unable to migrate, but a few cells were capable of moving. This agrees with the wound healing assay, which indicated partially motility when only one MAPK inhibitor was used. However, we were unable to distinguish which of the three pathways is more important for the migration effect. Therefore, we focused on the reintroduction of non-cleavable MAPKK mutants by lentivirus infections to rescue the effect of LT. (**Table 4-3**) The EGFP controls showed the same motility phenotype seen in untreated and LT treated cells. (**Movie 9**, **Movie 10**) Interestingly, we observed no rescue effect, when we reintroduced a single MAPKK. (data not shown) In **Figure 2-15**, it is shown, that a MAPKK combination (MEK1+2, MKK3+6 and MKK4+7) lead to the activation of one MAPK pathway (ERK, p38 and JNK). Therefore, it is possible that the addition of only one upstream MAPKK is not sufficient. A double infection of MEK1+2 and MKK3+6 gave us a partially rescue effect in motility and decreased lamellipodia extension. (**Movie 11**, **Movie 12** untreated; **Movie 13**, **Movie 14** LT) MKK4+7 did not have any positive effects of the LT treated cells. (**Movie 15** untreated, **Movie 16** LT) The results of the movies indicate the involvement of the ERK and partially of the p38 pathway in motility defects, caused by LT induced MAPKK cleavage.

5.5 Rescue Effect of the Permeability and Resistance

Keratinocyte growth factor (KGF) and dexamethasone are used in clinical lung diseases to improve injuries. The mechanism behind the healing effect is not completely understood. It was shown, that KGF plays a role in repairing and protecting against lung injuries by stimulating the growth of alveolar type II cells. [208, 209] Dexamethasone is a glucocorticosteroid, which has anti-inflammatory and immunosuppressive effects. Conditions of neonatal chronic lung diseases improved after 72 hours of dexamethasone treatment, by maturing the surfactant phosphatidylcholine. [210] Dexamethasone reduced the expression of the mucin protein MUC5AC in lung epithelial cell, decreasing the mucus secretion. [211] This change in surfactant and mucus production helped in the protection of lung injuries.

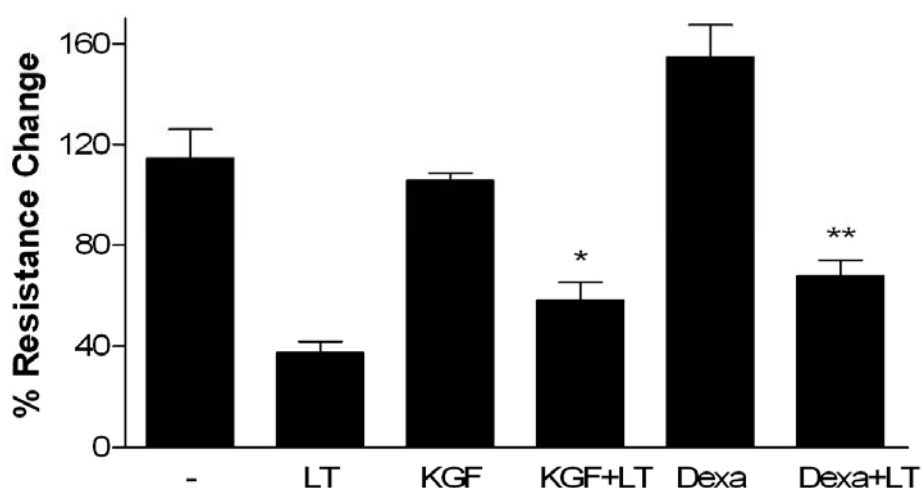


Figure 5-28: Rescue of resistance by KGF and dexamethasone.

Three weeks differentiated NHBE were pretreated with 250ng/ml KGF and 10 μ M dexamethasone for one hour and stimulated with 1 μ g/ml LT for 48 hours. KGF and dexamethasone led to increased resistance. Resistance was determined by usage of an EVOMX. Abbreviations: -, untreated; Dexa, dexamethasone; KGF, keratinocyte growth factor; LT, lethal toxin.

We determined if the pretreatment with both substances, would have a rescue effect on the epithelial cell disruption in 3D. After one hour pretreatment with KGF or dexamethasone and 48 hours of LT treatment a significant improvement of resistance and permeability was detected. (Figure 5-29, Figure 5-30) Dexamethasone increased the resistance of untreated and LT treated cell, whereas KGF influenced only LT damaged cells. Even if KGF and dexamethasone could not rescue the permeability and resistance effect completely, it could be considered as a prophylactic treatment of patients with anthrax infection to decrease the respiratory distress.

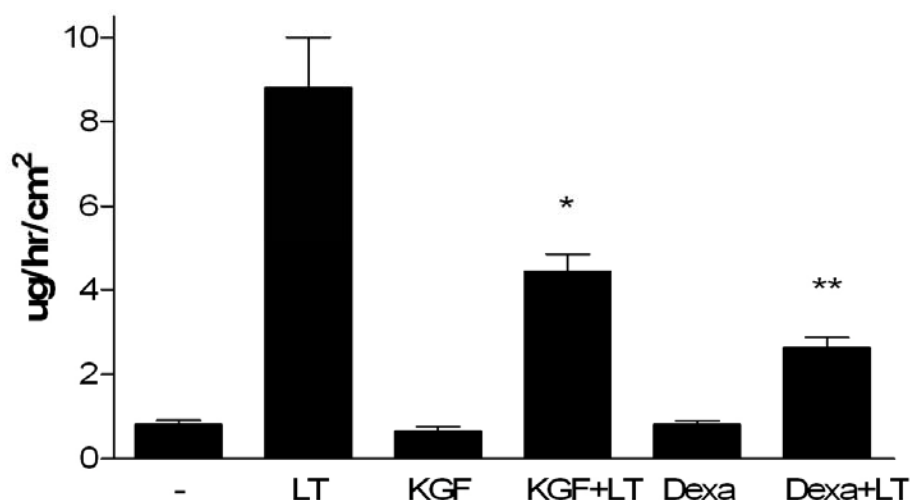


Figure 5-29: Rescue of permeability increase by KGF and dexamethasone.

Three weeks differentiated NHBE were pretreated with 250ng/ml KGF and 10 μ M dexamethasone for 1hour and stimulated with 1 μ g/ml LT for 48 hours. KGF and dexamethasone rescued the permeability increase caused by LT. The cell permeability was determined by adding FITC-albumin on top of the cells and measuring amount of the dye leaking through the layer into the basal compartment. Abbreviations: -, untreated; Dexa, dexamethasone; KGF, keratinocyte growth factor; LT, lethal toxin.

To test if KGF and dexamethasone have also a positive effect on cell viability, we compared the release of the cytosolic protein LDH in the media. LT induced 12% of cytotoxicity, which could be decreased to 8% by dexamethasone and 5% after KGF treatment. (Figure 5-30) The reduction of cell death could be the reason for the decreased cell layer damage seen by resistance and permeability improvements.

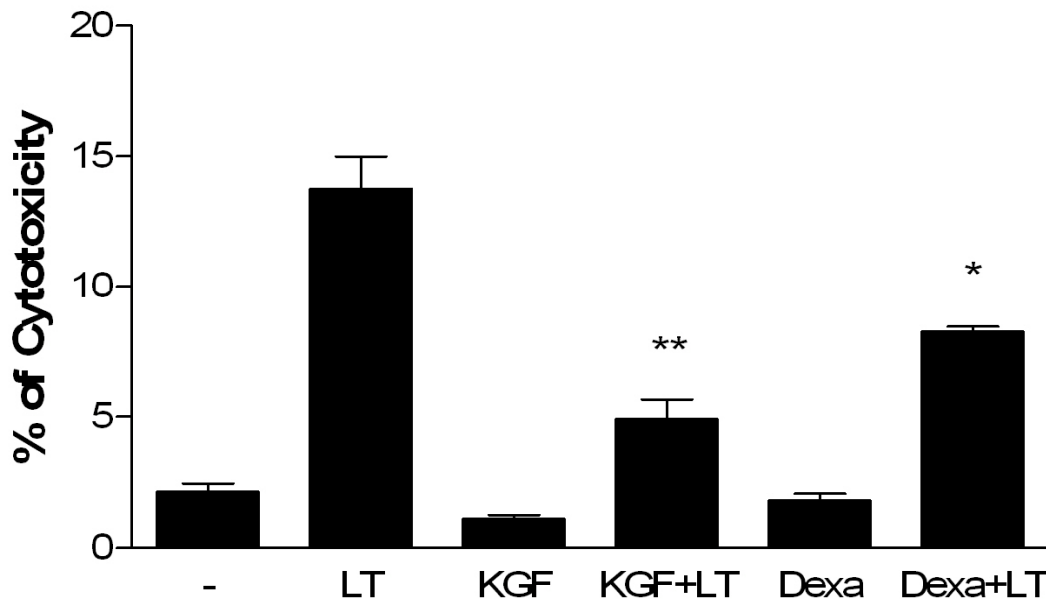


Figure 5-30: KGF and dexamethasone increase cell viability.

Three weeks differentiated NHBE were pretreated with 250ng/ml KGF and 10 μ M dexamethasone for one hour and stimulated with 1 μ g/ml LT for 48 hours. KGF and dexamethasone increased cell viability, which was determined in the basal media by LDH release. Abbreviations: -, untreated; Dexa, dexamethasone; KGF, keratinocyte growth factor; LDH, lactate dehydrogenase; LT, lethal toxin.

5.6 Cell Viability After LT Treatment

Murine macrophages from susceptible mouse strains undergo cell death in less than 3 hours after lethal toxin treatment. Human cells were proven to be more resistant. To determine, if human bronchial epithelial cells have a decreased cell viability, we used several different cell death assays.

First, we determined the membrane integrity by phosphatidylserine exposure. (Figure 5-31) Apoptotic cells flip phosphatidylserine towards the outer membrane side. Lethal toxin treated and untreated cells did not reveal increased membrane damage after 48 hours. (Figure 5-31, B-C) As control the protein synthesis inhibitor cyclohexamide was used and caused in 18% of the cells a membrane breakdown resulting in the exposure of phosphatidylserine to the outer membrane. (Figure 5-31, A)

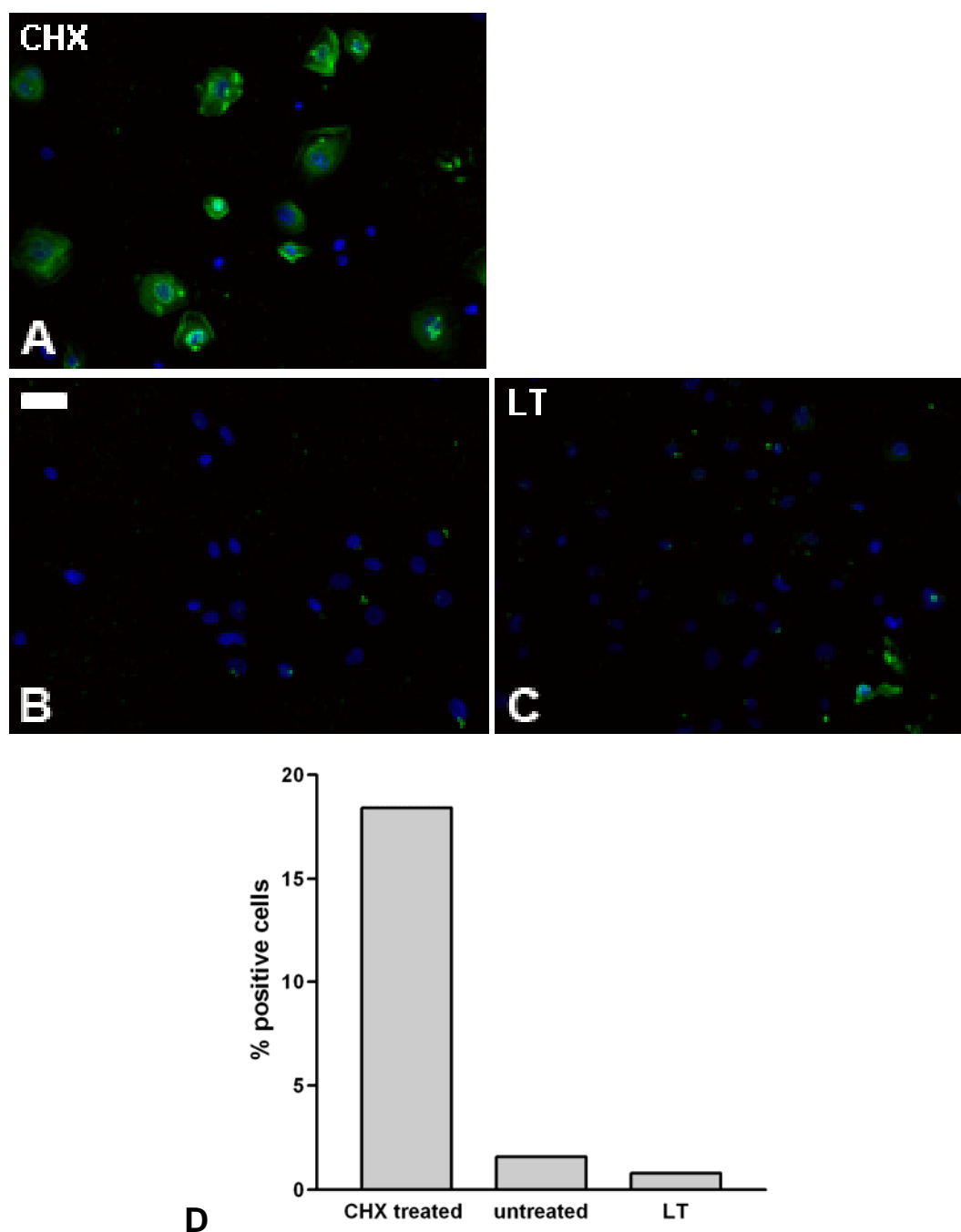


Figure 5-31: Lethal toxin does not alter membrane integrity.

A) Cyclohexamide is an inhibitor of protein synthesis and was used as positive control inducing the phosphatidylserine exposure to the outside of the cell. B) untreated and C) LT treated cells did not show any significant membrane integrity change. DAPI stained the DNA in the nucleus (blue). D) Quantification of 500 cells was shown in % of positive cells. Abbreviation: -, untreated; %, percent; CHX, cyclohexamide; DAPI, 4',6-diamidino-2-phenylindole dihydrochloride; LT, lethal toxin.

Apoptotic cells show fragmentations of nuclear DNA, which can be detected by connecting fluorescence dUTPs with a transferase into DNA strand breaks. To detect the total amount of cells, we stained the nuclei also. DNase1 nicked the DNA and was used as positive control and caused in all cells breakage of the DNA. (Figure 5-32, A) This was not observed in untreated or LT treated cells, which was shown by the quantification of 500 cells. (Figure 5-32, B) Therefore, LT does not affect DNA integrity.

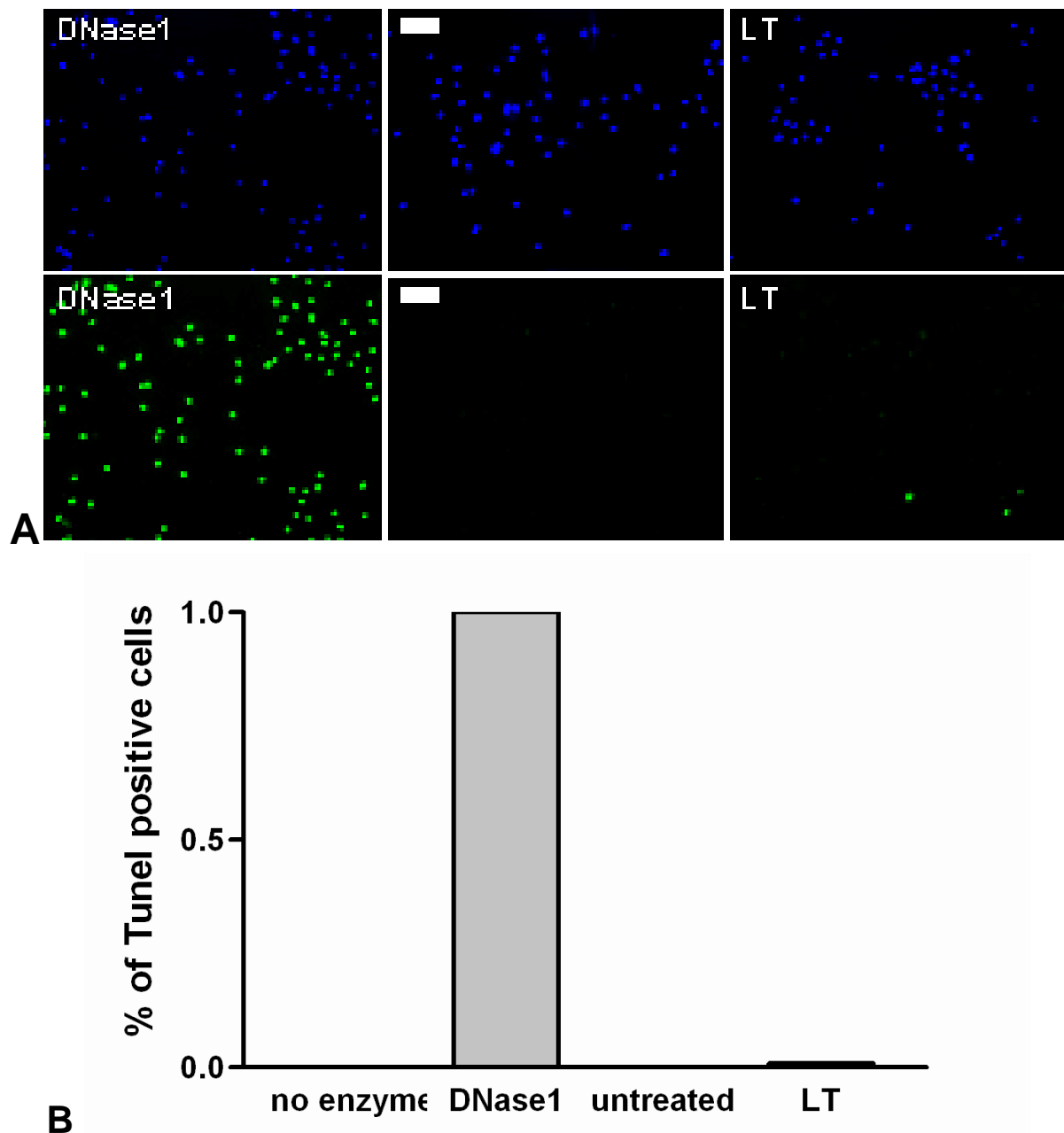


Figure 5-32: Minimal DNA strand breaks after LT treatment measured in a TUNEL assay.

A) Immunofluorescence to visualize DNA strand breaks (green). DNase 1 was used as positive control to introduce nicks in the DNA. No increase in DNA damage was seen in untreated or LT treated cells. DAPI (blue) was used to visualize the nucleus of the cells. B) Quantification of 500 cells is shown in the bar graph. Abbreviation: -, untreated; DAPI, 4',6-diamidino-2-phenylindole dihydrochloride; LT, lethal toxin.

Caspases are cysteine proteases involved in apoptosis, cytokine production and inflammation. Caspases are synthesized as inactive pro-caspases. This allows rapid autoactivation and induction of the caspase cascade leading to cell death. Caspase 3 activity can be detected by the cleavage of proteins such as PARP and ROCK-1. After 48 hours of LT treatment, we did not observe any caspase activity. (Figure 5-33)

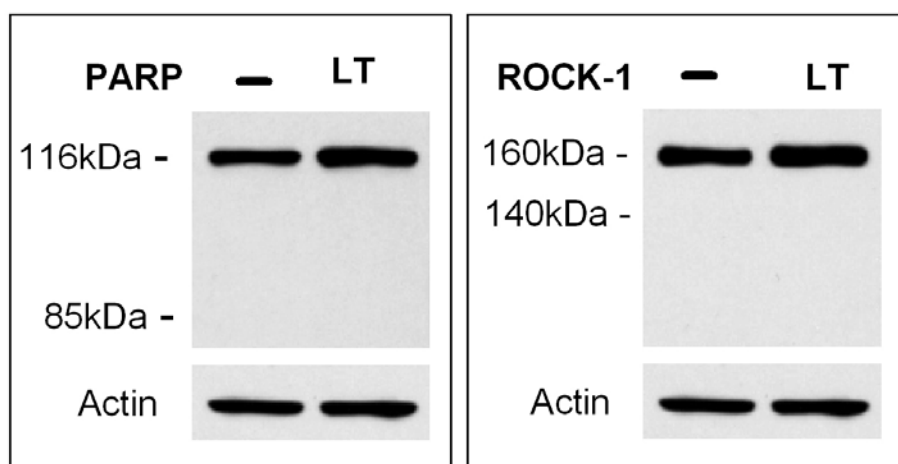


Figure 5-33: Caspase 3 activation is not induced by LT.

Western blot of PARP and Rock-1 cleavage after 48 hours of untreated and lethal toxin treated cells. Actin was used as loading control. Abbreviation: -, untreated; kDa, kilo Dalton; LT, lethal toxin; PARP, Poly ADP-ribosepolymerase; ROCK1, Rho-associated coiled-coil protein kinase 1.

5.6.1 Proliferation Decrease Due to Cell Cycle Arrest

Lethal factor did not induce any kind of cytotoxicity in epithelial cells after 48 hours of treatment, which was shown above. Also, the proliferation rate was not altered at that time point. (Figure 5-34, 48hr) However, when NHBE cells were grown longer than 48 hours lethal toxin treatment, they were unable to recover normal proliferation rates compared to untreated cells. Furthermore, slight losses of metabolic active cells were seen after 48+48 hours and 48+96 hours. (Figure 5-34)

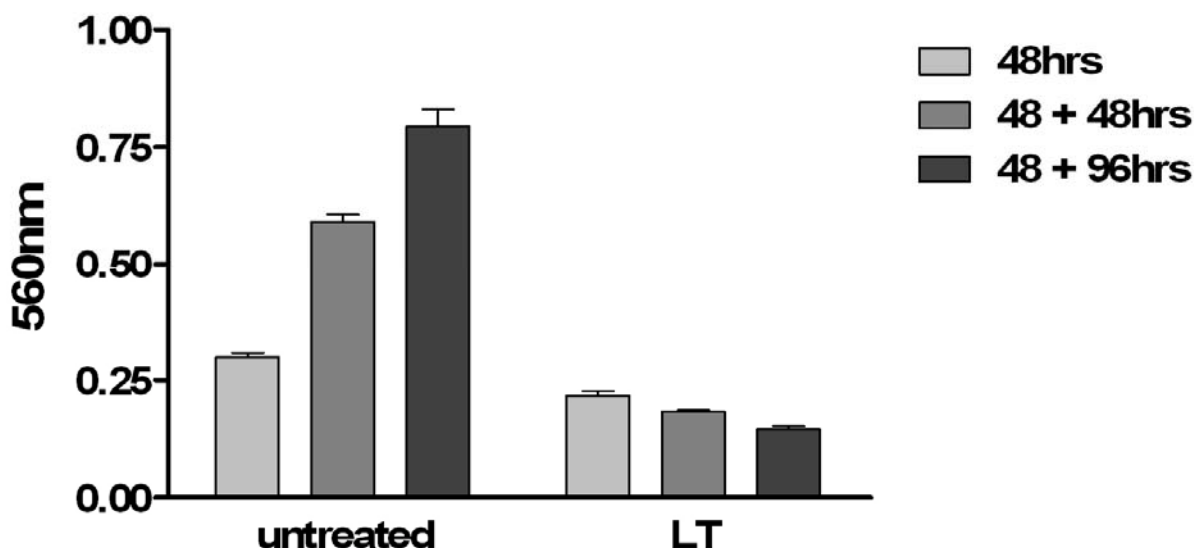


Figure 5-34: Blocked cell proliferation after LT treatment.

Proliferation measurements (MTT) were performed after 48 hours of LT treatment and an addition 48 hours and 96 hours of recovery in non-treated media. Abbreviation: hrs, hours; LT, lethal toxin; nm, nanometer.

Proliferation inhibition might be caused by a defect of cell cycle progression. Therefore, we determined the cell amount in the G1 phase versus S/G2/M at different time points. (Figure 5-35, C) After 48 hours treatment the levels were

comparable between untreated and lethal toxin treated cells. When lethal toxin was washed away and cells were grown for an additional 48 or 93 hours, the cell numbers in S/G2/M phase were decreased. One example is shown in Figure 5-35, A-B to demonstrate the G1 arrest. Looking at expression levels of proteins (cyclin B and E2) controlling the cell cycle did not show any changes after 48 hours of treatment. (data not shown) However, this G1 arrest was also shown in murine macrophages by the downregulation of cyclin D. [173] MAPKKs and the cytoskeleton are very important for cell division and might not only affect cytokineses, but also, the chromosome assembly and orientation of the MTOC in LT treated cells.

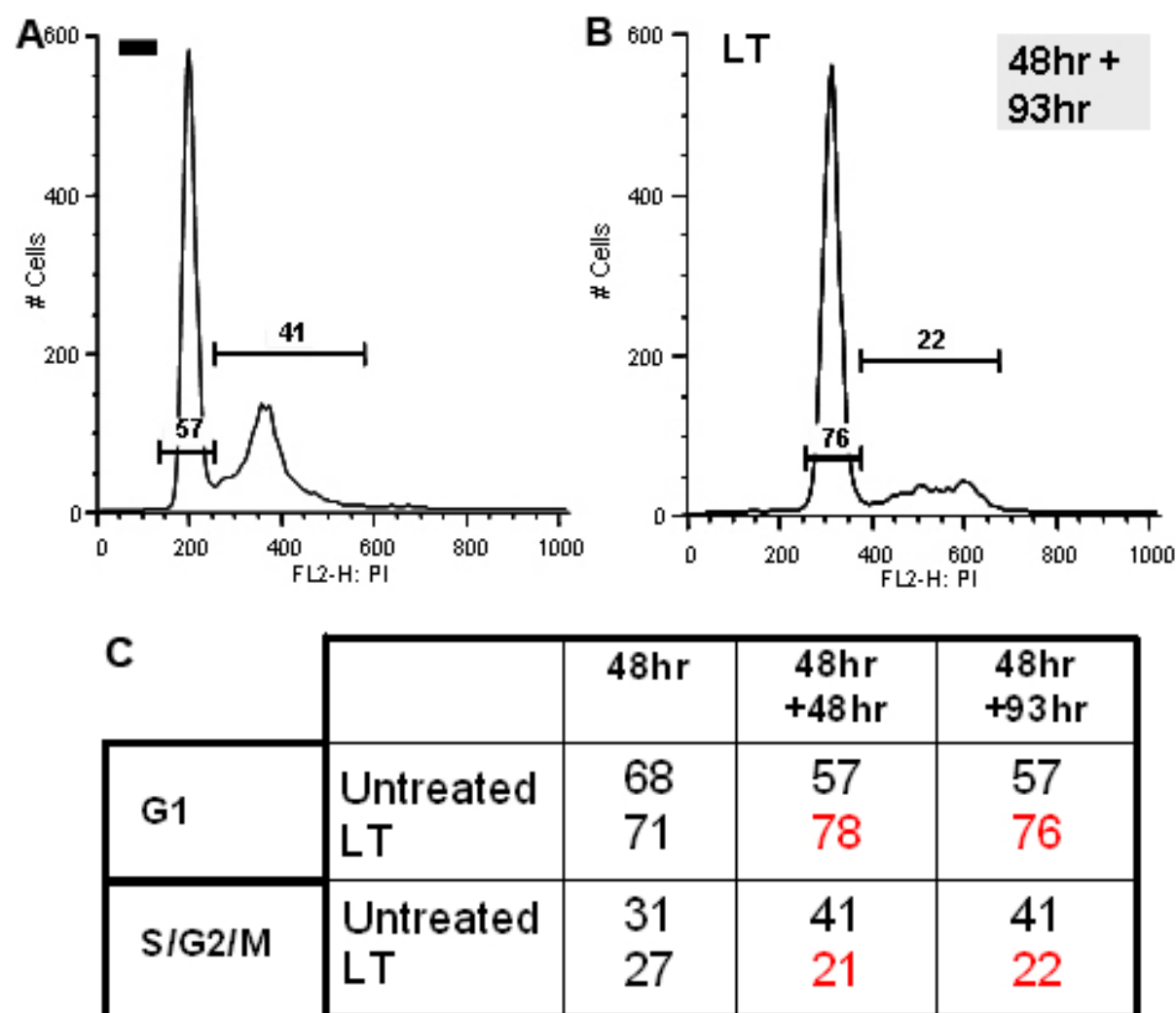


Figure 5-35: Increase of cells in G1 phase after LT treatment.

A,B) FACS histogram of PI stained cells untreated (A) or after 48 hours LT treatment (B) and 93 hours additional growth. First peak displays single the DNA content in G1 phase. Second lower peak contains double DNA content and include S/G2/M phase. C) The table shows the % of cells in each phase at three different time points. The biggest changes were highlighted in red. Abbreviation: -, untreated; hr, hours; LT, lethal toxin; M, mitosis phase; PI, propidium iodide; S, synthesis phase.

5.6.2 Mitochondrial Potential Changes

Lethal toxin impaired mitochondrial function, causing a decrease in membrane potential and succinate dehydrogenase (SDH) activity in murine macrophages (J774A.1). This event was predicted to be one of the key players of toxin induced cytotoxicity. [166] We determined, if the proliferation inhibition could be caused

through a mitochondria dysfunction. **Figure 5-36, A** displays a significant difference in untreated and LT treated cells. It seemed that LT treatment led to two types of cells. One peak was similar to the untreated one, whereas a second peak shifts to the right towards hyperpolarization. Since the three MAPK inhibitor combinations have a comparable LT profile, the MAPK pathway might be involved in the mitochondria alteration. (**Figure 5-36, A**) The single inhibitors had unique pattern. JNK was similar to LT treated cells. p38 inhibition showed only one population at the hyperpolarized side. The reduction of MEK1/2 caused the opposite effect, a shift towards the hypopolarized side.

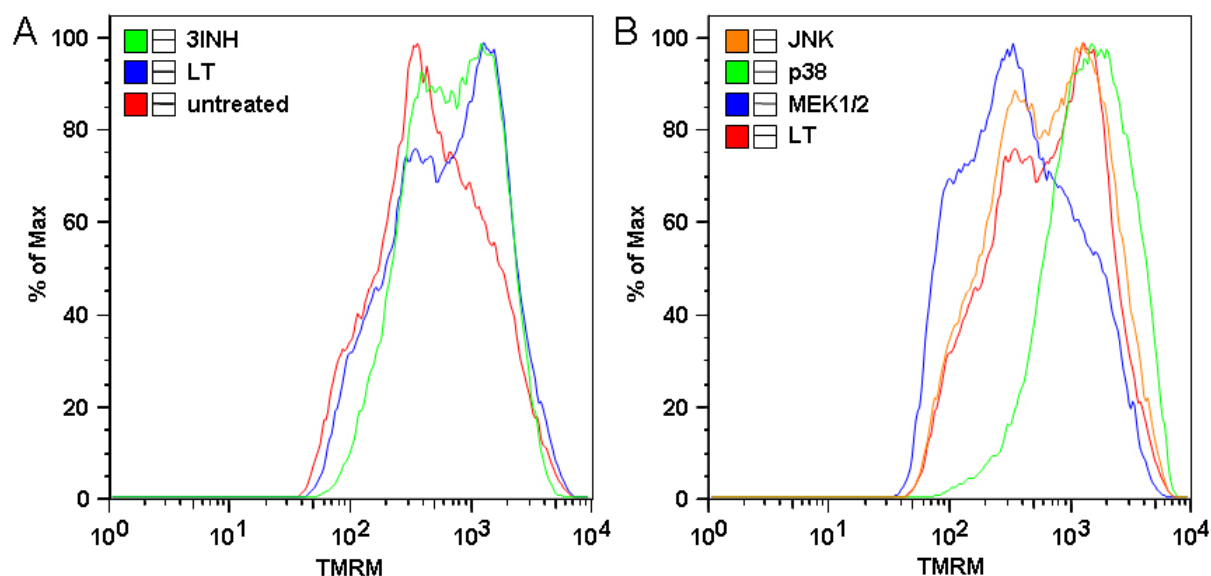


Figure 5-36: Mitochondrial potential alteration caused by MAPKK cleavage.

A) Comparison of untreated, LT and 3 MAPK inhibitor treated cells in their mitochondrial potential. B) Comparison of the mitochondrial potential of LT with single MAPKK inhibitor. FACS analysis of TMRM stained NHBE after 48 hours treatment in starving media. Abbreviation: 3INH, 3 inhibitor MAPK combination; LT, lethal toxin; TMRM, tetramethyl rhodamine methyl ester; %, percent.

5.6.3 Proteasome Impairment

The proteasome complex is involved in the cytotoxic effect induced by LT, since inhibitors partially prevent cell death. The importance of MAPKK in cell death would be implicated, if proteasome inhibitors would rescue MAPKK cleavage. **Figure 5-37, A** shows the recovery of MEK2 expression when the proteasome inhibitor is added shortly (90min) after lethal toxin treatment. After longer incubations (48hrs) with LT, inhibitors did not have any rescue effect on the cleavage of MAPKK. (**Figure 5-37, B**) Epoxomicin is a specific proteasome inhibitor, whereas MG132 can also reduce lysosomal protein degradation. The MEK2 expression could only be rescued by the proteasome and not by the lysosomes, since MEK2 expression assays performed with chloroquine, a lysosomal inhibitor, did not recover MEK2 expression after short toxin incubation. (data not shown)

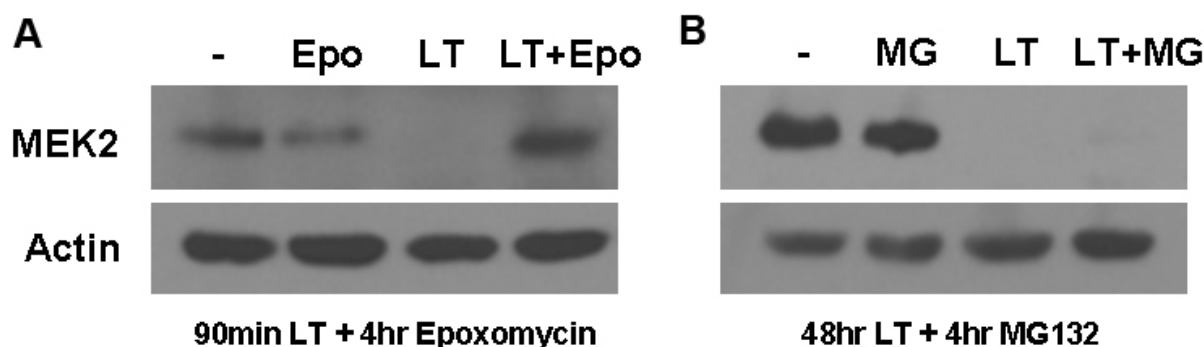


Figure 5-37: MAPKK expression induced by proteasome inhibitors.

A) MEK2 cleavage rescue after 90 minutes LT treatment followed by 4 hours epoxomycin. B) 4 hours MG132 after LT 48 hours treatment was unable to gain MEK2 protein expression. Actin was used as loading control. Abbreviation: -, untreated; Epo, epoxomycin; hr, hours; LT, lethal toxin; MEK-2, mitogen activated ERK kinase; MG, MG132 inhibitor; MKK-3, mitogen activated kinase kinases.

Analysis of the proteasome activity might give more inside information in the mechanism of cell death. Proteasome activity was measured for 60 minutes and showed a significant reduction through LT treatment. This reduction could be partially due to MAPKK cleavage, since a three inhibitor combination (MEK1/2, ERK, JNK) lowered the proteasome activity to around 50% of the LT levels. (data not shown) MG132, a proteasome inhibitor, was used as a control for complete inhibition of its activity. The reduction of proteasome activity was confirmed by the expression levels of LRP2, a protein in the proteasome involved in its activity, which was slightly reduced after LT treatment. (data not shown)

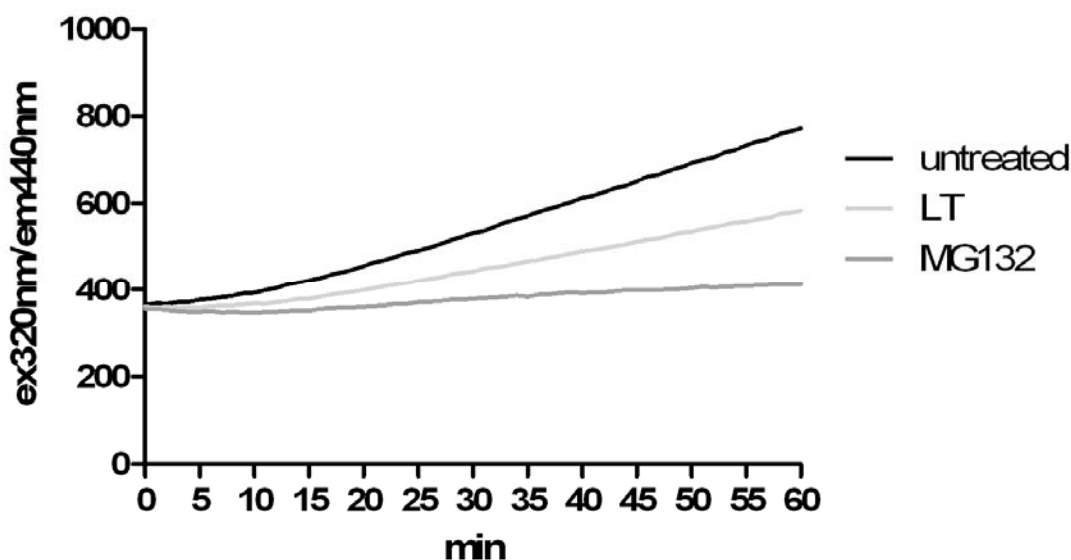


Figure 5-38: Reduced proteasome activity after LT treatment.

The proteasome activity was measured after 48 hours of LT treated NHBE and proteasome inhibitor MG132 for 4 hours. Abbreviation: LT, lethal toxin; min, minutes; nm, nanometer; ex, excitation; em, emission.

5.7 Continues MAPKK Cleavage Due to Lethal Toxin Residues

Recently, it was shown by LF inhibitor studies (LF protease inhibitor III), that lethal factor can be stored in the cell after exposure, causing constant MAPKK cleavage. [167] In Figure 5-39 we observed, that after 48 hours of lethal toxin exposure, MKKs

are completely cleaved. However, when we washed the outside LT away and incubated the cells for another 48 hours with media only, we did not regain MKK expression.

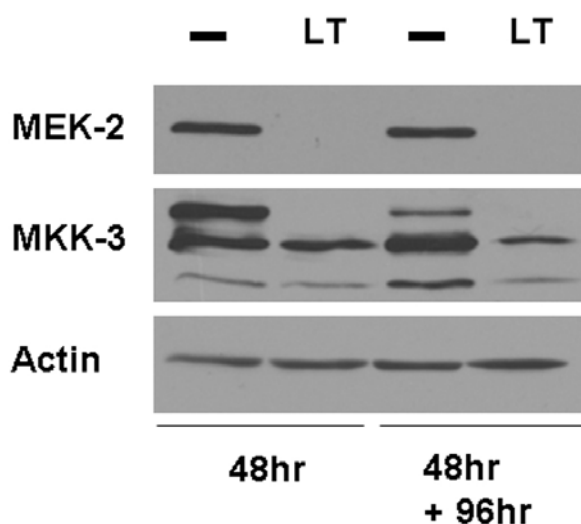


Figure 5-39: Continuous MAPKK cleavage after 48 hours of LT treatment.

Western blot of MAPKK cleavage after 48 hours of LT treatment and an additional 96 hours of normal growth stimulation. Actin was used as loading control. Abbreviation: -, untreated; hr, hours; LT, lethal toxin; MEK-2, mitogen activated ERK kinase; MKK-3, mitogen activated kinase kinases.

Since mRNA levels were not affected and resynthesis of MKKs took place [167] lethal factor might be stored in epithelial cells. Therefore, we treated NHBE for 24 hours, washed all extracellular LT away, infected the cells with a MEK2 wild-type lentivirus and determined its cleavage. If lethal toxin would be degraded or loses its activity in the cell, it should not be able to cleave the newly introduced MEK2 wt. However, if LT is stored somewhere in the cell, the cleavage should be observed. We detected cleavage of MEK2, which was shown in **Figure 5-40**.

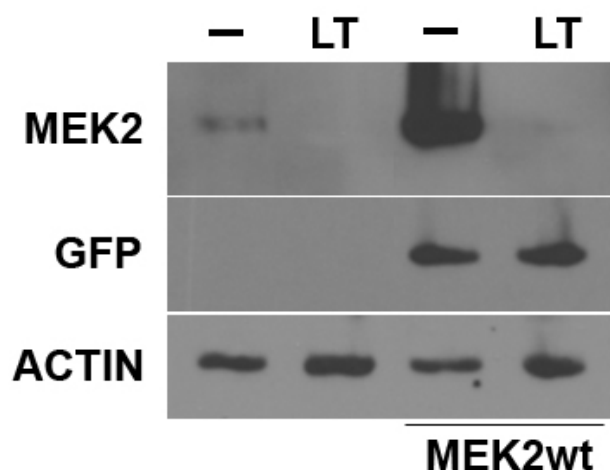


Figure 5-40: LT residues stored in cell.

NHBE were infected with MEK2wt as indicated after 24 hours of LT treatment. Overexpression and MEK2 cleavage were compared to uninfected cells. Residual LT caused cleavage of reintroduced MEK2wt. Equal infection rates were visualized with the GFP antibody, since the lentivirus construct contains EGFP. Actin was used as loading control. Abbreviation: -, untreated; GFP, green fluorescence protein; LT, lethal toxin; MEK-2, mitogen activated ERK kinase; wt, wild type.

With these findings, we had evidence, that lethal factor accumulates in the cell, causing constant MKK cleavage. But its location was not identified. Antibodies against lethal factor do not perform well. Therefore, we biotinylated LF (LFbio) to determine its storage in the cell. To ensure, that biotinylated LF tagged with histidine (LFhis) was also able to cleave MAPKK, we performed a MAPPKide assay. This assay emits fluorescent light upon MAPPKide cleavage. The similar kinetic cleavage curves are shown in **Figure 5-41**.

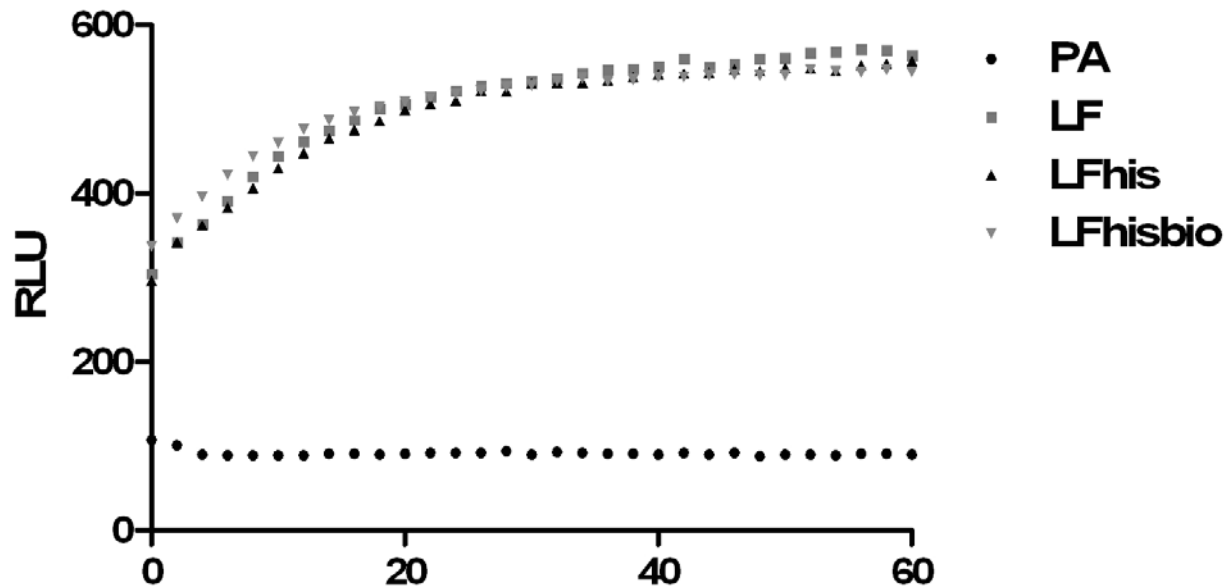


Figure 5-41: Similar MAPKK cleavage activity of different LFs.

The kinetic of the cleavage from the fluorescent MAPPKide by LF and its modified forms were followed over time. PA did not cleave MAPKK, whereas all LF forms had similar activity. Abbreviation: PA, protective antigen; LF, lethal factor; LFhis, histidine tagged lethal factor; LFhisbio, histidine tagged lethal factor biotinylated; RLU relative light units.

Visualizing the localization of biotinylated LF by immunofluorescence was not possible due to high background stain caused by the streptavidin conjugated FITC secondary antibody. We were unable to distinguish between unspecific binding and real signals. Therefore, we conjugated LF with Alexa-488 to detect a better signal. The result showed a very weak IF performance, from which we were also not capable of determining any significant location in the cell.

Another option was to fractionate membrane and cytosol of the LF-biotinylated treated cell lysates. **Figure 5-42** showed that LF is stored in membrane compartments and was probably slowly released in the cytosol, where it cleaved the MAPKK. After 48 hours treatment and washing away all extracellular toxin, MAPKK cleavage continued to locate (48hr+48hr) in the membrane compartments. GDI was used as a cytosolic marker.

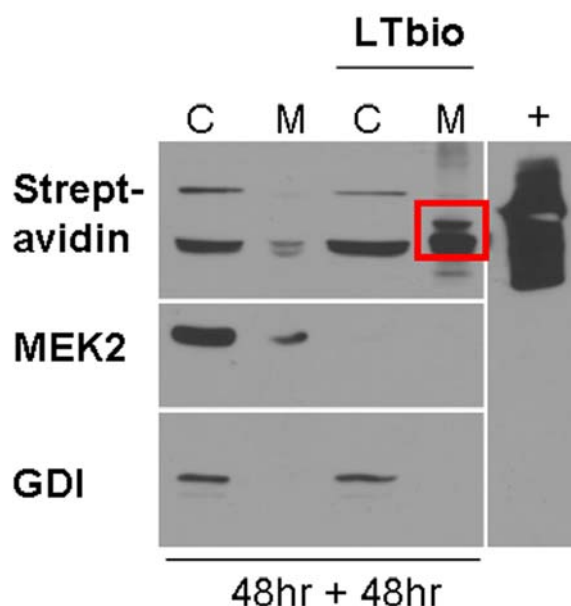


Figure 5-42: LF is localized in membrane compartments.

Western blot analysis to localize LFbio with a strept-avidin antibody. MEK2 cleavage after LTbio treatment was observed in the cytosolic fraction. GDI was used as cytosolic loading control. Abbreviation: hr, hours; C, cytosol; M, membrane; LTbio, lethal toxin biotinylated, MEK2, mitogen activated ERK kinase; GDI, guanine nucleotide dissociation inhibitor.

The incubation of LFhis with a crude Raw cell lysates would indicate its stability in the cytoplasm over time. After coating histidine-tagged LF on nickel beads, washing, cell lysates exposure and incubation with HIS antibodies and LF antibodies, LFhis could not be detected. This agrees with Leppla and coworkers observation that LT is degraded after 30-40 minutes in the cytosol and therefore cannot be stored there. (Figure 5-43)

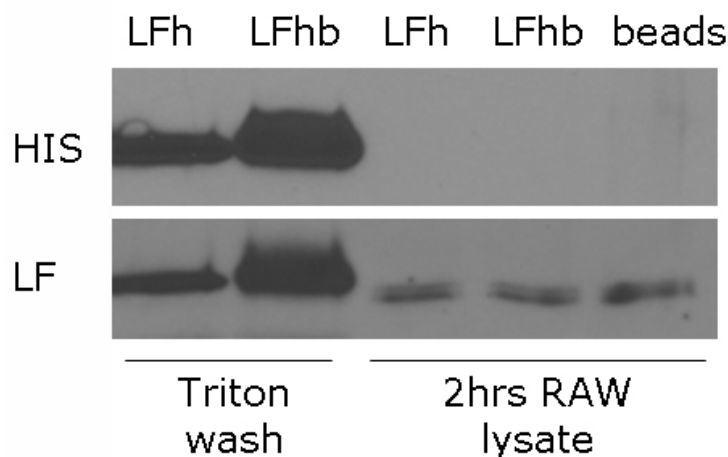


Figure 5-43: LF degradation after exposure to Raw cell lysates.

IP of LFhis and LFhisbio to nickel columns, washed with tritonX containing buffer or after exposure to Raw cell lysates for 2 hours. LFhis and LFhisbio were visualized with a His and LF antibody. Abbreviation: HIS, histidine antibody; LF, lethal factor; hrs, hours; LTh, histidine tagged lethal toxin; LThb, biotinylated histidine tagged lethal toxin.

5.8 Modification of Lethal Factor Influences Its Cytotoxic Effect

Murine macrophages from susceptible mouse strains undergo cell death in less than 3 hours. This is a fast way to detect the cytotoxicity effects of lethal toxin. We choose a macrophage cell line called RAW 264.7 and performed a dose dependent cell

viability assay after 3 hours of LT incubation. Lethal factor and protective antigen are by themselves non-toxic and were used as negative controls. Lethal toxin caused over 60% of cell death when a concentration of 50ng/ml was added, which was also showed for histidine tagged LF (LFhis) in combination with PA. Biotinylated LThis did not have the any cytotoxic effect. (Figure 5-44)

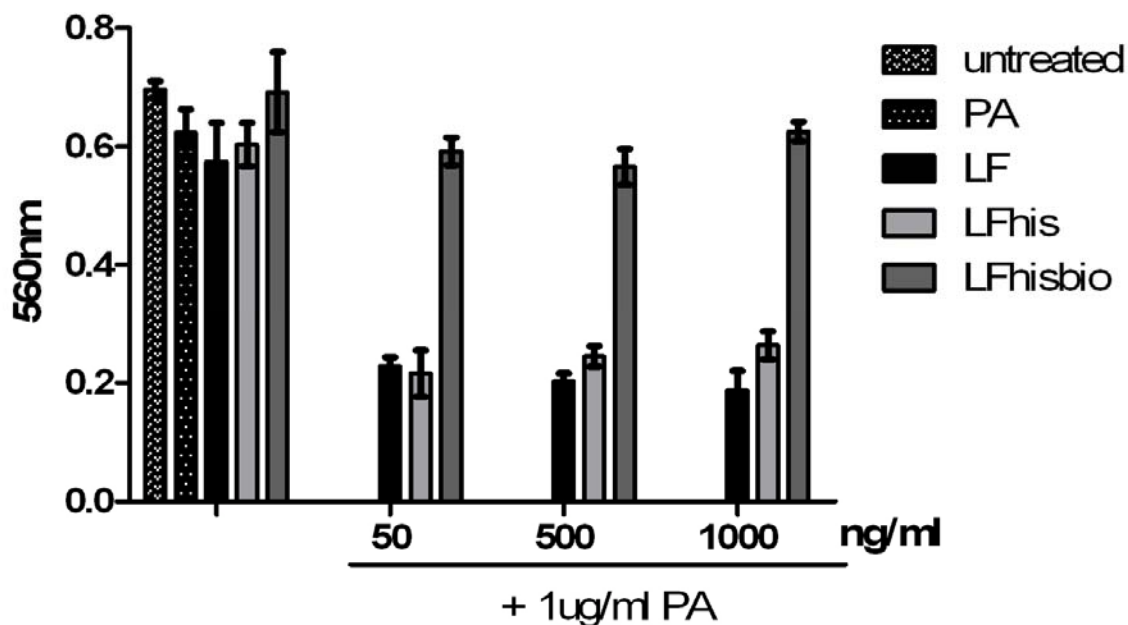


Figure 5-44: Biotinylated lethal factor did not alter cell viability.

MTT assay to determine viable cells after dose dependent incubation with LThis, LThisbio and LT after 3 hours treatment in Raw cells. Lethal toxin caused a dramatically decrease in cell viability, whereas LThisbio did not. Abbreviation: nm, nanometer; ug, microgram; ml, milliliter; ng, nanogram; PA, protective antigen; LF, lethal factor; LFhis, histidine tagged lethal factor; LFhisbio, biotinylated histidine tagged lethal factor.

To prove, that the decrease in toxicity is not due to the inhibited uptake of biotinylated LF, expression levels of MAPKK were determined. LFbio was able to enter the cell and cleave MEK2 comparable to LT, which is shown in Figure 5-45.

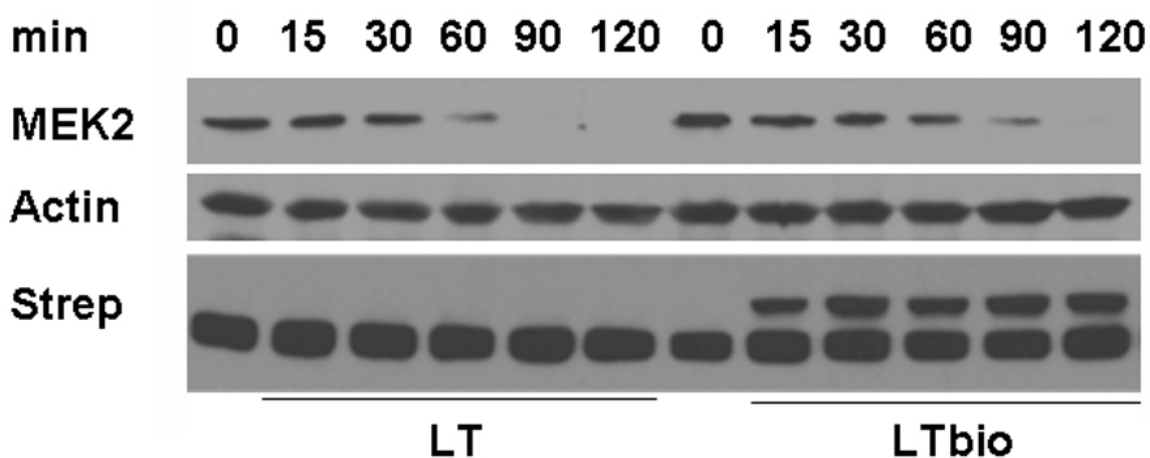


Figure 5-45: MAPKK cleavage time course.

Time dependent MEK2 cleavage in RAW cells. The uptake of biotinylated LT was shown by a streptavidin stain. Actin was used as loading control. Abbreviation: MEK2, mitogen activated ERK kinase; LTbio, biotinylated lethal toxin; Strep, streptavidin; min, minutes; LT, lethal toxin.

All other MKKs including MKK3 and MKK6, which can decrease toxicity, displayed also cleavage. (data not shown) Since there might be a delay in cell death we increased the incubation time to 24 hours. Even at such a late time point LThisbio did not induce cell death compared to LT. (Figure 5-46) However, a slight decrease in metabolic active cells after 24 hours was seen. This might not be induced by cell death, instead we believe that the proliferation was inhibited.

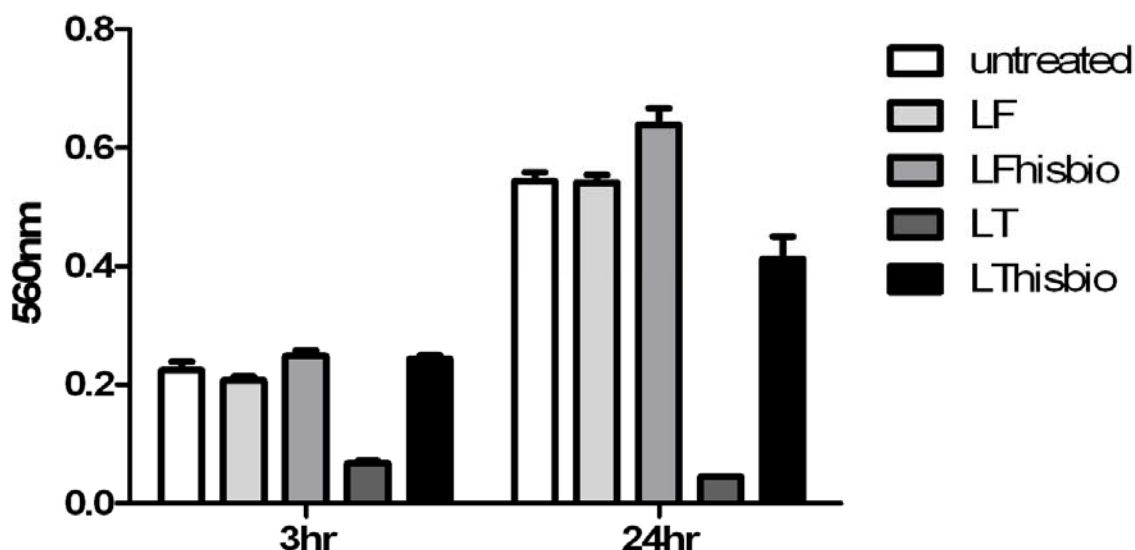


Figure 5-46: LFhisbio does not induce cell death within 24 hours treatment.

MTT assay to determine viable cells after 3 and 24 hours of indicated treatment of RAW cells. Lethal toxin caused cell death after 3 hours, whereas LThisbio showed only a slight proliferation inhibition. Abbreviation: nm, nanometer; hr, hours; PA, protective antigen; LF, lethal factor; LFhis, histidine tagged lethal factor; LFhisbio, biotinylated histidine tagged lethal factor; LT, lethal toxin; LThisbio, biotinylated histidine tagged lethal toxin.

These findings predict that through random biotinylation of lysines on lethal factor, either an unknown binding protein is blocked or that the localization of LTbio inside the cell is altered. To detect the specific LTbio biotinylation sites responsible for rescue of Raw cell death, we analyzed the LTbio by mass spectrometry. Trypsin digest was performed and mass changes were detected with nano-LC-MS-MS. (TSRI Core facility) Figure 5-47 displays all identified biotinylated lysines of two experiments, which were detected. With sequence coverage of 80% some biotinylation sites were probably undetected.

It would be very time consuming to analyze every of those lysines by mutagenesis in a cytotoxicity assay to identify the specific lysine causing the decrease in cell death. We used his-tagged LF in immunoprecipitation studies to identify different binding partner between LFhis and LFhisbio. Unfortunately, we were unable to pull any binding partner down, since LFhis was degraded after 2 hours when exposed to Raw cell lysates. (Figure 5-43)

MNIKKEFIKVISMSCLVTAITLSGPVFIPLVQAGGGHGDVGMHVKEKEKNKDENRKRK
 DEERNK TQEEHLKEIMKHIVKIEV K GEEAVKKEAAEK LLEK VPSDVLEMY KAIGGKI
 YIVDGDITKHISLEALSSEDKK KIKDIYGK DALLHEHYVYAKEGYEPLVIQSSDYVE
 NTEKALNVYYEIGKILSRDILS K INQPYQKFLDVLNTIKNASDSDGQDLLFTNQLKEH
 PTDFSVEFLEQNSNEVQEVFAKAFAYYIEPQHRDVLQLYAPEAFNYMDKFNEQEINL
 SLEELKDQRMLSRYEKWEKI K QHYQHWSDSLSEEGR GLLKK LQIPIEPKKDDIIHSLS
 QEEK ELLKRIQIDSSDFLSTEEKEFLKQLDIRDSLSEEE K ELLNRIQVDSSNPLSE K E
 K EFLKKLKLDIQPYDINQRLQDTGGLIDSPSINLDVR K QYKRDIQNIDALLHQSIGSTL
 YNKIYLYENMNINLTATLGADLVDSTDN TKINR GIFNEFKK NFK YSISSNYMIVDIN
 ERPALDNERLKWRIQLSPDTRAGYLENGKLILQRNIGLEIK DVQIIKQSEKEYIRIDAK
 VVPKSKIDT K IQEQLNINQEWN K ALGLPK YTKLITFNVHNRYSNIVESAYLILNEW
 KNNIQSDLI K KVTNYLV DGNRFVFTDITLPNIAEQYTHQDEIYEQVHSGKGLYVPESR
 SILLHGPSK GVELR NDSEGFIFEFGHVA VDDYAGYLLDKNQSDLV TNSKK FIDIFKEEG
 SNLTSYGR TNEAEFFAEAFRLMHSTDHAERLKVQKNAP K TFQFINDQIKFIINS

Figure 5-47: Protein sequence of lethal factor with biotinylated lysines (K).

Single protein code of the LF sequence. Lysine (K) biotinylation of two mass spectrometry experiments are displayed with different colors. Sites identified in experiment 1 (yellow), in experiment 2 (red) and when experiments discovered in both experiments (green). Not all areas were found in mass spectrometry, which are marked as non-covered region (blue).

Proteasome changes and mitochondria dysfunction were involved in lethal toxin toxicity. We wanted to compare the proteasome activity and mitochondrial potential between LT and LThisbio. We showed before (Figure 5-38) that lethal factor decreases proteasome activity. This can also be seen in Figure 5-48. Biotinylated LT displayed normal proteasome activity and was therefore closer to the untreated curve.

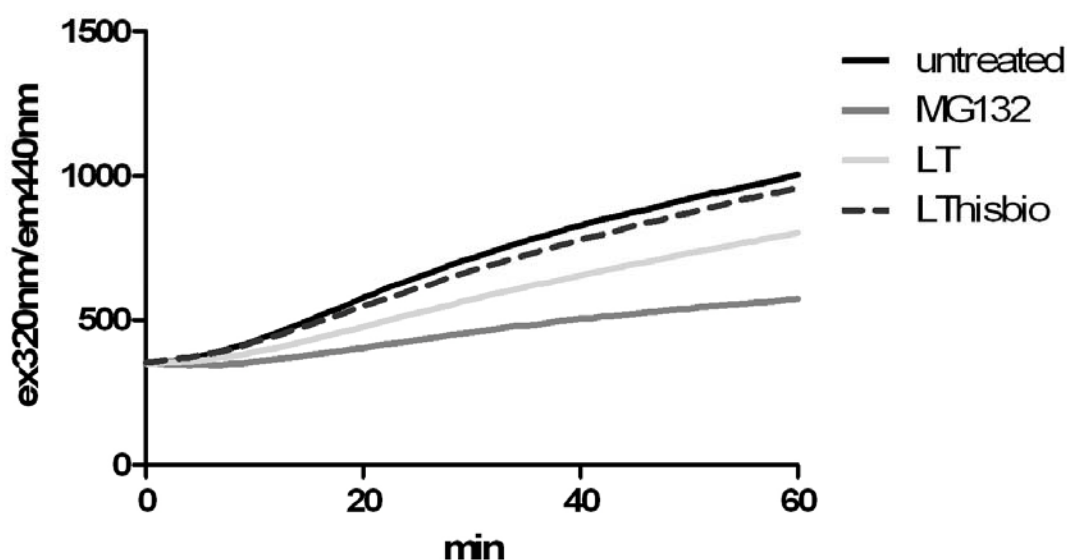


Figure 5-48: LThisbio does not reduce the proteasome activity in NHBE.

The proteasome activity was tested after 48 hours treated NHBE. The kinetic of indicated treatments were followed. Histidine tagged biotinylated LT did not decrease the proteasome activity compared to LT. MG132 is a proteasome inhibitor, reducing its activity. Abbreviation: LT, lethal toxin; LThisbio, histidine tagged lethal toxin; min, minutes; nm, nanometer; ex, excitation; em, emission.

The same observation was made in the mitochondria, where the membrane potential of LThisbio was similar to the untreated cell profile. (Figure 5-49) It showed three

populations of cells. Most LThisbio treated cells were hypopolarized (shift to left), others were similar to untreated cells and the rest showed cells in the hyperpolarized site such as LT. (Figure 5-49) Since LThisbio altered the proteasome and mitochondria in the opposite way compared to LT, it might be less toxic for cells.

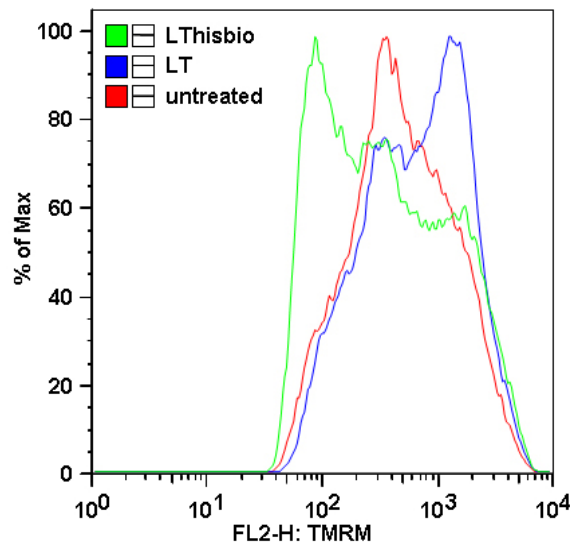


Figure 5-49: LThisbio causes mainly hypopolarization of the mitochondrial potential in NHBE. FACS analysis of TMRM stained NHBE after 48 hours treatment in starving media. Abbreviation: LT, lethal toxin; LThisbio, biotinylated histidine tagged lethal toxin; TMRM, tetramethyl rhodamine methyl ester; %, percent.

Lethal factor caused a variety of morphological and permeability changes in NHBE. Therefore, we investigated the effect of LTbio on junctions, cytoskeleton, motility and cytotoxicity. (data not shown) We observed very similar changes in all of these areas compared to LT. Junction formations were altered and caused a resistance decrease with permeability elevated. (Figure 5-50) The cytotoxicity assay performed in inserts displayed almost identically cell death. (Figure 5-50)

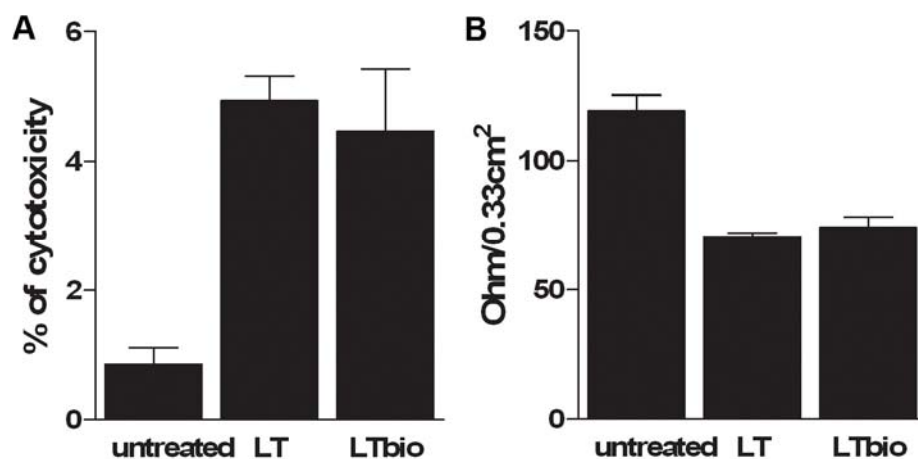


Figure 5-50: Cytotoxicity and resistance comparison of LT and LTbio in NHBE 3D. A) Comparison of LDH release after 48 hours of LT or LTbio treatment. B) Similar resistance changes were observed after incubation of LT or LTbio for 48 hours.

Furthermore, the stress fiber formations were increased, causing a defect in motility. Therefore, the cells treated with LTbio were studied in live cell imaging and showed exactly the same phenotype compared to LT. (Movie 17)

6 DISCUSSION

6.1 Polarized Lung Epithelial - An Excellent Model to Study LT Intoxication

B. anthracis infection in the lungs causes common flu-like symptoms, internal bleeding, respiratory distress and in rare cases meningitis. Most of the anthrax studies are performed on mice or in murine macrophages. Those were either resistant or susceptible to lethal toxin induced cell death. [212-216] Only a few studies have focused on human cells, which seem to be more resistant. Depending on the cell type, cell death started to occur as early as 18 hours or as late as 72 hours. [80, 172, 174, 177] In addition, it is not clear what causes the respiratory failure in the late pathogenesis. Therefore, we focused on the effect of the lethal toxin on the human respiratory system. To do so, we decided to work with primary human bronchial epithelial cells. The establishment of a differentiated, polarized 3D system gave us the possibility of studying LT intoxication under more physiological conditions. [217] NHBE are lung precursor cells which differentiated into pneumocytes, goblet, ciliated, and basal cells. The formation of desmosomes, tight and adherens junctions results in a very dense layer of cells, controlling tissue homeostasis and strength.

We observed that defense mechanisms such as cilia movement and the secretion of mucus and antimicrobial peptides such as defensins protect the apical side for environmental insults. Surfactants were found to be expressed to decrease surface tension. This shows that a differentiated epithelial system can be used to mimic human lung responses.

Furthermore, the expression of both anthrax receptors on the cell surface, which mediate the translocation of LT into the cell and in turn, led to MAPKK cleavage, makes the system best suitable for studying the effects of anthrax toxins.

Earlier observations in differentiated polarized T84 (human intestinal) cells proved the basolateral location of the anthrax receptors. [218] Protective antigen was only detected in the cells when treatment was performed from the basal side. [218] With this in mind, and knowing that LT would reach the lung epithelial cells from the vascular side, we carried out all our treatments from the basal side.

Taken together, normal tissue culture grown cells and the 3D model provided an excellent tool to understand lethal toxin effects in the human body.

6.2 Lethal Toxin Disrupts Barrier Function in Lungs

In humans anthrax pathogenesis causes blood vessel leakage and edema in the lungs, leading to severe bleeding and respiratory distress. Similar effects were seen in animal studies. [219, 220]

Using immunofluorescence, electron microscopy and protein expression assays, we observed alterations of junctions, cytoskeleton and adhesion complexes after lethal toxin treatment. In fact, LT disrupted the epithelial barrier by disturbing junction formation. Wide diffuse tight as well as adherens junctions indicated an assembly and remodeling defect in normal tissue culture plated cells.

Under more physiologic conditions in the form of a polarized epithelial system, we were able to identify phenotypical changes, which resemble diseased lungs. Staining of tight junctions revealed an enhanced connection failure at sites, where multiple

cells connect in one point. Naturally occurring multicellular junction sites have been identified in live cell imaging as the detachment of dead cells by extrusion. [203] Surrounding cells maintain those sites by reorganizing the junction complex and closing them up. We also encountered a slight increase in cell death in 3D, which could have been the cause of these described junction site disruptions.

We further confirmed those severe alterations in a cross section of the polarized system by electron microscopy. The basolateral site showed extremely wide intercellular space formations, causing the loss of integrity of that layer and swelling. Therefore, the junction defect seen in 2D was potentiated in 3D. This caused an increase in permeability and a decrease in resistance after 48 hours of lethal toxin treatment. Other investigators observed similar effects on the barrier function in the underlying lung endothelial cells. The disordered junctions were found to be triggered by a loss of peripheral F-actin, which was not seen in our studies after treating NHBE with LT. [80] Furthermore, Warfel et al. excluded cell death as a major mechanism responsible for permeability changes, as no significant apoptosis was observed in the first 72 hours of LT exposure. The probable cause may partially be due to the cleavage of MAPKKs. MKK1/2 and JNK inhibition increased the permeability in endothelial cells, whereas a reverse effect was seen by the decrease of p38. [80]

The permeability and resistance changes were rescued by pretreatment with dexamethasone and keratinocyte growth factor (KGF). This might be due to the induction of cell survival in the polarized epithelium. [221] Dexamethasone is a glucocorticoid hormone and known to decrease inflammation, severe edema and swelling. Lethal toxin was shown to repress the glucocorticoid receptor transactivation in a non-competitive manner. [222] This receptor repression is partially due to the inhibition of the p38 pathway, which was also seen to reduce glucocorticoid receptor-inducing gene expression. Early receptor activation by dexamethasone might prevent LT barrier disruption.

Pretreatment with KGF also increased the resistance of NHBE treated with LT. In animal studies it was shown that KGF prevents lung injury. [209] However, the mechanisms behind these effects are not well understood. In intestinal epithelial cells and pneumocyte type II cells, it induced cell proliferation, differentiation, migration and re-epithelialization. [209, 223] This might be due to the fact that KGF promotes ERK1/2 and p38 phosphorylation shown in cornea epithelial cells. [113] KGF pretreatment of the polarized system might cause an upregulation of the MAPKK pathway before lethal factor inhibits all of the MAPKK activation by cleavage.

6.3 Lethal Toxin Alters the Cytoskeleton

Previously it has been shown that LT induces elongated cell shape in monolayer formation of lung endothelial cells. This phenomenon was found to be due to increase in stress fiber formation at the center of the cells, whereas peripheral F-actin was reduced. [80] Other studies in human neutrophils described that LT inhibits the actin assembly. [87] This was explained by a lower F-actin content after LT treatment. However, this F-actin content was not altered when neutrophils were only incubated for 1 hour with lethal toxin. Longer treatments (2hrs) reduced the F-actin assembly when migration was induced by fMLP stimulation and also showed lower expression of actin in the triton-insoluble-cytoskeletal fraction. [87] In subsequent studies, this group connected the actin assembly defect with the inhibition of the p38

pathway in neutrophils, which blocks the phosphorylation of Hsp27. Hsp27 facilitates the transport of G-actin to regions of new actin filament growth and is therefore important for the assembly process. [88]

In contrast, we observed in epithelial cells that the accumulation of stress fibers (actin) and bundle-like tubulin structures resulted in an extremely ridged cytoskeleton. LT treatment caused the buildup of actin and tubulin filaments as seen after polymerization inhibition. To explore the possibility of an actin assembly defect seen in neutrophils by other investigators, we inhibited actin polymerization with reversible inhibitors after LT treatment. The assembly process was determined by IF showing the capability of the actin network to polymerize. Interestingly, actin polymerization led to the same stress fiber formation and inflexible cytoskeleton seen after LT treatment. Therefore, the idea of LT causing polymerization and depolymerization defects in lung epithelial cells could be excluded. In addition, we found that LT induces the stabilization of tubulin as a result of polyglutamination and acetylation modification as shown by inhibitor studies.

The above mentioned results do not explain why neutrophils showed a decreased actin assembly, whereas NHBE contained more filaments and had a normal turnover mechanism. However, compared to epithelial cells, neutrophils more motile cells, which allows them to migrate towards the site of infection, and might therefore differ in their regulation of the cytoskeleton compared to epithelial cells.

We believed that the lethal toxin induced phenotype of stress fiber and protrusion formation was caused by RhoGTPases alterations. Increased RhoA activity leads to stress fibers, whereas Rac1 forms lamellipodia. [224] Surprisingly, we did not detect any activity changes after 48 hours of LT treatment. Interestingly, an increase in activated Cdc42, which induces filopodia extensions, was identified after LT exposure. Cdc42 engages actin cytoskeletal reorganization, cell polarization and the reorientation of MTOC of migrating cells, which could contribute to the LT phenotype. [225]

Furthermore, MAPK pathways were shown to influence cytoskeletal rearrangements. ERK was shown to lower F-actin bundling by the phosphorylation of synapsin I in neuronal cells, which would be diminished by the downregulation of ERK activity. [102] In addition, p38 activates p16-Arc, a subunit of the Arp2/3 known to be crucial for actin rearrangements. [120, 121] In contrast, JNK activity can disrupt stress fiber formation. [226] Further investigations are required to prove which MAPK pathway has the most impact on cytoskeletal changes in epithelial cells. In summary, we showed that lethal toxin induced MAPKK cleavage and Cdc42 activation causes accumulation of actin and tubulin filament in bronchial epithelial cells.

6.4 Defective Motility and Wound Healing in the Lungs Caused by Lethal Factor Exposure

Cell migration depends on the coordinated interaction of three mechanisms: the polarization of the cells, the rearrangement of the cytoskeleton and the formation of adhesions. The previously described actin assembly defect in neutrophils paralyzes cell motility and prevents the directed migration towards a stimulus. [87]

We observed migration deficiencies in wound healing assays, due to the impaired cytoskeletal dynamics caused by LT. In fact, treating cells with lethal toxin abolished wound closure completely. The directed migration in a Boyden chamber experiment also displayed no movement towards the stimulus. In addition, live cell imaging experiments showed clearly that NHBE exposed to LT were capable of actin

polymerization. They formed multiple protrusions around the cell instead of one lamellipodium at the front. Therefore, their regulation and signal sensing were impaired.

Besides their role in the cytoskeleton, adhesion proteins are required to connect cell extensions with matrix proteins, resulting in their stabilization. By western blot analysis, we detected an increased amount of vinculin, a focal complex protein, in the cytoskeletal fraction. Paxillin, also known as a focal adhesion protein, was decreased in the cytosol, consequently impairing the assembly of focal complexes.

Similar effects were seen by different investigators in endothelial cells. LT treatment in combination with TNF α enhanced the expression of the adhesion protein called vascular cell adhesion molecule 1 (VCAM1). [227]

Although attachments through integrins were not impaired by LT, LT treated NHBE were unable to adhere to positively charged tissue culture plates or poly-L lysine. This might be explained by the finding of Popova et al., showing an increase in the shedding of syndecan 1 by epithelial membranes. The shedding might affect the charge or integrity of the cytoplasmic membrane required for attachment to positive surfaces. [228]

Many proteins are involved in the regulation of cell migration. Especially, GTPases were proven to play a major role in cytoskeletal rearrangements and motility. Rac1 and Cdc42 regulate actin polymerization in the front of the cell, forming lamellipodia and filopodia. [229] More interestingly, Cdc42 is required for cell polarity. [230] Therefore, an increased activity of Cdc42 could cause enhanced protrusion formation.

Other proteins, such as EB1, were also shown to be involved in polarity by positioning cues and regulating the connection between microtubules and cortical actin. [225] Lethal toxin treated cells might be disabled in sensing those cues by extracellular sensor downregulation/malfunction or intracellular signaling deficiency.

In addition, MAPK pathways are known to regulate cell motility. It was shown that downstream effectors of ERK induced membrane protrusion in polarized cells through the activation of myosin light chain kinase (MLCK) [109, 110] p38 controls adhesion dynamics by the phosphorylation of paxillin and actin filaments through inhibition of the Arp2/3 complex and therefore influences cell motility. [115] The downstream effector Hsp27 was shown to induce stress fibers and regulate actin polymerization in endothelial cells and neutrophils impaired in migration. [87, 117-119] In the JNK pathway many interacting proteins were observed to regulate locomotion. [122] Reduction of JNK impaired the motility causing improper wound healing. [125, 126] Faster migration was induced in lung carcinoma cell lines by activation of JNK and expression of constitutively active MKK4. [123, 124]

Wound healing and directed migration assays with the three MAPK inhibitor combinations proved the incapability of wound closure and chemotaxis. Single MAPK inhibitors displayed a partial migration into the wound. In addition, we performed live cell imaging experiments with either of these inhibitors and saw phenotypes similar to those seen with LT treatments. To prove, that the MAPK pathway was responsible for the protrusion formation and motility inhibition, we generated lentiviruses containing non-cleavable MKK mutants. The reintroduction of single MAPK did not have any positive effects on the LT induced phenotype. Partial motility rescues were observed in live cell imaging, when both of the MKKs upstream of p38 and ERK were expressed after lentivirus infection. This implied that single infections were not sufficient for the activation of the downstream pathways. Confirmation of these results is planned in more controlled settings, since we could

not exclude that the partial rescue effect was caused by expression of only MAPKK after double infection. Therefore, we will sort immortalized lung epithelial cells after single infections of MAPKKs (GFP), followed by a second infection with the MAPKK affecting the same downstream pathway. This guarantees a much higher expression of both MAPKK in one cell, required for a complete rescue effect in live cell experiments.

6.5 Lethal Factor Stored in Membrane Compartments Causing Continue MAPKK Cleavage

We decided to look further into the LT localization in NHBE due to the observation of continue MAPKK cleavage, when LT was not present in the extracellular media. A recent study showed that the MAPKK synthesis was not impaired by exposure to LT. [167] Therefore, our hypothesis was, that LT gets stored in the cell and is slow release in the cytosol to cleave MAPKK efficiently. To define the localization of LT we were constrained to biotinylated LF (LFbio) due to the unavailability of functional antibodies. By fractionation assays we were able to detect LFbio in membrane compartments.

However, to determine the type of membrane compartment, further experiments are required. The storage of LT in the membranes of multivesicular bodies in endosomes is likely since LT is endocytosed. In addition, cytosolic localization was excluded on the basis of rapid LF degradation after exposure to cell lysates.

Unpublished data from the group of Prof. van der Goot suggested that the release of LF might not be required for its action. They had evidence that MAPKKs are located close to endosomal compartments, where the cleavage could be performed by LT without its translocation. This might allow the storage of LF in endosomes for a longer time. Therefore, the uptake of only a minimal amount might be efficient to cause the constant cleavage.

6.6 Minimal Cytotoxicity Effect of LF in Human Lung Cells

Lethal toxin causes rapid cell death of murine macrophages from susceptible mouse strains and Fisher rats. [137, 231] Park J.M. et al. described the involvement of the p38 pathway, which is inhibited by LT induced MAPKK cleavage. The overexpression of a non-cleavable MKK6 mutant in murine macrophages was able to rescue the cells for cell death. [168]

However, it was shown that human cells such as endothelial cells and monocytic cell lines are more resistant against LT induced cytotoxicity. [80, 173, 174] Lethal toxin did not induce changes in membrane integrity, DNA strand breaks or activation of the death pathway by caspase3 cleavage in normal tissue culture treated cells. Even without the induction of cell death pathways, cell growth was compromised. We observed reduced proliferation when we continued cell growth after 48 hours of LT treatment in cells. Untreated cells divided and amplified exponentially, whereas LT kept their cell number steady for another 48 hours. Afterwards, slow death occurred, as shown by slightly lower levels of metabolically active cells. Further analysis of the cell cycle demonstrated arrest in the G1 phase which was also observed in human monocytic cell lines by another group. [173] They found the responsible mechanism for the cell cycle arrest to be the downregulation of cyclin D1/D2 and checkpoint kinase 1 (Chk1) by MEK1 cleavage. MEK1 was recovered when stabilized cyclin D

activated the PI3-K/Akt/GSK-3 β pathway. The importance of the MEK1/2-ERK, p38 and cyclin D in the cell cycle progression was also shown in different studies. [232, 233]

Moreover, we investigated the involvement of other processes in the inhibition of proliferation and induction of cell death, such as the alteration of mitochondrial potential and proteasome activity. Untreated and LT treated cells shared one peak but differed in the second one. LT led to an increase of hyperpolarized cells, whereas untreated cells were hypopolarized. Under normal cell culture conditions untreated cells should not display any depolarization effects. All of our treatments were performed in starving media resulting in some depolarization effects. The inhibition of all three MAPK pathways showed the same profile as LT treatment. This suggested an impact of the MAPKK pathway on mitochondrial dysfunction.

Other investigators detected a drop of SDH and mitochondrial potential after short LT incubations of murine macrophages, which indicated the involvement of mitochondrial potential changes in early cell death induction. [166] The reduced SDH activity was not due to the degradation of succinate dehydrogenase (SDH) or other mitochondrial proteins such as cytochrome c, as shown in western blots. [166] We did not detect similar changes in SDH activity after 48 hours of LT treatment. Furthermore, the mitochondrial proteins, Bnip3 and Bnip3L, are regulated by p38. [167] Their protein reduction was shown to cause more resistance to cytotoxicity in murine macrophages.

Susceptible murine macrophages were protected against lethal toxin induced cell death by the inhibition of the proteasome. [148] Interestingly, neither of the chymotrypsin-like, trypsin-like or peptidylglutamyl-like activities of the proteasome were increased in RAW macrophages after 1 hour of LT treatment. Also, the proteasome did not affect the cleavage of MAPKK, suggesting the involvement of a downstream pathway or other unknown substrates in the increase in cell survival. [147, 148, 167] In addition, macrophages reduce their levels of ubiquitination, which is required for protein degradation in the proteasome after 2 hours and was undetectable after 4 hours. [166]

In contrast, our findings showed rescue effects of MAPKK cleavage after short LT exposures (90min) followed by proteasome inhibition (4 hours) in NHBE. However, 5.5 hours of LT treatment did not change their proteasome activity. After 48 hours of LT exposure NHBE, proteasome activity was decreased. This was partially induced by MAPKK inhibition which caused 50% reduction of the activity compared to untreated cells. LT was shown to deplete ATP by the conversion to ADP and AMP in murine cells. [65] The protein degradation is an ATP-dependent process and could reduce the proteasome function.

Why the inhibition of the proteasome activity is beneficial for cell survival might be explained by the alteration of cell survival proteins by LT, which would, under normal conditions, not be degraded through the proteasome and induce apoptosis. Those proteins might be involved in cell cycle regulation or stabilization of membrane integrity. [148]

6.7 The Modification of LF on Lysines Abolished Induced Cell Death in Murine Macrophages

Biotinylation of LF (LFbio) was performed to localize LF inside NHBE. Interestingly, further cytotoxicity studies in susceptible murine macrophages showed complete viability after LTbio exposure. Since the biotinylation took place randomly, we

investigated by mass spectrometry the sites of biotin addition and detected 18 lysines to be modified. The observed MAPKK cleavages proved the internalization of LF through binding to protective antigen and its zinc metalloprotease activity. The time of cleavage was very similar to unbiotinylated LT, but in some cases a slight delay (15-30 minutes) occurred, which might lead to a later cell death. However, even after 24 hours of LTbio treatment cell death was not observed, but a slower proliferation rate was shown. In all other studies LTbio caused the same junction, cytoskeleton, adhesion and motility changes as LT.

Many inhibitors were shown to reduce LT induced cytotoxicity. (Table 2-3) However, this is the first report that a modification of LF by the addition of biotin abolished cell death. The biotinylation sites on LF might interfere with the interaction of a yet unknown substrate. Another possibility would be that biotin changes localization of LF in the cell, disabling signaling cascades important for LT induced cell death.

Further investigations showed that LTbio changed two major processes in epithelial cells compared to LT, the mitochondrial potential and proteasome activity. LTbio treated cells did not have the reduction in proteasome activity as seen in LT treated cells. The ATP reduction after LT treatment might be a cause for the decrease in proteasome activity, which might not have been influenced by LTbio. [65]

LThisbio treated cells were mainly hypopolarized even more than untreated cells, while LT treatment caused hyperpolarization. The combination of three MAPKK inhibitors with LT displayed a similar response. The single inhibition of MEK1/2, which reduces the effect of the ERK pathway, showed almost identical effects as LT treatment. This pathway is known to be involved in proliferation, which might be beneficial for cell survival.

7 SUMMARY

Inhalational anthrax is an acute infectious disease caused by exposure of the lungs to *B. anthracis* spores. Alveolar macrophages engulf spores causing them to germinate to the vegetative form of *B. anthracis*, which secretes edema toxin (ET) and lethal toxin (LT). The pathogenesis of inhalational anthrax is characterized by flu-like symptoms, respiratory distress, meningitis and shock, which is fatal in almost all cases.

The mechanism behind the respiratory distress is not well understood. Therefore, our goal was to determine the effects of lethal toxin in the human lung epithelium. To study alterations in a more physiological setting, we developed a differentiated, polarized lung epithelial system. Lethal toxin exposure disrupted the lung barrier function and wound healing. Assembly defects of junction proteins and additional multicellular junction sites resulted in a higher permeability. Pretreatment with keratinocyte growth factor (KGF) and dexamethasone increased the viability, resulting in the rescue of the permeability changes.

Upon LT treatment, a more rigid cytoskeleton was observed, evidenced by enhanced actin stress fiber formations and tubulin stabilization. Cytoskeleton and adhesion alterations prevented the epithelial cells from polarization, directed migration, and wound healing. The MAPK pathway and Cdc42 activity might be partially responsible for these motility defects.

Lethal toxin is known to induce rapid cell death in murine macrophages. In contrast, human epithelial cells are more resistant to the cytotoxic effect of LT. By following the growth of epithelial cells after LT treatment, we observed inhibited cell proliferation due to a cell cycle arrest in the G1 phase.

Surprisingly, biotinylated lethal factor did not induce cytotoxicity in murine macrophages. This is not due to an internalization or proteolytic activity defect; instead changes in the mitochondrial potential and proteasome activity were observed. Biotinylated LT did not reduce proteasome activity as seen in LT treated cells and caused hypopolarization of the mitochondria. However, it is possible that biotinylation of lethal toxin could prevent interaction of LT with proteins that induce cell death.

The major challenge for anthrax treatment is to find a treatment, which can act faster, is easy to use and can bring patient out of the dangerous physiological state in late pathogenesis. Our study has implications in saving the viability and barrier function of lung epithelial cells. One can devise better dosage and delivery of KGF and dexamethasone as treatment modality for post anthrax exposure to reduce respiratory distress. Furthermore, overcoming the cell cycle arrest by the development of a drug would reduce the damage of lung epithelial cells and induce proliferation. The discovery that biotinylated LT is non-toxic to murine macrophages could revolutionize treatment of anthrax infection. Exploring the types of post-translational modifications of LT that decrease toxicity and finding the mechanism behind it might, lead to therapies that directly counteract the effects of the lethal toxin *in vivo*.

8 REFERENCES

1. Keppie, J., P.W. Harris-Smith, and H. Smith, *The Chemical Basis of the Virulence of Bacillus Anthracis. Ix. Its Aggressins and Their Mode of Action*. British Journal of Experimental Pathology, 1963. **44**: p. 446-53.
2. Koehler, T.M., Z. Dai, and M. Kaufman-Yarbray, *Regulation of the Bacillus anthracis protective antigen gene: CO₂ and a trans-acting element activate transcription from one of two promoters*. Journal of Bacteriology, 1994. **176**(3): p. 586-95.
3. <http://www.wadsworth.org/databank/anthrax.htm>. [cited].
4. Tse, E., et al., *A cutaneous sore with black eschar in a cowhide worker*. Lancet, 2002. **360**(9329): p. 306.
5. Irmak, H., et al., *Cutaneous manifestations of anthrax in Eastern Anatolia: a review of 39 cases*. Acta Medica Okayama, 2003. **57**(5): p. 235-40.
6. Beatty, M.E., et al., *Gastrointestinal anthrax: review of the literature*. Archives of Internal Medicine, 2003. **163**(20): p. 2527-31.
7. Laforce, F.M., *Woolsorters' disease in England*. Bulletin of the New York Academy of Medicine, 1978. **54**(10): p. 956-63.
8. Meselson, M., et al., *The Sverdlovsk anthrax outbreak of 1979*. Science, 1994. **266**(5188): p. 1202-8.
9. Suffin, S.C., W.H. Carnes, and A.F. Kaufmann, *Inhalation anthrax in a home craftsman*. Human Pathology, 1978. **9**(5): p. 594-7.
10. Brachman, P.S., *Inhalation anthrax*. Annals of the New York Academy of Sciences, 1980. **353**: p. 83-93.
11. Jernigan, J.A., et al., *Bioterrorism-related inhalational anthrax: the first 10 cases reported in the United States*. Emerging Infectious Diseases, 2001. **7**(6): p. 933-44.
12. Dewan, P.K., et al., *Inhalational anthrax outbreak among postal workers, Washington, D.C., 2001*. Emerging Infectious Diseases, 2002. **8**(10): p. 1066-72.
13. Baldari, C.T., et al., *Anthrax toxins: A paradigm of bacterial immune suppression*. Trends in Immunology, 2006. **27**(9): p. 434-40.
14. Turk, B.E., *Manipulation of host signalling pathways by anthrax toxins*. Biochemical Journal, 2007. **402**(3): p. 405-17.
15. Makino, S., et al., *Molecular characterization and protein analysis of the cap region, which is essential for encapsulation in Bacillus anthracis*. Journal of Bacteriology, 1989. **171**(2): p. 722-30.
16. Green, B.D., et al., *Demonstration of a capsule plasmid in Bacillus anthracis*. Infection & Immunity, 1985. **49**(2): p. 291-7.
17. Uchida, I., et al., *Cloning and characterization of a gene whose product is a trans-activator of anthrax toxin synthesis*. Journal of Bacteriology, 1993. **175**(17): p. 5329-38.
18. Koehler, T.M., *Bacillus anthracis genetics and virulence gene regulation*. Current Topics in Microbiology & Immunology, 2002. **271**: p. 143-64.
19. Meynell, E. and G.G. Meynell, *The Roles of Serum and Carbon Dioxide in Capsule Formation by Bacillus Anthracis*. Journal of General Microbiology, 1964. **34**: p. 153-64.
20. Drysdale, M., et al., *atxA controls Bacillus anthracis capsule synthesis via acpA and a newly discovered regulator, acpB*. Journal of Bacteriology, 2004. **186**(2): p. 307-15.

21. Drysdale, M., A. Bourgoigne, and T.M. Koehler, *Transcriptional analysis of the Bacillus anthracis capsule regulators*. Journal of Bacteriology, 2005. **187**(15): p. 5108-14.
22. Molloy, S.S., et al., *Human furin is a calcium-dependent serine endoprotease that recognizes the sequence Arg-X-X-Arg and efficiently cleaves anthrax toxin protective antigen*. Journal of Biological Chemistry, 1992. **267**(23): p. 16396-402.
23. Welkos, S.L., et al., *Sequence and analysis of the DNA encoding protective antigen of Bacillus anthracis*. Gene, 1988. **69**(2): p. 287-300.
24. Gao-Sheridan, S., S. Zhang, and R.J. Collier, *Exchange characteristics of calcium ions bound to anthrax protective antigen*. Biochemical & Biophysical Research Communications, 2003. **300**(1): p. 61-4.
25. Petosa, C., et al., *Crystal structure of the anthrax toxin protective antigen*. Nature, 1997. **385**(6619): p. 833-8.
26. Singh, Y., et al., *The chymotrypsin-sensitive site, FFD315, in anthrax toxin protective antigen is required for translocation of lethal factor*. Journal of Biological Chemistry, 1994. **269**(46): p. 29039-46.
27. Lacy, D.B., et al., *Structure of heptameric protective antigen bound to an anthrax toxin receptor: a role for receptor in pH-dependent pore formation*. Proceedings of the National Academy of Sciences of the United States of America, 2004. **101**(36): p. 13147-51.
28. Mogridge, J., M. Mourez, and R.J. Collier, *Involvement of domain 3 in oligomerization by the protective antigen moiety of anthrax toxin*. Journal of Bacteriology, 2001. **183**(6): p. 2111-6.
29. Singh, Y., et al., *The carboxyl-terminal end of protective antigen is required for receptor binding and anthrax toxin activity*. Journal of Biological Chemistry, 1991. **266**(23): p. 15493-7.
30. Bradley, K.A., et al., *Identification of the cellular receptor for anthrax toxin*. [see comment]. Nature, 2001. **414**(6860): p. 225-9.
31. Brossier, F., et al., *Functional analysis of the carboxy-terminal domain of Bacillus anthracis protective antigen*. Infection & Immunity, 1999. **67**(2): p. 964-7.
32. Varughese, M., et al., *Identification of a receptor-binding region within domain 4 of the protective antigen component of anthrax toxin*. Infection & Immunity, 1999. **67**(4): p. 1860-5.
33. Krantz, B.A., et al., *A phenylalanine clamp catalyzes protein translocation through the anthrax toxin pore*. [see comment]. Science, 2005. **309**(5735): p. 777-81.
34. Melnyk, R.A. and R.J. Collier, *A loop network within the anthrax toxin pore positions the phenylalanine clamp in an active conformation*. Proceedings of the National Academy of Sciences of the United States of America, 2006. **103**(26): p. 9802-7.
35. Santelli, E., et al., *Crystal structure of a complex between anthrax toxin and its host cell receptor*. [see comment]. Nature, 2004. **430**(7002): p. 905-8.
36. Betsou, F., et al., *Cloning and sequence of the Bordetella bronchiseptica adenylate cyclase-hemolysin-encoding gene: comparison with the Bordetella pertussis gene*. Gene, 1995. **162**(1): p. 165-6.
37. Comer, J.E., et al., *Murine macrophage transcriptional and functional responses to Bacillus anthracis edema toxin*. Microbial Pathogenesis, 2006. **41**(2-3): p. 96-110.

38. Mock, M., et al., *Cloning and expression of the calmodulin-sensitive Bacillus anthracis adenylate cyclase in Escherichia coli*. *Gene*, 1988. **64**(2): p. 277-84.
39. Gordon, V.M., S.H. Leppla, and E.L. Hewlett, *Inhibitors of receptor-mediated endocytosis block the entry of Bacillus anthracis adenylate cyclase toxin but not that of Bordetella pertussis adenylate cyclase toxin*. *Infection & Immunity*, 1988. **56**(5): p. 1066-9.
40. Tournier, J.N., et al., *Anthrax edema toxin cooperates with lethal toxin to impair cytokine secretion during infection of dendritic cells*. *Journal of Immunology*, 2005. **174**(8): p. 4934-41.
41. Crawford, M.A., et al., *Bacillus anthracis toxins inhibit human neutrophil NADPH oxidase activity*. *Journal of Immunology*, 2006. **176**(12): p. 7557-65.
42. Hong, J., et al., *Anthrax edema toxin inhibits endothelial cell chemotaxis via Epac and Rap1*. *Journal of Biological Chemistry*, 2007. **282**(27): p. 19781-7.
43. Tessier, J., et al., *Contributions of histamine, prostanoids, and neurokinins to edema elicited by edema toxin from Bacillus anthracis*. *Infection & Immunity*, 2007. **75**(4): p. 1895-903.
44. Alam, S., M. Gupta, and R. Bhatnagar, *Inhibition of platelet aggregation by anthrax edema toxin*. *Biochemical & Biophysical Research Communications*, 2006. **339**(1): p. 107-14.
45. Cui, X., et al., *Bacillus anthracis edema and lethal toxin have different hemodynamic effects but function together to worsen shock and outcome in a rat model.[see comment]*. *Journal of Infectious Diseases*, 2007. **195**(4): p. 572-80.
46. Watson, L.E., et al., *Lethal and edema toxins of anthrax induce distinct hemodynamic dysfunction*. *Frontiers in Bioscience*, 2007. **12**: p. 4670-5.
47. Bragg, T.S. and D.L. Robertson, *Nucleotide sequence and analysis of the lethal factor gene (lef) from Bacillus anthracis*. *Gene*, 1989. **81**(1): p. 45-54.
48. Robertson, D.L. and S.H. Leppla, *Molecular cloning and expression in Escherichia coli of the lethal factor gene of Bacillus anthracis*. *Gene*, 1986. **44**(1): p. 71-8.
49. Pannifer, A.D., et al., *Crystal structure of the anthrax lethal factor.[see comment]*. *Nature*, 2001. **414**(6860): p. 229-33.
50. Lacy, D.B., et al., *Mapping the anthrax protective antigen binding site on the lethal and edema factors*. *Journal of Biological Chemistry*, 2002. **277**(4): p. 3006-10.
51. Quinn, C.P., et al., *Functional mapping of anthrax toxin lethal factor by in-frame insertion mutagenesis*. *Journal of Biological Chemistry*, 1991. **266**(30): p. 20124-30.
52. Liang, X., et al., *Involvement of domain II in toxicity of anthrax lethal factor*. *Journal of Biological Chemistry*, 2004. **279**(50): p. 52473-8.
53. Klimpel, K.R., N. Arora, and S.H. Leppla, *Anthrax toxin lethal factor contains a zinc metalloprotease consensus sequence which is required for lethal toxin activity*. *Molecular Microbiology*, 1994. **13**(6): p. 1093-100.
54. Kochi, S.K., et al., *Zinc content of the Bacillus anthracis lethal factor*. *FEMS Microbiology Letters*, 1994. **124**(3): p. 343-8.
55. Duesbery, N.S. and G.F. Vande Woude, *Anthrax lethal factor causes proteolytic inactivation of mitogen-activated protein kinase kinase*. *Journal of Applied Microbiology*, 1999. **87**(2): p. 289-93.
56. Vitale, G., et al., *Anthrax lethal factor cleaves the N-terminus of MAPKs and induces tyrosine/threonine phosphorylation of MAPKs in cultured*

- macrophages*. Biochemical & Biophysical Research Communications, 1998. **248**(3): p. 706-11.
57. Duesbery, N.S., et al., *Proteolytic inactivation of MAP-kinase-kinase by anthrax lethal factor*. [see comment]. Science, 1998. **280**(5364): p. 734-7.
58. Pellizzari, R., et al., *Anthrax lethal factor cleaves MKK3 in macrophages and inhibits the LPS/IFN γ -induced release of NO and TNF α* . FEBS Letters, 1999. **462**(1-2): p. 199-204.
59. Bardwell, A.J., M. Abdollahi, and L. Bardwell, *Anthrax lethal factor-cleavage products of MAPK (mitogen-activated protein kinase) kinases exhibit reduced binding to their cognate MAPKs*. Biochemical Journal, 2004. **378**(Pt 2): p. 569-77.
60. Chopra, A.P., et al., *Anthrax lethal factor proteolysis and inactivation of MAPK kinase*. Journal of Biological Chemistry, 2003. **278**(11): p. 9402-6.
61. Duesbery, N.S. and G.F. Vande Woude, *Anthrax toxins*. Cellular & Molecular Life Sciences, 1999. **55**(12): p. 1599-609.
62. Arora, N. and S.H. Leppla, *Fusions of anthrax toxin lethal factor with shiga toxin and diphtheria toxin enzymatic domains are toxic to mammalian cells*. Infection & Immunity, 1994. **62**(11): p. 4955-61.
63. Firoved, A.M., et al., *Anthrax edema toxin sensitizes DBA/2J mice to lethal toxin*. Infection & Immunity, 2007. **75**(5): p. 2120-5.
64. Pezard, C., P. Berche, and M. Mock, *Contribution of individual toxin components to virulence of Bacillus anthracis*. Infection & Immunity, 1991. **59**(10): p. 3472-7.
65. Hanna, P.C., S. Kochi, and R.J. Collier, *Biochemical and physiological changes induced by anthrax lethal toxin in J774 macrophage-like cells*. Molecular Biology of the Cell, 1992. **3**(11): p. 1269-77.
66. Carson-Walter, E.B., et al., *Cell surface tumor endothelial markers are conserved in mice and humans*. Cancer Research, 2001. **61**(18): p. 6649-55.
67. Collier, R.J. and J.A. Young, *Anthrax toxin*. Annual Review of Cell & Developmental Biology, 2003. **19**: p. 45-70.
68. Liu, S. and S.H. Leppla, *Cell surface tumor endothelium marker 8 cytoplasmic tail-independent anthrax toxin binding, proteolytic processing, oligomer formation, and internalization*. Journal of Biological Chemistry, 2003. **278**(7): p. 5227-34.
69. Bradley, K.A., et al., *Binding of anthrax toxin to its receptor is similar to alpha integrin-ligand interactions*. Journal of Biological Chemistry, 2003. **278**(49): p. 49342-7.
70. Bell, S.E., et al., *Differential gene expression during capillary morphogenesis in 3D collagen matrices: regulated expression of genes involved in basement membrane matrix assembly, cell cycle progression, cellular differentiation and G-protein signaling*. Journal of Cell Science, 2001. **114**(Pt 15): p. 2755-73.
71. Scobie, H.M., et al., *Human capillary morphogenesis protein 2 functions as an anthrax toxin receptor*. Proceedings of the National Academy of Sciences of the United States of America, 2003. **100**(9): p. 5170-4.
72. Wei, W., et al., *The LDL receptor-related protein LRP6 mediates internalization and lethality of anthrax toxin*. [see comment]. Cell, 2006. **124**(6): p. 1141-54.
73. Bann, J.G., L. Cegelski, and S.J. Hultgren, *LRP6 holds the key to the entry of anthrax toxin*. [comment]. Cell, 2006. **124**(6): p. 1119-21.

74. Young, J.J., et al., *LRP5 and LRP6 are not required for protective antigen-mediated internalization or lethality of anthrax lethal toxin*. PLoS Pathogens, 2007. **3**(3): p. e27.
75. Singh, Y., V.K. Chaudhary, and S.H. Leppla, *A deleted variant of Bacillus anthracis protective antigen is non-toxic and blocks anthrax toxin action in vivo*. Journal of Biological Chemistry, 1989. **264**(32): p. 19103-7.
76. Abrami, L., et al., *Anthrax toxin triggers endocytosis of its receptor via a lipid raft-mediated clathrin-dependent process.[see comment]*. Journal of Cell Biology, 2003. **160**(3): p. 321-8.
77. Abrami, L., et al., *Membrane insertion of anthrax protective antigen and cytoplasmic delivery of lethal factor occur at different stages of the endocytic pathway*. Journal of Cell Biology, 2004. **166**(5): p. 645-51.
78. Koehler, T.M. and R.J. Collier, *Anthrax toxin protective antigen: low-pH-induced hydrophobicity and channel formation in liposomes*. Molecular Microbiology, 1991. **5**(6): p. 1501-6.
79. Fasano, A. and J.P. Nataro, *Intestinal epithelial tight junctions as targets for enteric bacteria-derived toxins*. Advanced Drug Delivery Reviews, 2004. **56**(6): p. 795-807.
80. Warfel, J.M., A.D. Steele, and F. D'Agnillo, *Anthrax lethal toxin induces endothelial barrier dysfunction*. American Journal of Pathology, 2005. **166**(6): p. 1871-81.
81. Bruce Alberts, A.J., Julian Lewis, Martin Raff, Keith Roberts, and Peter Walter., *Molecular Biology of the Cell* fourth ed. 2002: Garland Science.
82. Harvey Lodish, A.B., S. Lawrence Zipursky, Paul Matsudaira, David Baltimore, James Darnell *Molecular Cell Biology*. fourth ed. 1999: W. H. Freeman and Company.
83. Holthofer, B., et al., *Structure and Function of Desmosomes*, in *International Review of Cytology*. 2007, Academic Press. p. 65-163.
84. Michael, Z.G., *Integrin signaling in epithelial cells*. Cancer letters, 2007. **247**(1): p. 1-25.
85. Wozniak, M.A., et al., *Focal adhesion regulation of cell behavior*. Biochimica et Biophysica Acta, 2004. **1692**(2-3): p. 103-19.
86. Chandra, H., et al., *Proteome analysis of mouse macrophages treated with anthrax lethal toxin*. Biochimica et Biophysica Acta, 2005. **1747**(2): p. 151-9.
87. During, R.L., et al., *Anthrax lethal toxin paralyzes neutrophil actin-based motility*. Journal of Infectious Diseases, 2005. **192**(5): p. 837-45.
88. During, R.L., et al., *Anthrax lethal toxin paralyzes actin-based motility by blocking Hsp27 phosphorylation*. EMBO Journal, 2007. **26**(9): p. 2240-50.
89. O'Brien, J., et al., *Effects of anthrax toxin components on human neutrophils*. Infection & Immunity, 1985. **47**(1): p. 306-10.
90. Campbell, N.A., *Biology*. fourth ed. 1996: Addison Wesley Publishing Company.
91. Takai, Y., T. Sasaki, and T. Matozaki, *Small GTP-binding proteins*. Physiological Reviews, 2001. **81**(1): p. 153-208.
92. Westermann, S. and K. Weber, *Post-translational modifications regulate microtubule function*. Nat Rev Mol Cell Biol, 2003. **4**(12): p. 938-948.
93. Pollard, T.D., *The cytoskeleton, cellular motility and the reductionist agenda.[comment]*. Nature, 2003. **422**(6933): p. 741-5.
94. Ridley, A.J., et al., *Cell migration: integrating signals from front to back*. Science, 2003. **302**(5651): p. 1704-9.

95. Martinez-Quiles, N., et al., *Erk/Src Phosphorylation of Cortactin Acts as a Switch On-Switch Off Mechanism That Controls Its Ability To Activate N-WASP*. *Mol. Cell. Biol.*, 2004. **24**(12): p. 5269-5280.
96. Johndrow, J.E., C.R. Magie, and S.M. Parkhurst, *Rho GTPase function in flies: insights from a developmental and organismal perspective*. *Biochemistry & Cell Biology*, 2004. **82**(6): p. 643-57.
97. Govek, E.E., S.E. Newey, and L. Van Aelst, *The role of the Rho GTPases in neuronal development*. *Genes & Development*, 2005. **19**(1): p. 1-49.
98. Desai, L.P., et al., *RhoA and Rac1 are both required for efficient wound closure of airway epithelial cells*. *American Journal of Physiology - Lung Cellular & Molecular Physiology*, 2004. **287**(6): p. L1134-44.
99. Nalbant, P., et al., *Activation of Endogenous Cdc42 Visualized in Living Cells*. *Science*, 2004. **305**(5690): p. 1615-1619.
100. Yang, L., L. Wang, and Y. Zheng, *Gene targeting of Cdc42 and Cdc42GAP affirms the critical involvement of Cdc42 in filopodia induction, directed migration, and proliferation in primary mouse embryonic fibroblasts*. *Molecular Biology of the Cell*, 2006. **17**(11): p. 4675-85.
101. http://www.cellsignal.com/reference/pathway/pdfs/MAPK_Cascades.pdf. [cited.
102. Lewis, T.S., P.S. Shapiro, and N.G. Ahn, *Signal transduction through MAP kinase cascades*. *Advances in Cancer Research*, 1998. **74**: p. 49-139.
103. Crews, C.M., A. Alessandrini, and R.L. Erikson, *The primary structure of MEK, a protein kinase that phosphorylates the ERK gene product*. *Science*, 1992. **258**(5081): p. 478-480.
104. Alessi, D.R., et al., *Identification of the sites in MAP kinase kinase-1 phosphorylated by p74raf-1*. *EMBO Journal*, 1994. **13**(7): p. 1610-9.
105. Rosen, L.B., et al., *Membrane depolarization and calcium influx stimulate MEK and MAP kinase via activation of Ras*. *Neuron*, 1994. **12**(6): p. 1207-1221.
106. Cowley, S., et al., *Activation of MAP kinase kinase is necessary and sufficient for PC12 differentiation and for transformation of NIH 3T3 cells*. *Cell*, 1994. **77**(6): p. 841-52.
107. Webb, D.J., D.H. Nguyen, and S.L. Gonias, *Extracellular signal-regulated kinase functions in the urokinase receptor-dependent pathway by which neutralization of low density lipoprotein receptor-related protein promotes fibrosarcoma cell migration and matrigel invasion*. *Journal of Cell Science*, 2000. **113**(Pt 1): p. 123-34.
108. Huang, C., K. Jacobson, and M.D. Schaller, *MAP kinases and cell migration*. *Journal of Cell Science*, 2004. **117**(Pt 20): p. 4619-28.
109. Totsukawa, G., et al., *Distinct roles of MLCK and ROCK in the regulation of membrane protrusions and focal adhesion dynamics during cell migration of fibroblasts*. *J. Cell Biol.*, 2004. **164**(3): p. 427-439.
110. Webb, D.J., et al., *FAK-Src signalling through paxillin, ERK and MLCK regulates adhesion disassembly*. *Nature Cell Biology*, 2004. **6**(2): p. 154-61.
111. Glading, A., et al., *Epidermal growth factor activates m-calpain (calpain II), at least in part, by extracellular signal-regulated kinase-mediated phosphorylation*. *Molecular & Cellular Biology*, 2004. **24**(6): p. 2499-512.
112. Hunger-Glaser, I., et al., *Bombesin, lysophosphatidic acid, and epidermal growth factor rapidly stimulate focal adhesion kinase phosphorylation at Ser-*

- 910: *requirement for ERK activation*. Journal of Biological Chemistry, 2003. **278**(25): p. 22631-43.
113. Sharma, G.D., J. He, and H.E. Bazan, *p38 and ERK1/2 coordinate cellular migration and proliferation in epithelial wound healing: evidence of cross-talk activation between MAP kinase cascades*. Journal of Biological Chemistry, 2003. **278**(24): p. 21989-97.
114. Hedges, J.C., et al., *A Role for p38MAPK/HSP27 Pathway in Smooth Muscle Cell Migration*. J. Biol. Chem., 1999. **274**(34): p. 24211-24219.
115. Huang, C., et al., *Phosphorylation of paxillin by p38MAPK is involved in the neurite extension of PC-12 cells*. J. Cell Biol., 2004. **164**(4): p. 593-602.
116. Tamara Mirzapioazova, I.A.K.L.R.J.G.N.G.A.D.V., *The role of caldesmon in the regulation of endothelial cytoskeleton and migration*. Journal of Cellular Physiology, 2005. **203**(3): p. 520-528.
117. Rousseau, S., et al., *p38 MAP kinase activation by vascular endothelial growth factor mediates actin reorganization and cell migration in human endothelial cells*. Oncogene, 1997. **15**(18): p. 2169-77.
118. Benndorf, R., et al., *Phosphorylation and supramolecular organization of murine small heat shock protein HSP25 abolish its actin polymerization-inhibiting activity*. Journal of Biological Chemistry, 1994. **269**(32): p. 20780-4.
119. Lavoie, J.N., et al., *Modulation of actin microfilament dynamics and fluid phase pinocytosis by phosphorylation of heat shock protein 27*. Journal of Biological Chemistry, 1993. **268**(32): p. 24210-4.
120. Singh, S., et al., *Identification of the p16-Arc subunit of the Arp 2/3 complex as a substrate of MAPK-activated protein kinase 2 by proteomic analysis*. Journal of Biological Chemistry, 2003. **278**(38): p. 36410-7.
121. Werz, O., et al., *5-lipoxygenase is phosphorylated by p38 kinase-dependent MAPKAP kinases*. Proceedings of the National Academy of Sciences of the United States of America, 2000. **97**(10): p. 5261-6.
122. Yujiri, T., et al., *MEK kinase 1 gene disruption alters cell migration and c-Jun NH2-terminal kinase regulation but does not cause a measurable defect in NF-kappa B activation*. Proceedings of the National Academy of Sciences of the United States of America, 2000. **97**(13): p. 7272-7.
123. Hauck, C.R., et al., *Inhibition of focal adhesion kinase expression or activity disrupts epidermal growth factor-stimulated signaling promoting the migration of invasive human carcinoma cells*. Cancer Research, 2001. **61**(19): p. 7079-90.
124. Shin, E.Y., S.Y. Kim, and E.G. Kim, *c-Jun N-terminal kinase is involved in motility of endothelial cell*. Experimental & Molecular Medicine, 2001. **33**(4): p. 276-83.
125. Javelaud, D., et al., *Disruption of Basal JNK Activity Differentially Affects Key Fibroblast Functions Important for Wound Healing*. J. Biol. Chem., 2003. **278**(27): p. 24624-24628.
126. Huang, C., et al., *JNK phosphorylates paxillin and regulates cell migration*. Nature, 2003. **424**(6945): p. 219-223.
127. Otto, I.M., et al., *The p150-Spir protein provides a link between c-Jun N-terminal kinase function and actin reorganization*. Current Biology, 2000. **10**(6): p. 345-8.
128. Gdalyahu, A., et al., *DCX, a new mediator of the JNK pathway*. EMBO Journal, 2004. **23**(4): p. 823-32.

129. Chang, L., et al., *JNK1 is required for maintenance of neuronal microtubules and controls phosphorylation of microtubule-associated proteins*. *Developmental Cell*, 2003. **4**(4): p. 521-33.
130. Cote, C.K., N. Van Rooijen, and S.L. Welkos, *Roles of macrophages and neutrophils in the early host response to Bacillus anthracis spores in a mouse model of infection*. *Infection & Immunity*, 2006. **74**(1): p. 469-80.
131. Cleret, A., et al., *Lung dendritic cells rapidly mediate anthrax spore entry through the pulmonary route*. *Journal of Immunology*, 2007. **178**(12): p. 7994-8001.
132. Russell, B.H., et al., *Potential dissemination of Bacillus anthracis utilizing human lung epithelial cells*. *Cellular Microbiology*. **0**(0): p.???-???
133. Gutting, B.W., et al., *Differential susceptibility of macrophage cell lines to Bacillus anthracis-Vollum 1B*. *Toxicology in Vitro*, 2005. **19**(2): p. 221-9.
134. Hanna, P., *Anthrax pathogenesis and host response*. *Current Topics in Microbiology & Immunology*, 1998. **225**: p. 13-35.
135. Hanna, P., *Lethal toxin actions and their consequences*. *Journal of Applied Microbiology*, 1999. **87**(2): p. 285-7.
136. Kim, S.O., et al., *Sensitizing anthrax lethal toxin-resistant macrophages to lethal toxin-induced killing by tumor necrosis factor-alpha*. *Journal of Biological Chemistry*, 2003. **278**(9): p. 7413-21.
137. Popov, S.G., et al., *Lethal toxin of Bacillus anthracis causes apoptosis of macrophages*. *Biochemical & Biophysical Research Communications*, 2002. **293**(1): p. 349-55.
138. Boyden, E.D. and W.F. Dietrich, *Nalp1b controls mouse macrophage susceptibility to anthrax lethal toxin.[see comment]*. *Nature Genetics*, 2006. **38**(2): p. 240-4.
139. Bugge, T.H. and S.H. Leppla, *Anthrax target in macrophages unveiled.[comment]*. *Nature Genetics*, 2006. **38**(2): p. 137-8.
140. Ting, J.P. and B.K. Davis, *CATERPILLER: a novel gene family important in immunity, cell death, and diseases*. *Annual Review of Immunology*, 2005. **23**: p. 387-414.
141. Lamkanfi, M., et al., *Caspase-1 inflammasomes in infection and inflammation*. *Journal of Leukocyte Biology*, 2007. **82**(2): p. 220-5.
142. Cordoba-Rodriguez, R., et al., *Anthrax lethal toxin rapidly activates caspase-1/ICE and induces extracellular release of interleukin (IL)-1beta and IL-18*. *Journal of Biological Chemistry*, 2004. **279**(20): p. 20563-6.
143. Burns, K., F. Martinon, and J. Tschopp, *New insights into the mechanism of IL-1beta maturation*. *Current Opinion in Immunology*, 2003. **15**(1): p. 26-30.
144. Tschopp, J., F. Martinon, and K. Burns, *NALPs: a novel protein family involved in inflammation*. *Nature Reviews Molecular Cell Biology*, 2003. **4**(2): p. 95-104.
145. Wickliffe, K.E., S.H. Leppla, and M. Moayeri, *Anthrax lethal toxin-induced inflammasome formation and caspase-1 activation are late events dependent on ion fluxes and the proteasome*. *Cellular Microbiology*, 2008. **10**(2): p. 332-343.
146. Muehlbauer, S.M., et al., *Anthrax lethal toxin kills macrophages in a strain-specific manner by apoptosis or caspase-1-mediated necrosis*. *Cell Cycle*, 2007. **6**(6): p. 758-66.
147. Hanna, P.C., et al., *Role of macrophage oxidative burst in the action of anthrax lethal toxin*. *Molecular Medicine*, 1994. **1**(1): p. 7-18.

148. Tang, G. and S.H. Leppla, *Proteasome activity is required for anthrax lethal toxin to kill macrophages*. Infection & Immunity, 1999. **67**(6): p. 3055-60.
149. Hammond, S.E. and P.C. Hanna, *Lethal factor active-site mutations affect catalytic activity in vitro*. Infection & Immunity, 1998. **66**(5): p. 2374-8.
150. Menard, A., et al., *The vacuolar ATPase proton pump is required for the cytotoxicity of Bacillus anthracis lethal toxin*. FEBS Letters, 1996. **386**(2-3): p. 161-4.
151. Kau, J.H., et al., *Calyculin A sensitive protein phosphatase is required for Bacillus anthracis lethal toxin induced cytotoxicity*. Current Microbiology, 2002. **44**(2): p. 106-11.
152. Dell'Aica, I., et al., *Potent inhibitors of anthrax lethal factor from green tea*. EMBO Reports, 2004. **5**(4): p. 418-22.
153. Gaddis, B.D., L.V. Avramova, and J. Chmielewski, *Inhibitors of anthrax lethal factor*. Bioorganic & Medicinal Chemistry Letters, 2007. **17**(16): p. 4575-4578.
154. Shoop, W.L., et al., *Anthrax lethal factor inhibition*. Proceedings of the National Academy of Sciences of the United States of America, 2005. **102**(22): p. 7958-63.
155. Panchal, R.G., et al., *Identification of small molecule inhibitors of anthrax lethal factor*. Nature Structural & Molecular Biology, 2004. **11**(1): p. 67-72.
156. Johnson, S.L., et al., *Anthrax lethal factor protease inhibitors: synthesis, SAR, and structure-based 3D QSAR studies*. Journal of Medicinal Chemistry, 2006. **49**(1): p. 27-30.
157. Min, D.H., W.J. Tang, and M. Mrksich, *Chemical screening by mass spectrometry to identify inhibitors of anthrax lethal factor*. Nature Biotechnology, 2004. **22**(6): p. 717-23.
158. Lee, L.V., et al., *Inhibition of the proteolytic activity of anthrax lethal factor by aminoglycosides*. Journal of the American Chemical Society, 2004. **126**(15): p. 4774-5.
159. Schepetkin, I.A., et al., *Novel small-molecule inhibitors of anthrax lethal factor identified by high-throughput screening*. Journal of Medicinal Chemistry, 2006. **49**(17): p. 5232-44.
160. Fridman, M., et al., *Dual effect of synthetic aminoglycosides: antibacterial activity against Bacillus anthracis and inhibition of anthrax lethal factor*. Angewandte Chemie. International Ed. in English, 2005. **44**(3): p. 447-52.
161. Jiao, G.S., et al., *Guanidinylated 2,5-dideoxystreptamine derivatives as anthrax lethal factor inhibitors*. Bioorganic & Medicinal Chemistry Letters, 2006. **16**(6): p. 1527-31.
162. Jiao, G.S., et al., *Selectively guanidinylated derivatives of neamine. Syntheses and inhibition of anthrax lethal factor protease*. Bioorganic & Medicinal Chemistry Letters, 2006. **16**(19): p. 5183-9.
163. Goldman, M.E., et al., *Cationic polyamines inhibit anthrax lethal factor protease*. BMC Pharmacology, 2006. **6**: p. 8.
164. Salles, II, et al., *Toxin-induced resistance in Bacillus anthracis lethal toxin-treated macrophages*. Proceedings of the National Academy of Sciences of the United States of America, 2003. **100**(21): p. 12426-31.
165. Squires, R.C., S.M. Muehlbauer, and J. Brojatsch, *Proteasomes Control Caspase-1 Activation in Anthrax Lethal Toxin-mediated Cell Killing*. J. Biol. Chem., 2007. **282**(47): p. 34260-34267.

166. Alileche, A., et al., *Mitochondrial impairment is a critical event in anthrax lethal toxin-induced cytolysis of murine macrophages*. *Cell Cycle*, 2006. **5**(1): p. 100-6.
167. Ha, S.-D., et al., *Mitochondrial Proteins Bnip3 and Bnip3L Are Involved in Anthrax Lethal Toxin-induced Macrophage Cell Death*. *J. Biol. Chem.*, 2007. **282**(36): p. 26275-26283.
168. Park, J.M., et al., *Macrophage apoptosis by anthrax lethal factor through p38 MAP kinase inhibition*. *Science*, 2002. **297**(5589): p. 2048-51.
169. Fang, H., et al., *Anthrax lethal toxin has direct and potent inhibitory effects on B cell proliferation and immunoglobulin production*. *Journal of Immunology*, 2006. **176**(10): p. 6155-61.
170. Paccani, S.R., et al., *Anthrax toxins suppress T lymphocyte activation by disrupting antigen receptor signaling.[see comment]*. *Journal of Experimental Medicine*, 2005. **201**(3): p. 325-31.
171. Fang, H., et al., *Anthrax lethal toxin blocks MAPK kinase-dependent IL-2 production in CD4+ T cells*. *Journal of Immunology*, 2005. **174**(8): p. 4966-71.
172. Koo, H.M., et al., *Apoptosis and melanogenesis in human melanoma cells induced by anthrax lethal factor inactivation of mitogen-activated protein kinase kinase*. *Proceedings of the National Academy of Sciences of the United States of America*, 2002. **99**(5): p. 3052-7.
173. Ha, S.-D., et al., *Critical role of PI3-K/Akt/GSK-3beta signaling pathway in recovery from anthrax lethal toxin-induced cell cycle arrest and MEK cleavage in macrophages*. *J. Biol. Chem.*, 2007: p. M707622200.
174. Paddle, B.M., V.K. Wong, and B.D. Muller, *The cytotoxic effect of anthrax lethal toxin on human lung cells in vitro and the protective action of bovine antibodies to PA and LF*. *Journal of Applied Toxicology*, 2006. **26**(2): p. 162-8.
175. Kirby, J.E., *Anthrax lethal toxin induces human endothelial cell apoptosis*. *Infection & Immunity*, 2004. **72**(1): p. 430-9.
176. Kassam, A., S.D. Der, and J. Mogridge, *Differentiation of human monocytic cell lines confers susceptibility to Bacillus anthracis lethal toxin*. *Cellular Microbiology*, 2005. **7**(2): p. 281-92.
177. Popov, S.G., et al., *Effect of Bacillus anthracis lethal toxin on human peripheral blood mononuclear cells*. *FEBS Letters*, 2002. **527**(1-3): p. 211-5.
178. Guidi-Rontani, C., E. Duflot, and M. Mock, *Anthrax lethal toxin-induced mitogenic response of human T-cells*. *FEMS Microbiology Letters*, 1997. **157**(2): p. 285-9.
179. Jason E. Comer, A.K.C., Johnny W. Peterson, and Rolf König, *Direct Inhibition of T-Lymphocyte Activation by Anthrax Toxins In Vivo* *Infection and Immunity*, 2005. **73**(12): p. 8275-8281.
180. Huang, D., et al., *Inhibition of MAPK Kinase Signaling Pathways Suppressed Renal Cell Carcinoma Growth and Angiogenesis In vivo*. *Cancer Res*, 2008. **68**(1): p. 81-88.
181. Depeille, P., et al., *Anthrax Lethal Toxin Inhibits Growth of and Vascular Endothelial Growth Factor Release from Endothelial Cells Expressing the Human Herpes Virus 8 Viral G Protein Coupled Receptor*. *Clin Cancer Res*, 2007. **13**(19): p. 5926-5934.
182. Dixon, T.C., et al., *Anthrax.[see comment]*. *New England Journal of Medicine*, 1999. **341**(11): p. 815-26.
183. Grinberg, L.M., et al., *Quantitative pathology of inhalational anthrax I: quantitative microscopic findings*. *Modern Pathology*, 2001. **14**(5): p. 482-95.

184. Mohamed, N., et al., *A high-affinity monoclonal antibody to anthrax protective antigen passively protects rabbits before and after aerosolized Bacillus anthracis spore challenge*. Infection & Immunity, 2005. **73**(2): p. 795-802.
185. Peterson, J.W., et al., *Human monoclonal anti-protective antigen antibody completely protects rabbits and is synergistic with ciprofloxacin in protecting mice and guinea pigs against inhalation anthrax*. Infection & Immunity, 2006. **74**(2): p. 1016-24.
186. Darly J. Manayani, D.T., Kelly A. Dryden, Vijay Reddy, Marc E. Siladi, John M. Marlett, G. Jonah A. Rainey, Michael E. Pique, Heather M. Scobie, Mark Yeager, John A. T. Young, Marianne Manchester, Anette Schneemann, *A Viral Nanoparticle with Dual Function as an Anthrax Antitoxin and Vaccine*. PLoS Pathogens, 2007. **3**(10).
187. de Jong, P.M., et al., *Ciliogenesis in human bronchial epithelial cells cultured at the air-liquid interface*. American Journal of Respiratory Cell & Molecular Biology, 1994. **10**(3): p. 271-7.
188. Gray, T.E., et al., *Mucociliary differentiation of serially passaged normal human tracheobronchial epithelial cells*. American Journal of Respiratory Cell & Molecular Biology, 1996. **14**(1): p. 104-12.
189. Bottenstein, J., et al., *The growth of cells in serum-free hormone-supplemented media*. Methods in Enzymology, 1979. **58**: p. 94-109.
190. Wu, R., Y.H. Zhao, and M.M. Chang, *Growth and differentiation of conducting airway epithelial cells in culture*. European Respiratory Journal, 1997. **10**(10): p. 2398-403.
191. Martin, W.R., et al., *Growth and differentiation of primary tracheal epithelial cells in culture: regulation by extracellular calcium*. Journal of Cellular Physiology, 1991. **147**(1): p. 138-48.
192. Floryk, D. and J. Houštek, *Tetramethyl Rhodamine Methyl Ester (TMRM) is Suitable for Cytofluorometric Measurements of Mitochondrial Membrane Potential in Cells Treated with Digitonin*. Bioscience Reports, 1999. **19**(1): p. 27-34.
193. Alley, M.C., et al., *Feasibility of drug screening with panels of human tumor cell lines using a microculture tetrazolium assay*. Cancer Research, 1988. **48**(3): p. 589-601.
194. Gorczyca, W., J. Gong, and Z. Darzynkiewicz, *Detection of DNA strand breaks in individual apoptotic cells by the in situ terminal deoxynucleotidyl transferase and nick translation assays*. Cancer Research, 1993. **53**(8): p. 1945-51.
195. Chapman, R.S., et al., *Further characterisation of the in situ terminal deoxynucleotidyl transferase (TdT) assay for the flow cytometric analysis of apoptosis in drug resistant and drug sensitive leukaemic cells*. Cytometry, 1995. **20**(3): p. 245-56.
196. Korzeniewski, C. and D.M. Callewaert, *An enzyme-release assay for natural cytotoxicity*. Journal of Immunological Methods, 1983. **64**(3): p. 313-20.
197. Decker, T. and M.L. Lohmann-Matthes, *A quick and simple method for the quantitation of lactate dehydrogenase release in measurements of cellular cytotoxicity and tumor necrosis factor (TNF) activity*. Journal of Immunological Methods, 1988. **115**(1): p. 61-9.
198. Radyuk, S.N., et al., *In vitro-generated respiratory mucosa: a new tool to study inhalational anthrax*. Biochemical & Biophysical Research Communications, 2003. **305**(3): p. 624-32.

199. <http://www.antibodybeyond.com/reviews/cell-marker-reviews.htm>. [cited.
200. Ganz, T. and R.I. Lehrer, *Defensins*. Current Opinion in Immunology, 1994. **6**(4): p. 584-9.
201. Bonuccelli, G., et al., *ATR/TEM8 is highly expressed in epithelial cells lining Bacillus anthracis' three sites of entry: implications for the pathogenesis of anthrax infection*. American Journal of Physiology - Cell Physiology, 2005. **288**(6): p. C1402-10.
202. Gumbiner, B.M., *Regulation of cadherin-mediated adhesion in morphogenesis*. Nature Reviews Molecular Cell Biology, 2005. **6**(8): p. 622-34.
203. Mickey Pentecost, G.O., Julie A Theriot, and Manuel R Amieva, *Listeria monocytogenes Invades the Epithelial Junctions at Sites of Cell Extrusion*. PLoS Pathology, 2006. **2**(1): p. 29-40.
204. Burridge, K., et al., *Focal adhesions: transmembrane junctions between the extracellular matrix and the cytoskeleton*. Annual Review of Cell Biology, 1988. **4**: p. 487-525.
205. Turner, C.E., *Paxillin interactions*. J Cell Sci, 2000. **113**(23): p. 4139-4140.
206. Sieg, D.J., et al., *FAK integrates growth-factor and integrin signals to promote cell migration*. Nat Cell Biol, 2000. **2**(5): p. 249-256.
207. Stefega, M., C. DerMardirossian, and G.M. Bokoch, *Affinity-based assay of Rho guanosine triphosphatase activation*. Methods of Molecular Biology, 2006. **332**: p. 269-79.
208. Sugahara, K., et al., *Alveolar epithelial cells: differentiation and lung injury*. Respirology, 2006. **11**(s1): p. S28-S31.
209. Ulrich, K., et al., *Keratinocyte growth factor therapy in murine oleic acid-induced acute lung injury*. Am J Physiol Lung Cell Mol Physiol, 2005. **288**(6): p. L1179-1192.
210. Ashton, M.R., et al., *Surfactant phosphatidylcholine composition during dexamethasone treatment in chronic lung disease*. Arch. Dis. Child. Fetal Neonatal Ed., 1994. **71**(2): p. F114-117.
211. Chen, Y., et al., *Dexamethasone-Mediated Repression of MUC5AC Gene Expression in Human Lung Epithelial Cells*. Am. J. Respir. Cell Mol. Biol., 2006. **34**(3): p. 338-347.
212. Roberts, J.E., et al., *Ltx1, a mouse locus that influences the susceptibility of macrophages to cytolysis caused by intoxication with Bacillus anthracis lethal factor, maps to chromosome 11*. Molecular Microbiology, 1998. **29**(2): p. 581-91.
213. Friedlander, A.M., et al., *Characterization of macrophage sensitivity and resistance to anthrax lethal toxin*. Infection & Immunity, 1993. **61**(1): p. 245-52.
214. Welkos, S.L., et al., *Resistance to the Sterne strain of B. anthracis: phagocytic cell responses of resistant and susceptible mice*. Microbial Pathogenesis, 1989. **7**(1): p. 15-35.
215. Singh, Y., et al., *Internalization and processing of Bacillus anthracis lethal toxin by toxin-sensitive and -resistant cells*. Journal of Biological Chemistry, 1989. **264**(19): p. 11099-102.
216. Welkos, S.L., T.J. Keener, and P.H. Gibbs, *Differences in susceptibility of inbred mice to Bacillus anthracis*. Infection & Immunity, 1986. **51**(3): p. 795-800.

217. Sachs, L.A., W.E. Finkbeiner, and J.H. Widdicombe, *Effects of media on differentiation of cultured human tracheal epithelium*. In *Vitro Cellular & Developmental Biology*. Animal, 2003. **39**(1-2): p. 56-62.
218. Beauregard, K.E., et al., *Anthrax toxin entry into polarized epithelial cells*. *Infection & Immunity*, 1999. **67**(6): p. 3026-30.
219. Moayeri, M., et al., *Bacillus anthracis lethal toxin induces TNF-alpha-independent hypoxia-mediated toxicity in mice.[see comment]*. *Journal of Clinical Investigation*, 2003. **112**(5): p. 670-82.
220. Cui, X., et al., *Lethality during continuous anthrax lethal toxin infusion is associated with circulatory shock but not inflammatory cytokine or nitric oxide release in rats*. *American Journal of Physiology - Regulatory Integrative & Comparative Physiology*, 2004. **286**(4): p. R699-709.
221. <http://www.emedicine.com/emerg/topic864.htm>. [cited.
222. Webster, J.I., et al., *Anthrax lethal factor represses glucocorticoid and progesterone receptor activity*. *Proceedings of the National Academy of Sciences of the United States of America*, 2003. **100**(10): p. 5706-11.
223. Tarnawski, A.S., *Cellular and molecular mechanisms of gastrointestinal ulcer healing*. *Digestive Diseases & Sciences*, 2005. **50**: p. S24-33.
224. Wennerberg, K. and C.J. Der, *Rho-family GTPases: it's not only Rac and Rho (and I like it)*. *Journal of Cell Science*, 2004. **117**(Pt 8): p. 1301-12.
225. Wehrle-Haller, B. and B.A. Imhof, *Actin, microtubules and focal adhesion dynamics during cell migration*. *The International Journal of Biochemistry & Cell Biology*, 2003. **35**(1): p. 39-50.
226. Rennefahrt, U.E., et al., *Constitutive JNK activation in NIH 3T3 fibroblasts induces a partially transformed phenotype*. *Journal of Biological Chemistry*, 2002. **277**(33): p. 29510-8.
227. Steele, A.D., J.M. Warfel, and F. D'Agnillo, *Anthrax lethal toxin enhances cytokine-induced VCAM-1 expression on human endothelial cells*. *Biochemical & Biophysical Research Communications*, 2005. **337**(4): p. 1249-56.
228. Popova, T.G., et al., *Acceleration of epithelial cell syndecan-1 shedding by anthrax hemolytic virulence factors*. *BMC Microbiology*, 2006. **6**: p. 8.
229. Raftopoulou, M. and A. Hall, *Cell migration: Rho GTPases lead the way*. *Developmental Biology*, 2004. **265**(1): p. 23-32.
230. Etienne-Manneville, S. and A. Hall, *Cdc42 regulates GSK-3beta and adenomatous polyposis coli to control cell polarity*. *Nature*, 2003. **421**(6924): p. 753-6.
231. Ivins, B.E., J.D. Ristroph, and G.O. Nelson, *Influence of body weight on response of Fischer 344 rats to anthrax lethal toxin*. *Applied & Environmental Microbiology*, 1989. **55**(8): p. 2098-100.
232. Ussar, S. and T. Voss, *MEK1 and MEK2, different regulators of the G1/S transition*. *Journal of Biological Chemistry*, 2004. **279**(42): p. 43861-9.
233. Yee, A.S., et al., *The HBP1 transcriptional repressor and the p38 MAP kinase: unlikely partners in G1 regulation and tumor suppression*. *Gene*, 2004. **336**(1): p. 1-13.

9 INDEX OF FIGURES

Figure 2-1: Electron microscopy of spores and vegetative form of anthrax.	4
Figure 2-2: Plasmids pXO1 and pXO2 of <i>B. anthracis</i> contain genes, which encode virulence factors.	5
Figure 2-3: Protective antigen crystal structure and pore formation from [35].	6
Figure 2-4: Crystal structure of lethal factor from [49].	7
Figure 2-5: Alignment for MAPKK cleavage site.	8
Figure 2-6: Lethal factor interacting region.	9
Figure 2-7: Alternative splice variants of the TEM8 receptor.	10
Figure 2-8: The splice variants of the CMG2 receptor.	11
Figure 2-9: Anthrax toxin cycle.	12
Figure 2-10: Overview of the junction complex.	13
Figure 2-11: Cytoskeletal polymers.	15
Figure 2-12: Mechanism of actin turnover from [93].	17
Figure 2-13: Cell migration key players.	18
Figure 2-14: Signaling cascade of Rho, Rac and Cdc42 and their influence on the cytoskeleton.	19
Figure 2-15: MAPK pathway.	20
Figure 2-16: ERK signaling pathway causes motility changes.	21
Figure 2-17: p38 signaling pathway causes motility changes.	22
Figure 2-18: JNK signaling pathway causes motility changes.	23
Figure 4-1: Differentiated airway system.	37
Figure 4-2: Resistance measurement of 3D grown cells with an electrical voltohmmeter.	46
Figure 5-1: Morphology of normal tissue culture treated NHBE and polarized 3D cells in EM.	50
Figure 5-2: Pneumocyte characterization.	51
Figure 5-3: mRNA and protein expression of MUC5AC in the 3D system.	52
Figure 5-4: Anthrax receptor expression.	52
Figure 5-5: Effect of LT treatment on the protein and mRNA levels of MAPKKs.	53
Figure 5-6: Resistance and permeability change.	54
Figure 5-7: LDH release after LT treatment in the 3D system.	54
Figure 5-8: Increase of multicellular junction sites after LT treatment at the apical side.	55
Figure 5-9: Electron microscopy pictures of LT treated, polarized NHBE.	56
Figure 5-10: Lethal toxin induces tight junction alterations.	56
Figure 5-11: A diffuse adherens junction stain occurred after LT treatment.	57
Figure 5-12: Junctional proteins increase in membrane and cytoskeleton after LT exposure.	57
Figure 5-13: Stress fiber and tubulin bundle accumulations after LT treatment.	57
Figure 5-14: Quantification of increased actin filaments after LT treatment and actin polymerization inhibition.	57
Figure 5-15: Actin assembly is not inhibited after LT treatment.	57
Figure 5-16: Increased actin amounts in cytoskeletal fraction after LT treatment.	57
Figure 5-17: Increased tubulin stabilization after LT treatment.	57
Figure 5-18: Wound healing defect caused by LT.	57
Figure 5-19: Chemotaxis defect of LT and MAPK inhibitors treated cells.	57
Figure 5-20: Live cell imaging picture.	57
Figure 5-21: Elongation of focal adhesion.	57
Figure 5-22: Fractionation of adhesion proteins and their regulatory proteins.	57
Figure 5-23: Phosphorylation of adhesion proteins are not altered after LT treatment.	57

Figure 5-24: Adhesion defect to positive charged surfaces after LT treatment.	57
Figure 5-25: RhoGTPase mRNA and protein activity measurements.	57
Figure 5-26: MAPK pathways are important for wound healing.	57
Figure 5-27: Quantification of wound healing defects.	57
Figure 5-28: Rescue of resistance by KGF and dexamethasone.	57
Figure 5-29: Rescue of permeability increase by KGF and dexamethasone.	57
Figure 5-30: KGF and dexamethasone increase cell viability.	57
Figure 5-31: Lethal toxin does not alter membrane integrity.	57
Figure 5-32: Minimal DNA strand breaks after LT treatment measured in a TUNEL assay.	57
Figure 5-33: Caspase 3 activation is not induced by LT.	57
Figure 5-34: Blocked cell proliferation after LT treatment.	57
Figure 5-35: Increase of cells in G1 phase after LT treatment.	57
Figure 5-36: Mitochondrial potential alteration caused by MAPKK cleavage.	57
Figure 5-37: MAPKK expression induced by proteasome inhibitors.	57
Figure 5-38: Reduced proteasome activity after LT treatment.	57
Figure 5-39: Continuous MAPKK cleavage after 48 hours of LT treatment.	57
Figure 5-40: LT residues stored in cell.	57
Figure 5-41: Similar MAPKK cleavage activity of different LFs.	57
Figure 5-42: LF is localized in membrane compartments.	57
Figure 5-43: LF degradation after exposure to Raw cell lysates.	57
Figure 5-44: Biotinylated lethal factor did not alter cell viability.	57
Figure 5-45: MAPKK cleavage time course.	57
Figure 5-46: LFhisbio does not induce cell death within 24 hours treatment.	57
Figure 5-47: Protein sequence of lethal factor with biotinylated lysines (K).	57
Figure 5-48: LThisbio does not reduce the proteasome activity in NHBE.	57
Figure 5-49: LThisbio causes mainly hypopolarization of the mitochondrial potential in NHBE.	57
Figure 5-50: Cytotoxicity and resistance comparison of LT and LTbio in NHBE 3D.	57

10 INDEX OF TABLES

Table 2-1: Resistant and susceptible macrophage cell lines or mouse strains.	9
Table 2-2: Posttranslational modification of tubulin.	16
Table 2-3: Inhibitors for lethal toxin induced cytotoxicity.	25
Table 2-4: Symptoms of 10 Inhalational anthrax cases between October-November of 2001.	27
Table 4-1: Antibody List.	33
Table 4-2: Primer list.	34
Table 4-3: Non-cleavable MKK mutants.	44
Table 12-1: Lung cell markers	57

11 INDEX OF MOVIES

- Movie 1:** Untreated cells imaged every minute for 2 hours.
- Movie 2:** Lethal toxin treated cells imaged every minute for 2 hours.
- Movie 3:** Untreated cells imaged every 30 seconds for 40 minutes.
- Movie 4:** Lethal toxin treated cells imaged every 30 seconds for 40 minutes.
- Movie 5:** Three MAPK inhibitor combination imaged every 30 seconds for 40min.
- Movie 6:** MKK1/2 inhibitor imaged every 30 seconds for 40min.
- Movie 7:** p38 inhibitor imaged every 30 seconds for 40min.
- Movie 8:** JNK II inhibitor imaged every 30 seconds for 40min.
- Movie 9:** Infection of VECTOR EGFP CONTROL imaged every 30 seconds for 40min.
- Movie 10:** Infection of VECTOR EGFP CONTROL and 24hr LT treatment imaged every 30 seconds for 40min.
- Movie 11:** Infection of non-cleavable mkk1 and 2 MUTANTS imaged every 30 seconds for 40min.
- Movie 12:** Infection of non-cleavable mkk3 and 6 MUTANTS imaged every 30 seconds for 40min.
- Movie 13:** Infection of non-cleavable mkk1 and 2 MUTANTS and 24 HR LT TREATMENT imaged every 30 seconds for 40min.
- Movie 14:** Infection of non-cleavable mkk3 and 6 MUTANTS and 24 HR LT TREATMENT imaged every 30 seconds for 40min.
- Movie 15:** Infection of non-cleavable mkk4 and 7 MUTANTS imaged every 30 seconds for 40min.
- Movie 16:** Infection of non-cleavable mkk4 and 7 MUTANTS and 24 HR LT TREATMENT imaged every 30 seconds for 40min.
- Movie 17:** Biotinylated lethal Toxin imaged every 30 seconds for 40min.

12 APPENDIX

12.1 Summary of Characteristically Marker of Lung Cells

Pneumocyte I	Pneumocyte II	Clara Cells	Goblet Cells
Aquaporin 5 (PMID:9374640)	Surfactant Protein A (PMID: 8425584)	CC10 (PMID: 9070353)	MUC5AC (PMID: 16261889)
T1alpha (PMID: 11748153)	Surfactant Protein B (PMID: 11152647)	CC16 (PMID: 9517618)	Muc2 (PMID: 16143030)
HTI56 (PMID: 10706135)	Surfactant Protein C (PMID: 15268776)	CC26 (PMID: 10483522)	MUC5B (PMID: 12568489)
Caveolins (PMID: 9662443)	Surfactant Protein D (PMID: 11061091)	CCSP (PMID: 11704549)	PKD (PMID: 17208228)
Bauhinia purpurea lectin (PMID: 7894248)	TF antigen (PMID: 10071237)	SP-A (PMID: 16540737)	CDX-2 (PMID: 12559945)
	KL-6 (PMID: 11557124)	SP-B (PMID: 10383422)	cytokeratin 7 (PMID: 12412423)
	MUC1 (PMID: 15974816)	SP-C (PMID: 1591008)	CK20 (PMID: 16932021)
	CD208 (PMID: 14982840)	SP-D (PMID: 1527377)	Trefoil factor 3 (PMID: 10194185)
	gp600 (PMID: 2647848)	Urinary protein 1 (PMID: 1488625)	UJA-1 (PMID: 11073062)
	CD44v6 (PMID: 12940087)	Uteroglobin (PMID: 12838427)	
		UGRP1 (PMID: 11682631)	
		CYP2F2/CYP2B4 (PMID: 8652187)	
		Cytochrome P-450 (PMID: 9575866)	

Table 12-1: Lung cell markers
(adapted from [199])

12.2 Abbreviations

2D	two dimensional
3D	three dimensional
³ H	tritium
%	percent
Å	angstrom
aa	amino acids
ADF	actin depolymerization factor
ADP	adenosine diphosphate
AKT	V-akt murine thymoma viral oncogene homolog
Ala	alanine (A)
ALI	airway surface liquid
APS	ammonium persulfate
Arp2/3	actin related protein 2/3
ASC	apoptosis-associated speck-like protein
ATP	adenosine triphosphate
ATR	anthrax receptor
AVA	anthrax-vaccine absorbed
BCA	bicinchoninic acid
BD-1	beta-defensin-1
BD-2	beta-defensin-2
BEGM	bronchial epithelial growth media
bp	base pairs
BSA	bovine serum albumin
Ca	calcium
Ca ²⁺	calcium ion
cAMP	cyclic adenosine monophosphate
CapZ	capping protein from the Z-disc of muscle
CARD	caspase recruiting domain
CCCP	carbonyl cyanide 3-chlorophenylhydrazone
cDNA	coding DNA
CHO	chinese hamster ovary cell line
CMG2	capillary morphogenesis gene 2
CO ₂	carbon dioxide
Cortactin	cortical cortex binding protein
CRK	v-crk sarcoma virus CT10 oncogene homolog
Da	dalton
DAPI	4',6-diamidino-2-phenylindole dihydrochloride
dH ₂ O	deionized water
DIC	differential interference contrast
DMSO	dimethyl sulfoxide
DNA	deoxyribonucleic acid
e.g.	exempli gratia, latin; for example
ECL	enhanced chemiluminescent
ECM	extracellular matrix
EDTA	ethylenediaminetetraacetic acid
EF	edema factor
EGCG	epigallocatechin gallate
EGF	epithelial growth factor

EGTA	ethylenebis (oxyethylenenitrilo) tetraacetic acid
EM	electronmicroscope
ERK	extracellular signal-regulated kinases
ET	edema toxin
EtBr	ethidium bromide
EVOM	epithelial voltohmmeter
F-actin	filamentous actin
FAK	focal adhesion kinase
FBS	fetal bovine serum
Fc	fragment, crystallizable
Fig	figure
FITC	fluorescein isothiocyanate
for	forward
FSC	forward scattering
g	gram
G-actin	globular actin
GDP	guanosine diphosphate
Glu	glutamic acid (E)
GM130	cis-golgi matrix protein 130kDa
GTP	guanosine triphosphate
HBSS	hank's balanced salt solution
hr	hour
HRP	horseradish peroxidase
hrs	hours
Hsp	heat shock protein
HUVEC	human umbilical vein endothelial cells
IF	immunofluorescence
IL	interleukin
IP	immunoprecipitation
JNK	Jun N-terminal kinase
kb	kilo base pairs
kDa	kilo dalton
KGF	keratinocyte growth factor
Kif1c	kinesin family member 1c
LDH	lactate dehydrogenase
LF	lethal factor
LFIR	lethal factor interacting region
LPS	lipopolysaccharide
LRP2	low-density lipoprotein receptor-related protein 2
LRR	leucine-rich repeats
LT	lethal toxin
mA	milliampere
MAP	mitogen-activated protein
MAPK	MAP kinase
MAPKAPK 2/3	MAPK-activating protein kinase 2/3
MAPKK	MAP kinase kinases
MAPKKK	MAP kinase kinase kinases
MAPs	microtubule-associated proteins
MDCK	Madin-Darby Canine Kidney Epithelial Cells
MEK	MAP ERK kinase

mg	milligram
MIDAS	metal ion-dependent adhesion site
min	minutes
ml	milliliter
MLCK	myosin light chain kinase
MMP	matrix metalloproteinase
mRNA	messenger RNA
MT	microtubules
MTOC	microtubules organizing center
MTT	3-(4, 5-Dimethyl-2-thiazolyl)-2, 5-diphenyl-2H-tetrazolium bromide
MUC5AC	mucin 5AC
NaCl	sodium chloride
NADPH	nicotinamide adenine dinucleotide phosphate oxidase
Nalp1	NACHT, leucine rich repeat and PYD (pyrin domain) containing1
NaN3	sodium azide
nano-LC-MS-MS	nano-liquid chromatography-mass spec-mass spec
NaOH	sodiumhydroxide
NCBI	national center for biotechnology information
ng	nanogram
NHBE	normal human bronchial epithelial cells
NIH	national institute of health
NLR	NOD-like receptor protein
nm	nanometer
nmol	nanomolar
NOD	nucleotide-binding oligomerization domain
NP-40	nonidet P-40
PA	protective antigen
PAGE	polyacrylamide gel electrophoresis
PAK	p21-activated kinase
PARP	poly (ADP-ribose) polymerase-1
PBS	phosphate buffered saline
PCR	polymerase chain reaction
PET	polyester
PFA	paraformaldehyde
PI	propidium iodide
PI3K	Phosphoinositide-3 kinase
PIP ₂	phosphatidylinositol bisphosphate
PIX	PAK-interacting exchange factor
PLC	phosphorlipase C
PMSF	phenylmethylsulphonylfluoride
Pro	proline (P)
RA	retinoic acid
RCC	renal cell carcinoma
Rev	reverse
RIPA	radioimmuno-precipitation assay buffer
RNA	ribonucleic acid
ROCK	Rho-associated coiled-coil protein kinase 1
ROS	reactive oxygen species
rpm	rounds per minute

RT	room temperature
SAEC	small airway epithelial cells
SAGM	small airway growth media
Scar	suppressor of cAMP receptor
SDS	sodium dodecyl sulfate
sec	seconds
SP-A	surfactant A
SP-B	surfactant B
SSC	side scattering
T	thymidine
TAE	tris acetate EDTA
TBS	tris buffered saline
TBST	tris-buffered saline with tween
TE	tris EDTA buffer
TEER	trans epithelial electric resistance
TEM	transmission electron microscopy
TEM8	tumor endothelial marker 8
TEMED	N,N,N',N',tetramethylethylene diamine
THP-1	human acute monocytic leukemia cell line
Thr	threonine (T)
TMRM	tetramethyl rhodamine methyl ester
TNF α	tumor necrosis factor α
TNS	trypsin neutralizing solution
TSRI	The Scripps Research Institute
TUNEL	terminal deoxynucleotidyl transferase biotin-dUTP nick end labeling
Tyr	tyrosine (Y)
V	volts
VCAM-1	vascular cell adhesion molecule 1
VIP2	vegetative insecticidal protein 2
VWAI	von Willebrand Factor type A domain/integrin inserted domain
WASP	wiskott aldrich syndrome protein
μ g	microgram
μ l	microliter
μ M	micromolar

12.3 Alphabetical List of Companies

Aaper Alcohol Co	Shelbyville, KY
Abgene	United Kingdom
Airgas West	San Diego, CA
Alpha Innotech	San Leandro, CA
Amersham Bioscience	Uppsala, Sweden
Applied Biosystems	Foster City, CA
BD Biosciences	San Jose, CA
Beckman Coulter	Fullerton, CA
Bellco Glass INC	Vineland, NJ
BioRad Laboratories	Hercules, CA
Brinkman Instruments Inc.	Westbury, NY
Lonza	Walkersville, MD

Cell Sciences	Canton, MA
EG + G Berthold	Bad Wildbach, Germany
Electron Microscopy Sciences	Hatfield, PA
EMD Biosciences	San Diego, CA
Eppendorf AG	Hamburg, Germany
Fisher Scientific	Hampton, NH
GE Healthcare	Piscataway, NJ
Genesee Scientific	San Diego, CA
Gibco Invitrogen	Carlsbad, CA
Integrated DNA Technology (IDT)	Coralville, IA
Invitrogen	Carlsbad, CA
J.T. Baker	Phillipsburg, NJ
Konica Minolta	Wayne, NJ
Labnet International Inc	Edison, NJ
Leica	Wetzlar, Germany
Perkin Elmer Instruments	Wellesley, MA
List Biological Laboratories	Campbell, CA
Mettler	Toledo, Switzerland
Millipore	Temecula, CA
Molecular Devices	Sunnyvale, CA
MP Biomedical	Solon, OH
NanoDrop Technologies	Wilmington, DE
Nikon	Melville, NY
NUAIRE	Plymouth, MN
Olympus	Center Valley, PA
Perkin Elmer	Wellesley, MA
Pharmacia Biotech	Cambridge, UK
Philips	New York, NY
Pierce	Rockford, IL
Promega	Madison, WI
Qiagen	Valencia, CA
Reichert	Depew, NY
Roche	Basel, Switzerland
Santa Cruz	Santa Cruz, CA.
Sigma-Aldrich Co	St. Louis, MO
Southern Biotech	Birmingham, AL
STERIS Corporation	Mentor, Ohio
Stratagene	La Jolla, CA
Thermo Forma Scientific	Waltham, MA
ThermoHybaid	Heidelberg, Germany
VWR	West Chester, PA
World Precision Instruments	Sarasota, FL
Zeiss	Goettingen, Germany

12.4 Publications

ORIGINAL PUBLICATIONS:

Mandy Lehmann, Deborah Noack, Martha Perego, Angelika M. Vollmar and Ulla G. Knaus. "Lethal Toxin Induced Respiratory Distress Caused by Cell Motility and Junctions Alteration." in preparation.

Mandy Lehmann, Martha Perego, Angelika M. Vollmar and Ulla G. Knaus. "Lysine Modification of Lethal Factor Prevents Cell Death in Murine Macrophages." in preparation.

Vladimir V. Kravchenko, Gunnar F. Kaufmann, John C. Mathison, David A. Scott, Alexander Z. Katz, David C. Grauer, **Mandy Lehmann**, Michael M. Meijler, Kim D. Janda, Richard J. Ulevitch. "A small bacterial molecule specifically alters gene expression via disruption of NF- κ B signaling." submitted.

Sandrine Pacquelet, **Mandy Lehmann**, Sylvia Luxen, Karine Regazzoni, Monika Frausto, Deborah Noack and Ulla G. Knaus. "Inhibitory Action of Noxa1 on Duox Activity in Airway Cells." submitted.

Kravchenko VV, Kaufmann GF, Mathison JC, Scott DA, Katz AZ, Wood MR, Brogan AP, **Lehmann M**, Mee JM, Iwata K, Pan Q, Fearn C, Knaus UG, Meijler MM, Janda KD, Ulevitch RJ. "N-(3-oxo-acyl) homoserine lactones signal cell activation through a mechanism distinct from the canonical pathogen-associated molecular pattern recognition receptor pathways." *J Biol Chem*. 2006 Sep 29;281(39):28822-30.

Rutsch, F., Ruf, N., Vaingankar, S., Toliat, M.R., Suk, A., Hoehne, W., Schauer, G., **Lehmann, M.**, Roscioli, T., Schnabel, D., Epplen, J. T., Knisley, A., Superti-Furga, A., McGill, J., Filippone, M., Sinaiko, A. R., Vallance, H., Hinrichs, B., Smith, W., Ferre, M., Terkeltaub, R., Nuernberg, P. (2003). "Mutations in ENPP1 are associated with 'idiopathic' infantile arterial calcification." *Nat Genet* 34(4): 379-81.

POSTERS:

Frontiers of Clinical Investigation Symposium – Host Defense 2006: From Bench to Bedside, October 5-7, 2006 Estancia Hotel La Jolla, CA: Model of the human airway system – A tool to study lung disease.

Gordon Research Conference: Microbial Toxins & Pathogenicity, July 16- 21, 2006 Proctor Academy Andover, NH: Effect of *B. anthracis* lethal toxin on the respiratory epithelium.

International Symposium of the Collaborative Research Center 577, Berlin September 29-30, 2003: Role of the Ank protein in the regulation of skeletal homeostasis.

12.5 Acknowledgements

The present study was carried out at the Scripps Research Institute in San Diego in exchange with the Ludwig-Maximilians University in Munich, during the years 2003-2008. It is my great pleasure to thank the following persons, who have given their effort and support to this work:

First and foremost, I want to thank Dr. Ulla G. Knaus and Prof. Dr. Angelika M. Vollmar for giving me the opportunity to perform this doctoral thesis. Their guidance, encouragement, scientific knowledge and optimism throughout my study have been invaluable. It is an honor to do this exchange and gain international experience. I am deeply grateful it.

Special thanks go to my thesis committee.

I am indebted to my many colleagues for providing a stimulating and fun environment in which I was able to learn and grow. I am especially grateful to Monika Frausto, Sylvia Luxen, Katrina Schreiber, Dr. Michael Ye and Suzel Davanture-Verdeil.

Without the critical suggestions on my writing by Dr. Marina Tsatmali, Sylvia Luxen, Katrina Schreiber and Dr. Monica Ruse this thesis would not be what it is right now.

Debbie Noack helped me with cloning of lentiviral constructs, which was very challenging and I am grateful for her help.

Thanks also to the stimulating suggestions from members of the Bokoch laboratory in our joined lab meetings.

Dr. Malcolm Wood instructed me to use the confocal and electron microscope and Dr. Theresa Fassel prepared all EM slides for which I am thankful.

A special thanks to Dr. Cristian Ruse, who introduced me in mass spectrometry.

Furthermore, I would like to thank Dr. Aimee DeCathelineau and Dr. Peri Nalbant for their expert guidance and constant support.

Dr. Mario Tschan did a wonderful job in teaching me real-time PCR and the handling of lentivirus in the BSL3 facility. I would like to say thanks for this.

I wish to thank Karen Commons, Dr. Rajesh Grover, Rafer Willenberg and John Huang for helping me get through the difficult times, and for all the emotional support and caring they provided.

Lastly, and most importantly, I wish to thank my mother, Sabine Lehmann. She has always supported my dreams and aspirations even over the distance. I'd like to thank her for all she is, and all she has done for me. It is hard for a mother and a child to be separated, especially at times of sickness or holidays. To her, I dedicate this thesis.

12.6 Curriculum Vitae

PERSONAL INFORMATION:

Name	Mandy Lehmann
Date of Birth	18.04.1978
Place of Birth	Frankfurt/Oder
Nationality	German
Marital Status	Single

EDUCATION:

Nov. 2003 – April 2008 LUDWIG-MAXIMILIANS UNIVERSITY, Munich, Germany
External Ph.D. Student in exchange with The Scripps Research Institute, La Jolla, USA

Sep. 1997 – April 2002 PHILIPPS UNIVERSITY, Marburg, Germany
Diplom (American Master's Degree Equivalent) Human Biology
Main Emphasis: Human Genetics
Minor Emphases: Immunology and Pharmacology
Thesis: Pathophysiology of Craniometaphyseal Dysplasia: Testing functional changing's of the ANKH mutations in cellular system

Sep. 1991 – June 1997 GYMNASIUM BEESKOW, Beeskow, Germany

Sep. 1984 – June. 1991 CLARA-ZETKIN OBERSCHULE, Beeskow, Germany

WORK EXPERIENCE:

April 2003 – Oct. 2003 MAX-PLANCK INSTITUTE FOR MOLECULAR GENETICS, Berlin, Germany
Research Assistant

April 2002 – April 2003 MAX-DELBRUECK CENTER FOR MOLECULAR BIOLOGY, Berlin, Germany
Research Assistant

Sep. 2002 – Mar. 2003 RHEUMATOLOGY GROUP VETERAN'S ADMINISTRATION HOSPITAL, La Jolla, CA
Research Assistant – Exchange Program

April 2001 – April 2002 CHARITÉ CLINICS, Humboldt University, Berlin, Germany
Laboratory Technician